Technische Universität Dortmund

Fakultät für Chemie und Chemische Biologie

Dissertation zur Erlangung des akademischen Grades Doktor der Naturwissenschaften

---

The cytosolic state of the integrin adhesome and its relation with cell-matrix adhesion sites

---

vorgelegt von:

Jan-Erik Hoffmann

Betreuer:

Dr. (IL) Eli Zamir und

Prof. Dr. Philippe Bastiaens

Dezember 2013

Erstgutachter: Prof. Dr. Philippe Bastiaens
Zweitgutachter: Prof. Dr. Frank Wehner

Declaration of Authorship

Erklärung:

Ich versichere hiermit an Eides statt, dass ich die vorliegende Dissertation "The cytosolic state of the integrin adhesome and its relation with cell-matrix adhesion sites" selbstständig und ohne unzulässige fremde Hilfe erbracht habe. Ich habe keine anderen als die angegebenen Quellen und Hilfsmittel benutzt, sowie wörtliche und sinngemäße Zitate kenntlich gemacht. Die Arbeit hat in gleicher oder ähnlicher Form noch keiner Prüfungsbehörde vorgelegen.

Unterschrift: _____

Dortmund, den: _____

Curriculum Vitae

Jan-Erik Hoffmann

Born 20.05.1985 in Hagen

Abitur 2004 at the Gesamtschule Schwerte

Bachelor of Science in Chemical Biology 2007 at Dortmund University

Master of Science in Chemical Biology 2009 at Dortmund University of Technology

Lebenslauf

Jan-Erik Hoffmann

Geboren 20.05.1985 in Hagen

Abitur 2004 an der Gesamtschule Schwerte

Bachelor of Science in Chemischer Biologie 2007 an der Universität Dortmund

Bachelor of Science in Chemischer Biologie 2009 an der Technischen Universität Dortmund

Abstract

Integrin mediated cell-matrix adhesion plays an important role in cellular attachment and migration, signal transduction and control of the cytoskeleton and is therefore of major interest for the treatment of cancer metastasis and developmental disorders. More than 100 proteins, collectively called the integrin adhesome, are localized in adhesion sites and have a cytosolic fraction. In order to understand how adhesion sites are assembled and maintained, it is essential to study the state of their components in the cytosolic pool.

Using FCCS, the pairwise associations of 13 key proteins were quantified, thereby revealing a high extent of interconnections between them in the cytosol. FRAP measurements show a rapid exchange of material between focal adhesions and the cytosol. By combining these methods, the cytosolic pool was characterized to consist of diverse building blocks that are confined in size.

In steady state focal adhesion exchange material symmetrically with the cytosol, releasing proteins in the same interaction and phophorylation state as they entered. This ensures a standardized cytosolic pool of building blocks and prevents a gradient of altered components around adhesion sites that could have lead to communication between focal adhesions. In contrast, rapidly disassembling focal adhesions release their material asymmetrically in large complexes, as was determined by perturbating the actomyosin contractility of cells.

To enable the detection of high order complexes, a novel correlation spectroscopy approach was developed. By separating fluorophores by both their fluorescence lifetime and spectrum, associations between three components per complex were resolved simultaneously.

Zusammenfassung

Die Integrin-mediierte Zell-Matrix Adhäsion spielt eine wichtige Rolle bei der Anheftung und Bewegung von Zellen, der Signaltransduktion und der Kontrolle des Cytoskeletts und ist daher von großem Interesse für die Bekämpfung von Krebsmetastasen und Entwicklungsstörungen. Mehr als 100 Proteine, die zusammen das Integrin-Adhesom bilden, lokalisieren in Adhäsionsstellen und haben einen cytosolischen Anteil. Um zu verstehen, wie Adhäsionsstellen gebildet und instandgehalten werden, ist es essentiell, den Zustand des cytosolischen Reservoirs von Adhäsionsproteinen und ihr Verhältnis zu Adhäsionsstellen zu untersuchen.

Durch FCCS wurde die paarweise Assoziation von 13 Schlüsselproteinen quantifiziert und ein hoher Grad an Vernetzung untereinander im Cytosol gefunden. FRAP Messungen zeigen einen schnellen Materialaustausch zwischen Adhäsionsstellen und Cytosol. Die Kombination dieser Methoden zeigt, dass das cytosolische Reservoir aus verschiedenartigen und in ihrer Größe beschränkten Bausteinen besteht.

Im Gleichgewichtszustand tauschen Adhäsionsstellen ihr Material symmetrisch mit dem Cytosol aus, so dass Proteine die Stellen im gleichen Interaktions- und Phosphorylierungszustand verlassen, in dem sie sie betreten haben. Dadurch wird sichergestellt, dass die Bausteine im cytosolischen Reservoir standardisiert sind und verhindert, dass sich ein Gradient um Adhäsionstellen bildet, der zu Kommunikation zwischen Adhäsionen führen könnte. Im Gegensatz dazu setzen schnell auseinanderfallenden Adhäsionsstellen ihr Material asymmetrisch in großen Komplexen frei, wie durch die Störung des Cytoskeletts gezeigt werden konnte.

Für die Untersuchungen von Komplexen mit hochdimensionaler Zusammensetzung wurde ein neuartiger Ansatz der Korrelationspektroskopie entwickelt. Durch das separieren von Fluorophoren anhand ihrer Fluoreszenzlebenszeit und ihres Spektrums, konnte die Assoziation von drei Komponenten pro Komplex gleichzeitig gemessen werden.

Acknowledgements

Contents

List of Figures

Abbreviations

α-Act	α-Actinin
α-Par	α-Parvin
AOTF	**A**cousto-**O**ptical **T**unable **F**filter
ARP	**A**ctin-**R**elated **P**rotein
CAS	**C**rk-**A**ssociated **S**ubstrate
CSK	**C**-**S**rc **K**inase
DNA	**D**esoxyribo **N**ucleic **A**cid
EVA	**E**na/**V**ASP **H**omology
FAK	**F**ocal **A**dhesion **K**inase
FAT	**F**ocal **A**dhesion **T**argeting
FBS	**F**etal **B**ovine **S**erum
FCCS	**F**luorescence **C**ross **C**orrelation **S**pectroscopy
FCS	**F**luorescence **C**orrelation **S**pectroscopy
FLIM	**F**luorescence **L**ifetime **I**maging **M**icroscopy
FRAP	**F**luorescence **R**ecovery **A**fter **P**hotobleaching
GEF	**G**uanine **N**ucleotide **E**xchange **F**actor
HEPES	4-(2-**H**ydroxy**e**thyl)-1-**P**iperazin**e**thane**s**ulfonic acid
ILK	**I**ntegrin **L**inked **K**inase
LD	**L**eucine-aspartate motif
LIM	**L**in11 **I**sl-1 **M**ec-3
MAD	**M**edian **A**bsolute **D**eviation
NA	**N**umerical **A**perture
PBS	**P**hosphate **B**uffered **S**aline
PCR	**P**olymerase **C**hain **R**eaction

PDGF	**P**latelet **D**erived **G**rowth **F**actor
PXN	Paxillin
QD	**Q**uantum **D**ot
RHO	**R**as **Ho**mology gene family
ROCK	Rho associated protein kinase
SH2	**S**rc **H**omology 2
sSMCC	**S**ulfo**s**uccinimidyl-4-(N-**m**aleimidomethyl)**c**yclohexane-1-**c**arboxylate
TLN	Talin
TNS	Tensin
VASP	**Va**sodilator **S**timulated **P**hosphoprotein
VCL	Vinculin
ZXN	Zyxin

Für meine Großeltern...

Dedicated to my Grandparents...

Chapter 1

Introduction

1.1 Biological background

1.1.1 Cell-matrix adhesion sites

In order to attach, arrange and sense their enviroment, cells require a protein machinery that connects the cellular structures and signaling networks with their surrounding. The connective tissue of all metazoa (animals) is made up of an extracellular matrix and cells connect to it by structures formed around a family of transmembrane receptors, the integrins. Upon binding to the extracellular matrix, integrins form heterodimers made up of an α and β subunit. There are at least 18 α and 8 β chains in humans that are further processed by cleavage and modification after translation and can form a variety of dimers [Hynes, 1987]. Among the most investigated are the $\alpha_5\beta_1$ integrin that binds to fibronectin and the $\alpha_v\beta_3$ integrin that binds to vitronectin [Zamir and Geiger, 2001]. Unbound integrins are in an inactive state and are activated by binding to extracellular ligands or intracellularly by binding to adaptor proteins like talin, upon which they undergo a conformational change that allows them to bind their ligand and opens up binding sites on the intracellular domain [Wehrle-Haller, 2012b]. Small integrin clusters form at the lamellipodium and recruit a number of cytosolic proteins to form nascent adhesions, also called focal complexes. Some of these proteins connect the actin cytoskeleton to the newly formed adhesions and bundle actin filaments, marking the maturation of the short-lived nascent adhesions into focal adhesions [Yu et al., 2011]. The force applied to the adhesions by the actin stress fibers can be sensed

1

by adaptor proteins and the integrins themselves and lead to further integrin clustering, protein recruitment and the growth into a micrometer-sized focal adhesion, as depicted in figure 1.1. Integrin clustering and activation is also regulated by the composition of membrane lipids [Legate et al., 2011, Wehrle-Haller, 2012b]. A mature focal adhesion site has an adaptor protein layer of around 40 nm thickness, connecting integrins to actin filaments [Kanchanawong et al., 2010]. Focal adhesions may slide within a cell in a treadmill like manner, where integrins and adaptor proteins detach on the trailing side and assemble on the leading edge, leading to a constant exchange of material. This treadmilling is driven by actomyosin contractility and directed towards the cell center. Mature focal adhesions can further develop into elongated, phosphotyrosine-poor fibrillar adhesions that are responsible for the fibronectin fibrillogenesis [Stanchi et al., 2009, Zamir et al., 2000]. At the rear edge of a migrating cell, adhesion sites disassemble in a proteolysis dependent manner, induced by changes in the actomyosin contractility and the membrane composition [Wehrle-Haller, 2012a].
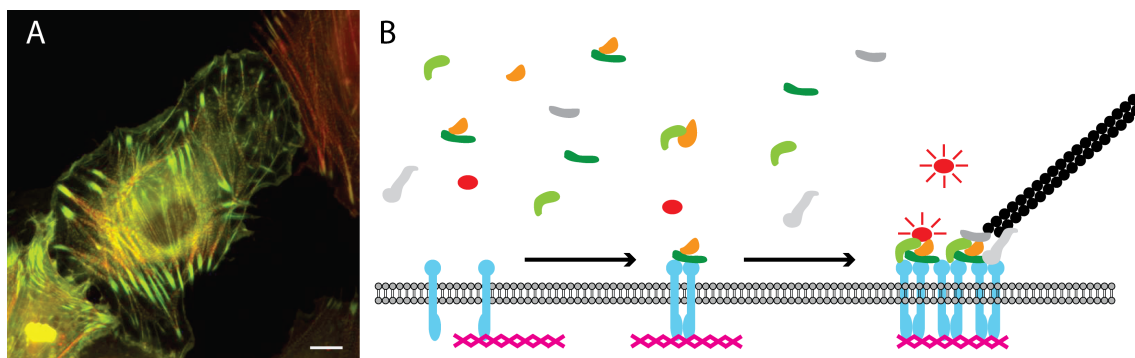
FIGURE 1.1: A) Fluorescence microscopy image of focal adhesions and the cytoskeleton. Stained proteins are actin (red) and α-actinin (green). Scale bar = 10 μm. B) Simplified scheme of the assembly and function of cell-matrix-adhesions: The transmembrane protein integrin (blue) binds to the extracellular matrix (pink) and is activated upon forming a heterodimer with another integrin. Scaffold proteins (green), e.g. talin, bind to the intracellular part of integrins and recruit additional proteins, e.g. kinases (orange) and adaptors of the cytoskeleton (grey), promoting focal adhesion growth. Mature adhesions are linked to actin stress fibers (black) and form platforms to which signaling proteins (red) are recruited and can be modified and activated. The building blocks of focal adhesions also have a cytosolic pool, in which they can exist as monomers or preformed complexes.

The primary functions of cell-matrix adhesions are attachment, anchoring of the

cytoskeleton and signaling. They form a tight connection to the surrounding tissue of around 10-15 nm width [Zamir and Geiger, 2001], holding the cell in place. By providing a fixed anchor point for the stress fibers they enable the cell to remodel its shape and move by actomyosin contractility. Focal adhesions form a signaling hub by allowing spatial regulation of kinase activity and specific recruitment of effector proteins. Among other things, they remodulate the cytoskeleton by affecting rho-family proteins [Deakin and Turner, 2008] and can regulate gene expression [Hirota et al., 2000].

Understanding the dynamics of cell-matrix adhesions and how they are regulated is key in understanding embryonic development, morphogenesis and wound healing and the related deficiencies and diseases [Burridge and Chrzanowska-Wodnicka, 1996]. Additionally, the ability to attach and migrate is a hallmark capability of aggressive cancer, in particular metastasis [Hanahan and Weinberg, 2011]. Therefore, interactions of proteins that are upregulated in cancer, but perform no vital function in adult organisms, can be valuable drug targets for the inhibition of cancer metastasis [Danen, 2013].

Until recently it was disputed if cell-matrix adhesion sites, like those that are seen and investigated in two-dimensional cell culture, actually exist in organisms or if they might be an artifact of the attachment of cells to surfaces. Advancements in microscopy have proven the existence of adhesion sites in three-dimensional culture that behave like those observed in two-dimensional culture [Kubow and Horwitz, 2011], confirming it as a useful model for cell attachment and spreading.

1.1.2 Proteins examined in this work

More than 100 different proteins are associated to focal adhesions [Zaidel-Bar et al., 2007], a number too big to investigate in this work in all detail, as the number of necessary pairwise measurements increases quadratically with the number of observed proteins. Therefore a subset of 13 proteins, known to be key players in focal adhesion development and function and representing different protein classes like scaffold proteins, kinases and adaptors of the cytoskeleton, has been selected. All proteins have in common that they localize to focal adhesions in spread fibroblasts, while also maintaining a large cytosolic fraction. Proteins that are mostly membrane bound, like integrins, are not suitable for the microscopic approach used in this work. Also not considered are proteins known to be associated to integrin

signaling, but do not localize to focal adhesions themselves, like mitogen-activated protein kinases.

The selected proteins are described in the following section. Attached to the protein name is the Uniprot identity of the exact ortholog used.

α-actinin1 (P12814) is a scaffold protein of the spectrin superfamily that can bind to multiple actin fibers, thereby bundling them. It also binds to focal adhesions, creating a link between them and the stress fibers of the cytoskeleton [Sjöblom et al., 2008].

α-parvin (Q9NVD7) consists of two calponin-homology domains and regulates cell contractility by linking actin stress fibers to focal adhesions. It is part of the ILK-PINCH-parvin complex [Wickström et al., 2010].

p130CAS (P56945), also known as breast cancer anti-estrogen resistance protein 1, is a major adaptor protein in focal adhesions that can be phosphorylated on several tyrosine and serine residues and in return recruits several kinases to focal adhesions. It can therefore integrate and transduce signals from receptor tyrosine kinases and influence cell cycle progression and cytoskeleton dynamics [Barrett et al., 2013].

Csk (P41240) is a tyrosine kinase that phosphorylates kinases of the Src-family on their regulatory site and thereby inactivates them [Nada et al., 1991]. Csk is recruited to membrane receptors and focal adhesions in a phosphorylation dependent manner by its SH2-domain [Okada, 2012] and enhances dephosphorylation of adhesion proteins [Tobe et al., 1996].

FAK (Q05397), the focal adhesion kinase, is a tyrosine kinase that is autoinhibited in the cytosol [Lietha et al., 2007] and becomes active upon recruitment to the adhesion sites. Among its functions is the regulation of cell migration [Chacón and Fazzari, 2011], making it a necessary protein for embryonic development as well as a target for cancer treatment [Infusino and Jacobson, 2012].

ILK (Q13418), the integrin linked kinase, is a pseudokinase which also acts as a scaffold protein. While kinase activity has been shown *in vitro*, it is controversial whether this activity has any biological function [Wickström et al., 2010].
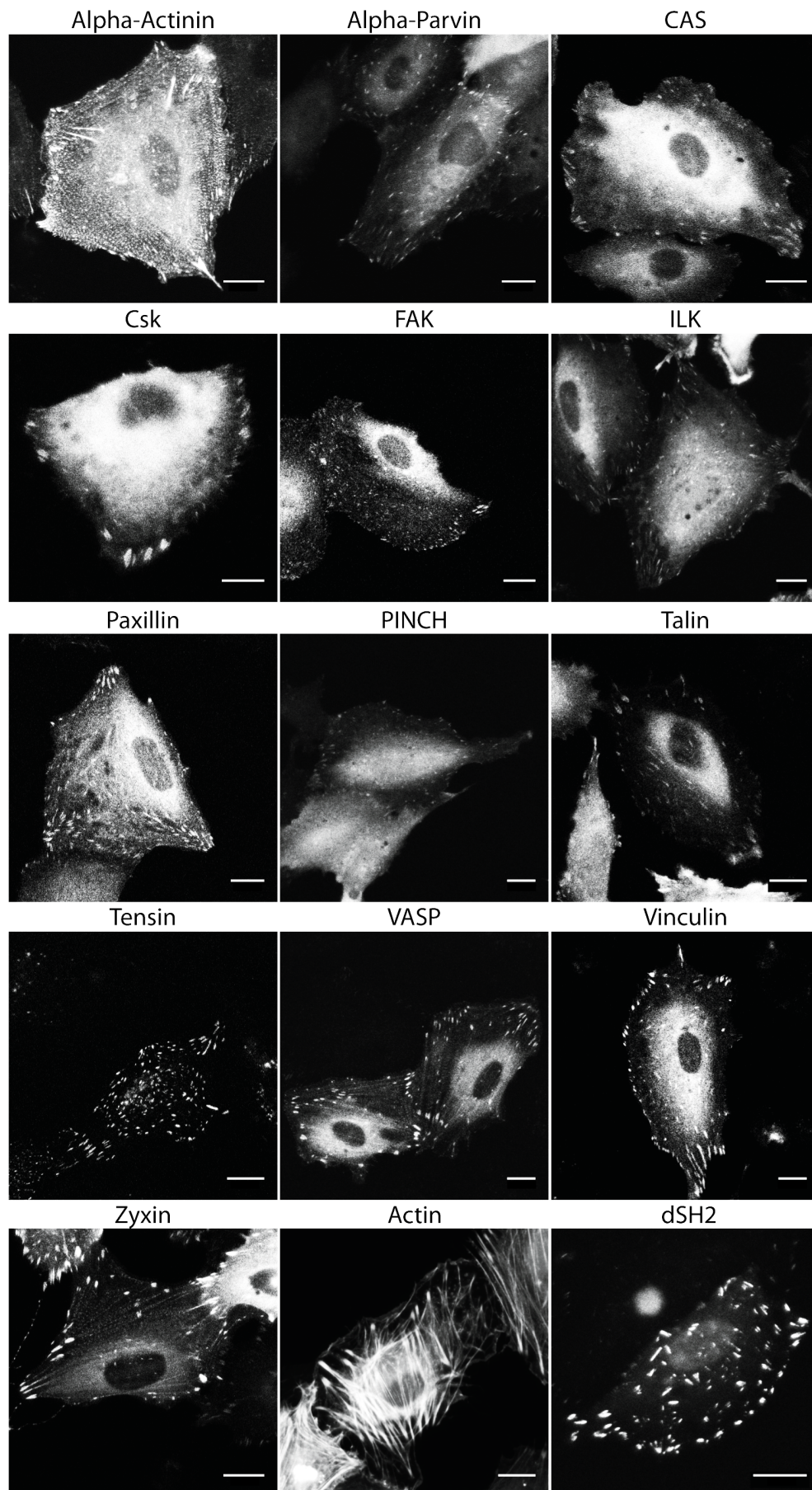
FIGURE 1.2: Localization of the examined proteins: Fluorescence microscopy images of all 13 proteins plus actin and the dSH2-sensor. Proteins are tagged with the fluorophore meGFP and expressed in REF52 cells. Scale bars = 15 μm.

Recent studies confirm the pseudokinase status of ILK, while also showing the essential role of the kinase domain for protein-protein interactions [Ghatak et al., 2013]. ILK directly binds to integrins and via a complex with parvin links them to the cytoskeleon [Qin and Wu, 2012].

Paxillin (P49023-2) is a major scaffold protein that is in the center of the integrin signaling network. It contains a proline rich region, five LD domains and 4 LIM domains and can be phosphorylated on several residues. Many of its interactions are mutual exclusive or phosphorylation dependent, which allows paxillin to integrate signals [Romanova and Mushinski, 2011]. Among its interaction partners are regulators of Rho-family GTPases that regulate the actin cytoskeleton [Deakin and Turner, 2008].

PINCH1 (P48059), also known as LIMS1, is a scaffold protein that consists of five LIM domains which have two zink fingers each. PINCH binds to focal adhesions via interaction with ILK and recruits mediators of different signaling pathways, such as the EGFR pathway [Kovalevich et al., 2011].

Talin1 (Q9Y490) is a high molecular weight protein that enters focal adhesions early in their development. It directly binds to β-integrin with its FERM domain and is required for integrin activation [Ratnikov et al., 2005]. Talin can recruit vinculin to focal adhesions and activate it by opening up the effector binding sites [Critchley, 2005].

Tensin1 (Q9HBL0) is recruited early in integrin activation and binds directly to phosphorylated β-integrin [Calderwood et al., 2003]. It can also bind multiple actin-filaments and acts as a binding platform for tyrosine-phosphorylated proteins with its SH2-domain [Lo, 2004].

VASP (P50552), the vasodilator-stimulated phosphoprotein, is located to focal adhesions by its EVH1 domain and can bind both F- and G-actin [Bear and Gertler, 2009]. In concert with the ARP2/3 complex it modulates the actin polymerization close to the plasma membrane and controls cell protrusion and cell shape [Trichet et al., 2008].

Vinculin (P18206-2) is an adaptor protein that consists of a head and a tail domain [Carisey and Ballestrem, 2011]. In the closed conformation, in which head and tail bind each other, many interaction sites are blocked, while open vinculin can recruit many effector molecule to focal adhesions [Ziegler et al., 2006]. Vinculin is also linked to the actin stress fibers [Ziegler et al., 2008].

Zyxin (Q15942) is a scaffold protein with a proline rich sequence and three LIM domains[Wang and Gilmore, 2003]. Due to an interaction with α-actinin, zyxin also localizes to the cytoskeleton [Reinhard et al., 1999]. Zyxin is also able to shuttle to the nucleus, possibly influencing gene expression [Hirota et al., 2000].

1.2 Microscopy

1.2.1 Principles of fluorescence microscopy

The investigation of dynamic cellular processes requires high spatial and temporal resolution that is provided by fluorescence microscopy. It is based on the effect of fluorescence, where a molecule absorbs a photon of a certain wavelength and reaches a higher energy excited state. After a certain time, usually a few nanoseconds, the molecule falls back into ground state while emitting a photon at a higher wavelength. Flourochromes are sensitive to a particular excitation wavelength, based on the energy gap between ground state and excited state that is broadened due to the fact that the fluorochrome has different vibrational levels. The reemitted photon has a lower energy than the absorbed one because energy is lost during internal conversion processes. Therefore fluorochromes possess a characteristic absorption and emission spectrum that is used in fluorescence microscopy [Ishikawa-Ankerhold et al., 2012]. Here the excitation and emission light is filtered and splitted with optical elements that are transparent or reflective only for light with certain wavelength, so that the emission of multiple fluorophores can be measured selectively. Microscopes route the emission light through a set of lenses before detecting it, to magnify the fluorescent object. The maximum magnification is limited by the wave properties of the light. The minimum d distance to resolve two points is given in equation 1.1, where λ is the wavelength of the emission light and NA the unitless numerical aperture for a specific objective that takes into account the angular apperture of the lens and the refractive index of

the medium.

$$d = \frac{\lambda}{2 \cdot \text{NA}} \tag{1.1}$$

All experiments in this work were performed with confocal laser scanning microscopes. They use monochromatic laser light as a light source that is combined with a set dichroic mirrors or an AOTF and coupled into the microscope with an optical fiber. Here a set of lenses inside the objective is used to focus the beam on a spot inside the sample, creating a femtoliter-sized excitation volume. The fluorophores excited in this volume emit light that is again channeled through the objective and separated from the excitation light with a dichroic mirror. In case of multiple fluorophores, the emission light is further separated and filtered and detected with photomultipliers or avalanche photodiodes. The resolution is further increased by putting a pinhole in the beampath that limits the light that can pass through to that of the confocal plane. By setting the pinhole size to one airy unit, only the light from the main peak of the diffraction pattern passes through. This method measures the fluorescence only in one point a time and to aquire an image, the confocal volume is rapidly moved through the sample with a scanning mirror to build up the image pixel by pixel [Ishikawa-Ankerhold et al., 2012]. A simplified beampath of the microscopes used is shown in figure 1.3.

In this work, fluorescent proteins [Tsien, 1998] were used as fluorophores. They were derived from proteins that occur in organisms like the jellyfish *Aequorea victoria* (eGFP) and the sea anemone *Entacmaea quadricolor* (mKate2) and include mutations that optimize their spectra and photostability [Cubitt et al., 1995]. After expression, these proteins form a β-sheet barrel and form a fluorochrome out of amino acid side chains in a one- or two-step reaction. The main advantage of using fluorescent proteins is that they can be genetically encoded and linked to target proteins. These genes can be transferred into cells that then express the fusion proteins without the need to first purifying the target proteins, labeling them and then injecting them into cells. Disadvantages include their large size of about 250 amino acids that can change the diffusion or binding properties of the labeled protein and their relatively broad spectrum that can lead to fluorescence bleedthrough.
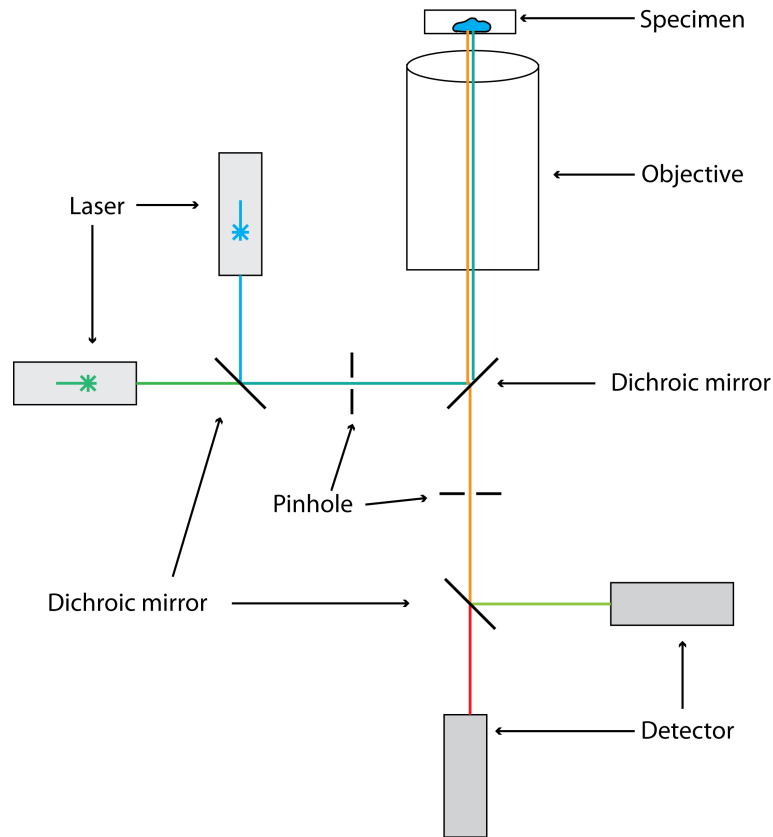
FIGURE 1.3: Simplified beampath of a confocal microscope: The excitation light from one or more lasers is combined with a dichroic mirror or AOTF, directed through a set of lenses in the objective and focussed on the specimen. Emission light is collected by the objective, separated from the excitation light, limited by a pinhole and directed to the different detectors.

Other fluorophores used in this work, in addition to fluorescent proteins, are quantum dots (QDs). QDs are semiconductor nanoparticles made of binary alloys, in case of this work an inner core of cadmium selenide and an outer shell of zinc sulfide. When absorbing a photon, QDs reach an excited state and emit fluorescence when falling back into ground state. Their wavelength depends on the gap between the valence and the conducting band, and thus, their size [Petryayeva et al., 2013]. Main advantages of QDs over organic fluorophores are the high quantum yield and high photostability that makes them bleach only under extreme circumstances [Arnspang Christensen et al., 2012, Shi et al., 2013]. They have a narrow emission spectrum and a broad excitation spectrum that starts about 100 nm below the emission wavelength and increases towards higher energy light. A known property of QDs is the so-called blinking, the loss and gain of fluorescence at time intervals in the range of seconds [Rombach-Riegraf et al., 2013]. This can be a problem when using them in single particle tracking, but is not an issue for the

techniques used in this work, as the timescale of blinking is much longer than their typical dwell times in a confocal volume.

QDs are typically around 10 nm in diameter and can be covered with a polymer coating to make them biocompatible and functionalize them with chemically reactive groups. While there have been efforts to create monovalent QDs with only one functional group per particle [Howarth et al., 2008], commercially available QDs are multivalent which can be both and advantage and disadvantage. QDs are not cell permeable and require the use of microinjection for intracellular applications.

1.2.2 Fluorescence recovery after photobleaching (FRAP)

Another disadvantage of fluorescent proteins and organic fluorophores in general is their tendency to bleach when exposed to light. The excact mechanism of this effect is still not fully understood [Henderson et al., 2007], but it likely results from irreversible modification of covalent bonds that happen while the fluorophore is in the triplet state, involving the creation of reactive oxygen species. [Duan et al., 2013, Hoebe et al., 2008]. While this effect is harmful for general fluorescence microscopy and especially for single molecule techniques like FCS, it can be utilized for methods such as fluorescence recovery after photobleaching (FRAP) [White and Stelzer, 1999]. In this method, intracellular regions or structures are selectively bleached by exposing them to high light intensities via laser scanning microscopy. It can then be observed how the surrounding, still fluorescent, material exchanges with the targeted region to measure diffusion speeds or exchange rates. FRAP has been used on focal adhesions in the past, to reveal their exchange with the cytosolic pool [Lele et al., 2008, Wolfenson et al., 2013], however, a systematic study of all relevant proteins is still missing.

1.2.3 Fluorescence correlation spectroscopy (FCCS)

FCS is based on the movement, in the simplest case free diffusion caused by Brownian motion, of fluorophores through a static volume created by a confocal microscope [Haustein and Schwille, 2007]. This confocal volume is usually approximated as an oval 3-dimensional gaussian intensity distribution that is limited by the decrease of light intensity to e^{-2} of the maximal intensity. For FCS a population of fluorophores, either in solution or inside living cells, is measured over a

certain time. The intensity I detected within this confocal volume will fluctuate around a certain mean value, caused by single flurophores entering and leaving the volume, as shown in figure 1.4 A+B. The fluorescence intensity I at a timepoint t is proportional to the number of fluorophores in the confocal volume at this timepoint. At a later timepoint $t + \tau$ the intensity $I(t + \tau)$ can be similar to $I(t)$, if τ is smaller than the time needed for flurophores to enter or leave the volume, or it can be unrelated if the time τ is much larger and all fluorophores have randomly exchanged. By comparing many different timepoints, the correlation value $G(\tau)$ is calculated for a broad range of different τ, as stated in equation 1.2.

$$G(\tau) = 1 + \frac{\langle \delta I(t) \cdot \delta I(t + \tau) \rangle}{\langle I \rangle^2} = \frac{\langle I(t) \cdot I(t + \tau) \rangle}{\langle I \rangle^2} \tag{1.2}$$

Depending on the convention used, the autocorrelation curve will decay to 1 or 0 for $G(\infty)$. Both is correct and widely used in the literature.

The process of calculating correlation values by comparing a trace with itself shifted by a lag time τ as well as the resulting autocorrelation function is illustrated in figure 1.4 C. This curve contains mainly two important parameters. First, the average number of particles in the confocal volume can be derived from the amplitude of the autocorrelation curve. Assuming the fluorescent particles are highly diluted and behave independently, the fluorescence fluctuations caused by the appearance of these particles in the observation volume are Poisson distributed. In poissonian statistics the average is equal to the variance of a random variable, so in case of the intensity distribution described above $\langle \delta I(t) \rangle^2$ equals $\langle I(t) \rangle$. Therefore for $\tau = 0$ the inverse of the correlation value equals the average number of particles in the confocal volume N [Elson, 2011, Lee et al., 2008].

$$G(0) = 1 + \frac{\langle \delta I(t) \rangle^2}{\langle I(t) \rangle^2} = \frac{N}{N^2} = \frac{1}{N} \tag{1.3}$$

If the size of the confocal volume is known, the absolute concentration of fluorophores can be derived.

The second parameter is the dwell time τ_D of a fluorophore, i.e. the average time a particle needs to cross the confocal volume. In case of three-dimensional free diffusion of one species of fluorescent particles, the inflection point of the autocorrelation curve corresponds to τ_D. Equation 1.4 shows a simple model to describe an autocorrelation curve
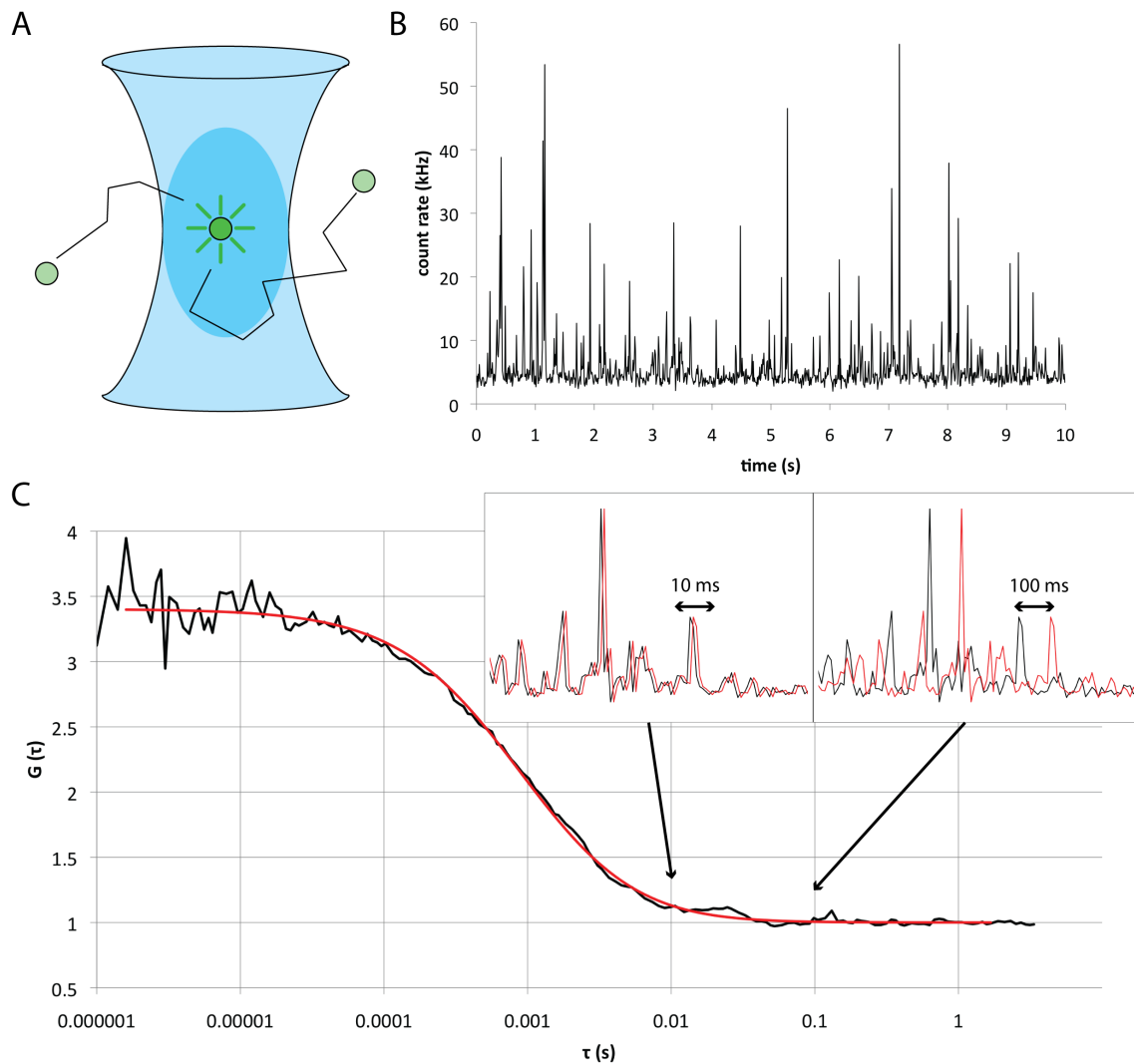
FIGURE 1.4: The principle of FCS: A) Fluorophores diffuse through the excitation volume and emit light that is detected within the femtoliter sized oval detection volume. B) Photons emitted by the fluorophores within the confocal volume are counted with an APD. The example shows a 10 s trace created by a solution of freely diffusing quantum dots. C) Autocorrelation curve of the time trace shown in B. Inserts show a portion of the time trace shifted against itself by different lag times τ and the corresponding part of the autocorrelation curve. The red line shows a fit with a single component free diffusion model.

$$G(\tau) = \frac{1}{N \cdot (1 + \frac{\tau}{\tau_D}) \cdot \sqrt{1 + \frac{\tau}{\tau_D \cdot S^2}}} \tag{1.4}$$

with N being the average number of particles in the confocal volume and S the structural parameter that is determined by the ratio of height z to width ω of the confocal volume. From this the diffusion coefficient D can be calculated [Rüttinger et al., 2008].

$$D = \frac{\omega^2}{4 \cdot \tau_D} \tag{1.5}$$

Assuming free diffusion the hydrodynamic radius r of the fluorescent particle can be calculated using the Stokes-Einstein equation 1.6, where k_B is the Boltzmann constant ($1.380\,648\,8(13) \times 10^{-23}$ JK^{-1}), T the temperature in K and η the viscosity of the medium [Ries and Schwille, 2012].

$$D = \frac{k_B \cdot T}{6 \cdot \pi \cdot \eta \cdot r} \tag{1.6}$$

In crowded environments where the particles cannot move freely, such as the cytosol, the model can be expanded to include anomalous diffusion [Weiss et al., 2004]. In cases where the fluorophore has different populations with different diffusion speeds, like freely diffusing monomers and nearly static complexes, a model with several dwell times can be used. Additionally, technical or photophysical effects, like the detector afterpulse or the triplet state of the fluorophore, can influence the shape of the autocorrelation curve at small τ. This can either be included in the model or excluded by limiting the fitting range.

FCS can be expanded if a second, spectrally separate, fluorophore is used that is excited in the same confocal volume and measured at the same time. In this case, additionally to the autocorrelation curves of the two fluorophores, the crosscorrelation can be measured by comparing the fluorescence trace of one fluorophore with the time-shifted trace of the other, as described in equation 1.7, where x and y are the two fluorophores.

$$G_{xy}(\tau) = 1 + \frac{\langle \delta I_x(t) \cdot \delta I_y(t + \tau) \rangle}{\langle I_x \rangle \langle I_y \rangle} \tag{1.7}$$

If the two fluorophores move independently, G_{xy} has the baseline value for all τ, but if there is association between them, they will simultaneously enter and leave the confocal volume more often than by chance. In this case G_{xy} will be above the baseline value for small τ, but decay at higher τ, depending on the diffusion speed of the complex, which leads to a cross-correlation curve shape similar to that of the autocorrelation curve. The number of complexes in the confocal volume N_{xy} can be calculated according to equation 1.8, where G_{xy} is the amplitude of the cross-correlation curve and N_x and N_y are the number of fluorophores x and y derived from the respective autocorrelation curves.

$$N_{xy} = G_{xy}(0) \cdot N_x \cdot N_y \tag{1.8}$$

Again, the absolute concentrations of fluorophores and complex can be calculated if the confocal volume is known. According to the law of mass action, the association constant K_a and dissociation constant K_d can be derived from the concentrations.

$$K_a = \frac{1}{K_d} = \frac{[xy]}{[x] \cdot [y]} \tag{1.9}$$

It is important to note that K_a can be disturbed, if the confocal volumes for both fluorophores do not perfectly overlap, as well as if the binding sites of potentially associating particles are occupied with non-fluorescent, endogenous proteins. In this case the apparent association constant K_a^{app} is measured and the actual K_a is likely to be underestimated.

In principle any fluorophore can be used for FC(C)S, however it is important that the fluorophores are bright enough so that a single molecule can be distinguished over the noise of background fluorescence and detector. Additionally the fluorophore should be photostable enough to survive a pass through the confocal volume, as photobleaching complicates the shape of the correlation curve and must be attributed during fitting. While the use of fluorescent proteins is often mandatory for live cell experiments, it is possible to improve their brightness by creating fusion proteins with several copies that act as one fluorophore in terms of diffusion behavior. Quantum dots are perfectly suited for FCS, if the experiment allows their use.

1.2.4 Fluorescence lifetime imaging (FLIM)

While FCCS is a powerful tool for the quantitative and sensitive measurement of protein-protein associations, it is important to keep in mind that it only measures co-diffusion and thus association, but not direct interaction, as the confocal volume is much bigger than the investigated protein complexes. For the detection of direct interaction, a method is needed that measures a parameter that is more sensitive to small distances between molecules [Sahoo and Schwille, 2011]. Förster resonance energy transfer is an effect that occurs when a fluorophore in an excited state returns to ground state by transferring its energy emissionless to a nearby acceptor molecule, that can be a fluorophore itself [Förster, 1948]. The efficiency E of this process, that is defined as the fraction of energy transfer relation to all processes in which the excited state can relax, is dependent on the distance R between the donor and acceptor molecule.

$$E = \frac{R_0^6}{R_0^6 + R^6} \tag{1.10}$$

R_0 is the Förster radius that is defined as the distance where halfmaximal FRET efficiency occurs and that is dependent on the fluorophore pair used. R_0 is made up according to equation 1.11

$$R_0^6 = 8.8 \cdot 10^{-5} \cdot \kappa^2 \cdot n^{-4} \cdot Q \cdot J \tag{1.11}$$

where n is the refractive index of the medium, Q the quantum yield of the donor fluorophore, κ^2 the orientation factor between the dipoles of the fluorophores and J the spectral overlap between donor emission and acceptor absorbance [Sun et al., 2011]. J is related to the wavelength λ and the extinction coefficient ϵ of the acceptor.

$$J = \frac{\epsilon \cdot \int_0^\infty f_D(\lambda) f_A(\lambda) \lambda^4 \mathrm{d}\lambda}{\int_0^\infty f_D(\lambda) \mathrm{d}\lambda} \tag{1.12}$$

Therefore a good FRET pair needs to have a high spectral overlap, without causing too much spectral bleedthrough. The orientation factor κ^2 can be assumed to be 2/3, if the fluorophores are freely rotating. This is likely the case for the proteins used in this work, that are separated from their fluorescent tag with a

linker.

Because of the steep distance dependence of the FRET efficiency, FRET can usually only be measured within 1.5 R_0, which corresponds to less than 10 nm for most commonly used FRET pairs [Piston and Kremers, 2007], far smaller than the optical resolution limit. Therefore FRET usually only occurs if the proteins labeled with donor and acceptor are in direct contact with each other, making it a method to measure interactions instead of associations. The principle of using FRET for the detection of protein-protein interactions is shown in figure 1.5 A.
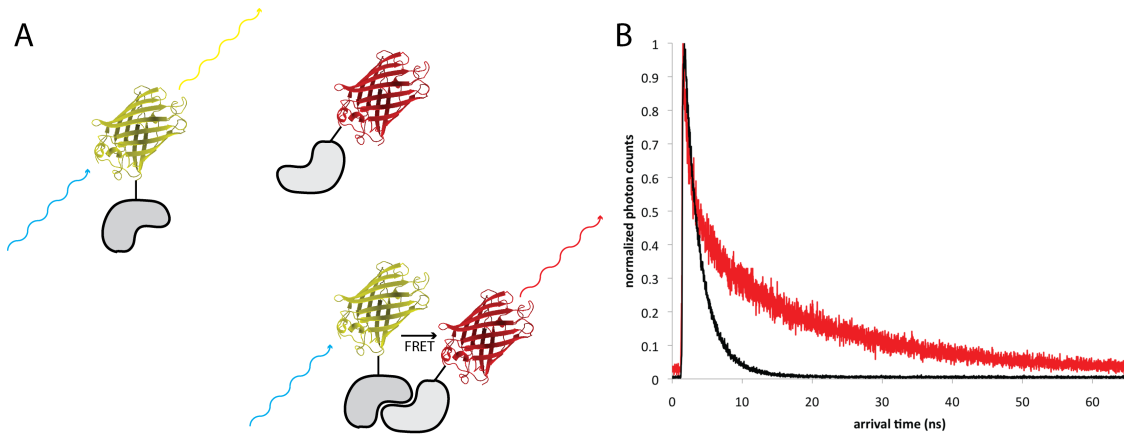
FIGURE 1.5: A) The principle of FRET: Two proteins are labeled with different fluorophores, e.g. mCitrine and mCherry, that form a FRET pair. The donor fluorophore is excited and in absence of an acceptor emits photons at a higher wavelength. When the proteins interact and the fluorophores come into close proximity, an excited donor can transfer the energy to the acceptor fluorphore, which then emits photons. Protein structures taken from [Ormö et al., 1996]. B) Time correlated single photon counting histograms of a low lifetime (eGFP, τ=2.5 ns) and a high lifetime (Quantum dot 525, τ=19.5 ns) fluorophore.

There are many ways to measure FRET, most of which are based on loss of donor fluorescence or gain of acceptor fluorescence [Zeug et al., 2012]. This work uses the technique fluorescence lifetime imaging (FLIM) , a technique based on the reduction of fluorescence lifetime due to FRET [Lakowicz and Berndt, 1991]. The fluorescence intensity I of a population of fluorophores decays exponentially. The simplest case of a monoexponential fluorophore is described in equation 1.13.

$$I(t) = I_0 \cdot \mathrm{e}^{-t/\tau} \tag{1.13}$$

The fluorescence lifetime τ is the rate by which the fluorescence decays and is a constant for every fluorophore at a given temperature and pH value. Processes that reduce the radiative decay, like FRET, apparently reduce this rate an lead to a decrease in τ.

Compared to other methods to measure FRET, like acceptor photobleaching, sensitized emission and ratiometric imaging, FLIM has several advantages. The detection of binary interactions requires only a single channel, reducing the issue of spectral bleedthrough and fluctuating excitation intensity in different channels. It is to a certain degree independent of fluorescence intensity and thereby allows the imaging of dim and bright structures at the same time and tolerates photobleaching [Wouters and Bastiaens, 1999]. Drawbacks include the high measurement time of up to several minutes to collect enough photons in every pixel, the expensive instrumental setup required to obtain high resolution photon counting histograms and the complex analysis of the raw data to get meaningful values.

This work employs the method time domain FLIM, where the donor fluorophores are excited simultaneously with a short laser pulse. After each laser pulse the arrival of emitted photons is measured with picosecond precision. By doing this repeatedly for each pixel, a photon counting histogram is built up, as shown in figure 1.5 B. This histogram is fitted with a model that includes the instrument response function, attributing to the shape of the laser pulse and the mono- or multi-exponential fluorescence decay [Walther et al., 2011]. To observe changes in the fluorescence lifetime τ, a non-FRETing donor-only sample is measured and compared with a sample in which FRET might occur. If the lifetime decay of the donor was only monoexponential, FRET can reveal a second lifetime component, τ_2. With these parameters, the fraction of FRETing donor fluorophores α can be calculated according to equation 1.14 with β being the fraction of photons contributed by the lifetime population τ_2.

$$\alpha = \frac{\beta/\tau_2}{(1-\beta)/\tau_1 + \beta/\tau_2} \tag{1.14}$$

This can be done globally for all photons or pixel-wise to image the spatial distribution of the FRETing fraction and thus the interaction between donor and acceptor.

1.2.5   Fluorescence lifetime correlation spectroscopy (FLCS)

Fluorescence Lifetime Correlation Spectroscopy (FLCS), first described in 2002 [Böhmer et al., 2002], uses the principle of FCS as described in 1.2.3 but, in addition, uses pulsed excitation and measures the arrival time of each photon in respect to both the start of the measurement and the latest laser pulse. With the first information, auto- and cross correlation curves can be calculated, while the second information allows the exclusion weighting of individual photons. This has been used to denoise correlation curves by cutting off or giving a low weight to photons that arrive right after the laser pulse and are likely artifacts from after-pulsing and photons that arrive at the end of the pulse window and are likely to result from background fluorescence, stray light or dark counts. Furthermore, the lifetime information can be utilized to unmix different species of spectrally similar fluorophores that have a different fluorescence lifetime. For this it is necessary to measure the decay pattern of each species individually and then calculate filter functions that are applied to a mixture of the fluorophores. A photon arriving early after the laser pulse is more likely to come from the lower lifetime fluorophore and is weighted high in respect to this species, while a photon arriving late after the pulse, when the fluorescence from the low lifetime fluorophore is expected to have already decayed, is weighted high in respect to the high lifetime species. This way, two different autocorrelation curves can be derived from a trace measured in only one channel [Kapusta et al., 2012]. It is also possible to cross-correlate the two channels generated by filtering a single fluorescent trace. This has been done to investigate the binding of an antibody to EGFR, both labeled with a green fluorophore [Chen and Irudayaraj, 2010], however, not yet in combination with a third, spectrally separated, fluorophore. To avoid artifacts, such as anticorrelation between two fluorophores, it is necessary to make sure that the contributions of both fluorophores to the overall intensity are similar and that the intensity is not too high [Kapusta et al., 2012].

1.3 Objective and approach of this work

1.3.1 The cytosolic interactome of adhesion proteins

There have been extensive studies about the interactions and associations of the components of cell-matrix adhesions [Zaidel-Bar et al., 2007]. However, many of these studies are based on methods that sample whole cell populations like pull down and western blotting and lack the spatial resolution required to selectively observe specific cellular compartments. Even preparation protocols that allow the separation of different cellular compartments, like membranes and cytosol, cannot rule out that a subpopulation of the cells is not in steady state, e.g. mitosis or apoptosis, and might have a completely different state of the interactome. Other studies focus particularly on the adhesion sites themselves, not taking into account the extensive cytosolic fraction that most proteins associated with adhesion sites have.

Proteins associated with focal adhesions are also present in the cytosol and make up the building blocks from which focal adhesions are assembled and maintained. Knowing the composition of these building blocks is of pivotal interest for understanding how proteins are recruited to adhesion sites and how they are regulated. To achieve this, a study of pairwise associations between the 13 key proteins described in section 1.1.2 was conducted in this work. In addition to the 78 possible pairwise associations between these proteins, the 13 possible multimerizations of these proteins were also measured by labeling different copies of a protein with different fluorophores. FCCS is the method of choice for this task as it can quantitatively measure association constants in a well defined spot inside a cell with high sensitivity. The disadvantage is that only one spot can be measured at the same time. Digman et al. used scanning image correlation spectroscopy to investigate the spatial distribution of vinculin-paxillin and FAK-paxillin associations [Digman et al., 2009a,b], but their approach is not sensitive enough for the detection of low affinity complexes. Another disadvantage of FCCS and other fluctuation based methods is their inability to distinguish between direct interactions and mediated associations. Therefore, FLIM was used also as a complementary method for selected protein pairs, providing high spatial resolution and a measure of direct interactions, at the expense of possible false negatives. The third technique that was employed is FRAP, by bleaching a fluorescently tagged protein in single adhesion sites and measuring its recovery speed and mobile fraction. This allows the

characterization of the exchange between adhesion sites and cytosol. With this information available, a picture of the composition and the dynamics of cytosolic building blocks was created.

Additionally to the investigation of the interactome of adherent cells in steady state, the effect of perturbations on the protein-protein associations was measured. For this, cells were treated with the rho kinase (ROCK) inhibitor Y-27632 [Ishizaki et al., 2000, Uehata et al., 1997]. Y-27632 is widely used for the perturbation of actomyosin contractility and focal adhesions [Coyer et al., 2012, Lavelin et al., 2013]. ROCK activates the LIM kinase that phosphorylates and inhibits the actin-depolymerizing protein cofilin. It also phosphorylates the myosin light chain and inhibits the myosin phosphatase, which increases actomyosin contractility. Thus ROCK is mandatory for the maintenance of actin stress fibers [Ai et al., 2001, Maekawa et al., 1999]. Blocking the rho kinase leads to a breakdown of stress fibers and a disassembly of focal adhesions, as the maintenance of these structures is force dependent [Geiger and Bershadsky, 2001, Zhang et al., 2011].

1.3.2 Resolving the exchange mode of material between focal adhesions and the cytosol

The second focus of this work was to study how the identified building blocks are being exchanged between adhesion sites and the cytosol. During their assembly and disassembly focal adhesions take up and release material, but even in steady state they constantly exchange proteins with the cytosolic pool. In principle, two general exchange models can be considered: A protein or protein complex can leave the adhesion site in the same state in which it entered, leading to symmetric exchange. This can mean, for example, that two proteins enter as monomers, bind to each other within the adhesion site and leave again as monomers. Similarly, a protein could enter unphosphorylated, gets phophorylated in the adhesion site and is desphosphorylated before or during getting released. The second model is asymmetric exchange, where a protein or complex leaves the adhesion site in an altered, e.g. phosphorylated or complex bound, way, thereby getting "primed" within the adhesion site and deprimed later in the cytosol. The two models and the special case of complex formation is depicted in figure 1.6.

The different exchange modes have huge consequences on the maintenance of focal adhesions. While both models allow for a steady state between adhesion
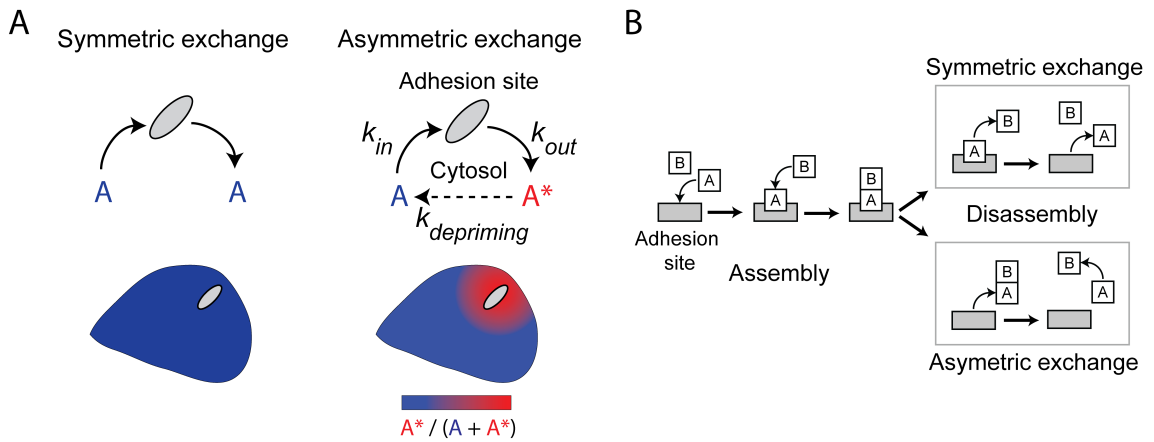
FIGURE 1.6: Symmetric *versus* asymmetric exchange of material between cytosol and focal adhesions: A) In case of symmetric exchange, proteins leave the adhesion site in the same state as they entered, leading to a homogeneous distribution inside the cytosol. In case of asymmetric exchange a protein is modified in adhesion sites (e.g. by phosphorylation or mediated interactions) and leaves them in this "primed" state. It is then deprimed in the cytosol, which leads to the formation of a gradient around adhesion sites. B) Proteins A and B enter the focal adhesion as monomers and interact there. They can leave either as monomers or as a complex that dissolves later in the cytosol.

sites and cytosol, the symmetric exchange model predicts a uniform distribution of protein states across the whole cytosol. The asymmetric model on the other hand predicts a gradient of primed components around adhesion sites, because proteins leave in primed state and are slowly getting deprimed while diffusing away from the site. This would allow adhesion sites to communicate with each other, e.g. a focal adhesion could release proteins in big complexes that might support the formation of new focal adhesions next to it. It also poses an engineering challenge for maintaining a stable environment in the cytosol, as primed proteins could lead to spontaneous formation of large structures within the cytosol around adhesion sites.

To resolve the mode in which adhesion sites exchange material with the cytosol, techniques with high spatial resolution are required. This work will therefore utilize the aforementioned methods FCCS and FLIM to look for differences in the protein-protein associations and interactions around adhesion sites. It will also check the phosphorylation state of the three proteins p130CAS, FAK and paxillin, that are known to be highly tyrosine phosphorylated in adhesion sites [Yu et al., 2004]. Therefore, a tyrosine phosphorylation sensor is used, consisting of two SH2 domains connected to a fluorescent protein that will bind to phosphorylated proteins [Kirchner, 2003].

1.3.3 Development of new microscopy techniques to measure high order protein associations

Standard FCCS is a powerful tool for the quantitative detection of protein-protein associations, but reaches its limit when encountering weak fluorophores, high background noise and weak associations where only a small fraction of the proteins is in complex. Zamir et al. developed a quantum dot based visual immunoprecipitation method, where a quantum dot is coated with a bait to recruit fluorescently labeled prey proteins [Niethammer et al., 2007, Zamir et al., 2010]. In addition to its high quantum yield and photostability, the quantum dot recruits multiple prey proteins at once, leading to a change of diffusion speed and apparent molecular brightness of the prey fluorophore. Combining these additional readout parameters with the cross-correlation between both molecules allows a much more sensitive determination of association strength than the cross-correlation alone. In this work the probe was further enhanced by making the interaction between quantum dot and bait protein switchable. This has the additional advantage of being able to measure a negative control in the same cell, allowing for the correction of background noise, before switching on the interaction. For this, the FKBP/FRB dimerization system was used. Upon addition of the drug rapamycin [Ley et al., 2009, Sehgal et al., 1975], the usually non-interacting protein FKBP12 (FK506 binding protein) and the FKBP-rapamycin-binding domain (FRB) of mTOR form a strong complex with a K_d of 2 nM [Hay and Sonenberg, 2004, Liang et al., 1999]. FRB contains only a single cysteine that is embedded in the structure (see figure 1.7A), thus expressing and purifying it with an additional cysteine attached to its free N-terminus provides a chemically active site to link it to amino-modified quantum dots using the bifacial linker sSMCC. Thereby a FRB functionalized quantum dot is created that can be injected into cells expressing a bait protein fused to the FKBP domain and a fluorescently labeled prey protein. As rapamycin interfers with the mTOR-patchway and can potentially influence focal adhesion [Liu et al., 2008], a mutation in the FRB domain is introduced to be able to use the non-toxic dimerizer AP21967 instead [Bayle et al., 2006].

The detection of high order protein complexes in living cells, but also *in vitro* and in cell extract, is a challenging task that is often beyond the abilities of existing microscopy techniques. Two-color FCCS is able to indicate potential high order complexes by measuring pairwise associations between proteins that are possibly
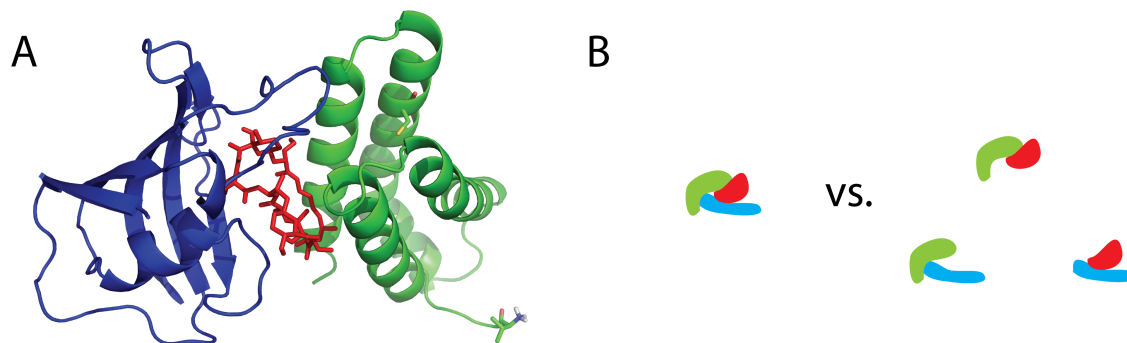
FIGURE 1.7: A) Crystal structure of FKBP (blue) and FRB (green) in complex with rapamycin (red) [Liang et al., 1999]. Highlighted are the N-terminus of FRB and the single cystein within its structure. B) Three proteins form a trimeric complex or have mutual exclusive associations with each other. The two cases cannot be told apart by pairwise two-color FCCS and require high order correlation spectroscopy.

associating, but cannot distinguish between cases like the one shown in figure 1.7B. In order to truly resolve high order complexes with FCCS, three or more fluorophores must be resolved at the same time. This work uses FLCS, as introduced in section 1.2.5, to resolve fluorophores both spectrally and by lifetime. For this, eGFP and the green quantum dot QD525 are used that have similar emission spectra, but a lifetime that is different by one order of magnitude (see figure 1.5). They are combined with a red fluorophore, here QD655, that is spectrally different from the other two fluorophores. To link the quantum dots to proteins of interest, antibodies or the rapamycin based system described above can be used.

Three-color-FCCS has been introduced by the groups of Schwille [Heinze et al., 2004] and Cramb [Blades et al., 2012, Wobma et al., 2012], using three spectrally separate organic dyes and quantum dots, respectively. They also developed the mathematical theory required to infer high order cross-correlation from this data. So far these methods are still limited to *in vitro* applications and require a complex instrumental setup with three detection channels. The method introduced in this work, based on lifetime separation by FLCS, has the advantage of requiring spectral separation of only two colors, which is achievable by most commercially available microscopes, as well as using single wavelength excitation which excludes

the problem of non-optimal excitation volume overlap.

Another method that would allow the measurement of three species with only two channels is pulsed interleaved excitation [Hendrix and Lamb, 2013, Müller et al., 2005], that is based on excitation with alternating laser pulses. Using fluorophores with high stokes-shift like mKeima [Kogure et al., 2008, Piatkevich et al., 2010] that can be excited at the same wavelength as a green fluorescent protein, while having the emission spectrum of a red fluorescent protein, it would be possible to observe this protein in the same channel as a regular red fluorescent protein, while only exciting one of them at a time. However, since the quantum yield of the available high-stokes-shift proteins is still inferior to conventional fluorescent proteins, this work concentrates on the abovementioned method FLCS.

Chapter 2

Material

2.1 Cell lines

2.1.1 REF52

Rat embryonic fibroblasts (REF52) were used as a model cell line for most of the experiments in this work. This cell line resembles cells from the connective tissue, shows prominent focal adhesions and has been used for the study of focal adhesions before [Zamir et al., 2008]. REF52 cells were originally generated by Logan et al. from primary 14-day-old rat embryos. They are subtetraploid and form single layers with a cell density of up to 10^4 cells/cm^2 [Logan et al., 1981]. Cells were used between passage number 44 and 90 and showed no morphological alterations during that period. For control experiments that required a uniform expression level, REF52 cells with a stable transfection of paxillin labeled with YFP, a variant of GFP, were used. They were provided by the Geiger and Spatz groups.

2.1.2 NIH3T3

To verify the findings of the experiments in REF52 cells, key experiments were repeated in the mouse embryonic fibroblast cell line NIH3T3. They were created by Jainchill et al. and have been used as a model cell line for fibroblasts [Jainchill et al., 1969].

2.1.3 XL10 Gold

For cloning and plasmid preparation the *E. coli* strain XL10 Gold from Stratagene (La Jolla, USA) was used. It has the following genotype:

Tetr Δ(mcrA)183 Δ(mcrCB-hsdSMR-mrr)173 endA1 supE44 thi-1 recA1 gyrA96 relA1 lac Hte [F' proAB lacIqZΔM15 Tn10 (Tetr) Amy Camr]

2.1.4 SCS110

Cloning strategies that required using methylation sensitive restriction enzymes made the use of a dam-methylase negative *E. coli* strain necessary. For these cases the strain SCS110 from Stratagene was used. It has the following genotype:

rpsL (Strr) thr leu endA thi-1 lacY galK galT ara tonA tsx dam dcm supE44 Δ(lac-proAB) [F' traD36 proAB lacIqZΔM15]

2.2 Plasmids

All backbones used for the transfection of eucaryotic cells were based on the N1- and C1-vectors from Clontech. They contain a kanamycin resistance and a CMV promoter.

For FCCS experiments proteins were tagged with meGFP and TDmKate2 fluorescent proteins by inserting their sequence into plasmid backbones containing the sequences of the fluorescent proteins. Monomeric GFP was created by introducing the mutation A206K [Zacharias et al., 2002] by mutagenesis PCR with the primers eGFP-meGFP-FP and eGFP-meGFP-RP.

mKate2-C1 was cloned on the basis of mKate2-N1 (Evrogen) by performing a PCR with primers mKate2 FP1 and mKate2 RP2, and inserting it into pEGFP with the restriction enzymes *Age*I and *Xho*I. TDmKate2 was cloned by inserting another copy of the fluorophore into mKate2-N1- or C1-vectors. For the C1 backbone a PCR was conducted on mKate2-C1 using primers mKate2 C1 FP1 and mKate2 C1 RP1. The product was cut with *Age*I and *BspE*I and inserted into mKate2-C1 backbone that was cut with *BspE*I. For the N1 backbone a PCR was conducted on mKate2-N1 using primers mKate2 N1 FP1 and mKate2 N1 RP1. The product was cut with *Age*I and *BspE*I and inserted into mKate2-N1 backbone

that was cut with *Age*I.

To correct for non-optimal overlap of confocal volumes in FCCS, a TDmKate2-Don1-meGFP positive control was cloned by separating the fluorophores with the inert yeast protein Don1, as described in [Maeder et al., 2007]. Don1 was amplified from yeast genomic DNA with primers Don1-FP and Don1-RP and cut with *Bgl*II and *Eco*RI. *Sal*I and *BamH*I restriction sites were introduced in meGFP using meGFP-N1 as template and meGFP-FP and meGFP-RP as primers. Both fragments were ligated into TDmKate2-C1.

In all cases α-actinin, Csk and VASP were tagged C-terminally, while α-parvin, CAS, FAK, ILK, paxillin, PINCH, talin, tensin, vinculin and zyxin were tagged N-terminally.

pEGFP-N1-**α-actinin** was obtained from Adgene. It was subcloned using the restriction sites *Eco*RI and *Xho*I.

α-parvin was amplified with primers parvin C1 FP1 and parvin C1 RP1 using HeLa cDNA as template. The product was cut with *Eco*RI and *Xho*I and inserted into the expression vectors.

p130CAS was obtained from Openbiosystems (p130CAS-pOTB7). A linker was introduced by PCR using the primers CAS C1 FP1 and CAS C1 RP1. The product was subcloned with *Xho*I and *Eco*RI.

Csk was amplified with primers Csk N1 FP1 and Csk N1 RP1 using HeLa cDNA as PCR template. The product was cut with *Sal*I and *BamH*I and inserted into the expression vectors.

FAK was amplified by PCR from HeLa cDNA. Restriction sites BglII and SalI for subcloning were introduced with the primers FAK C1 FP1 and FAK C1 RP1.

ILK was amplified with the primers ILK C1 FP1 and ILK C1 RP1 using HeLa cDNA as template. The product was subcloned with *Xho*I and *Eco*RI.

mCherry-α-**paxillin**-C1 was a gift of Irina Kaverina [Efimov et al., 2008]. It was subcloned with *Bgl*II and *Eco*RI. The paxillin used in this work deviated from human α-paxillin by having the mutation T284A. This amino acid is outside of the LIM or LD domains of paxillin and was not reported to have any function or biologically relevant posttranslational modification. A similar mutation appears in guinea pigs, elephants, chicken and turtles, among other animals.

PINCH1 was obtained from Openbiosystems in pDNR-LIB (Catalog number MHS1011-62408). Linker and restrictions sites for subcloning were introduced by

PCR using primers PINCH-FP2.

Talin was amplified by a 2-step real-time-PCR using U373 mRNA as a template and Talin C1 RP2 as primers. After a PCR with primers Talin C1 FP2 and Talin C1 RP2 the product was cut into two parts with the internal restriction site *Fse*I. The flanking restriction sites were *EcoR*I/*Fse*I and *Fse*I/*Sal*I for the two parts. Both parts were inserted into mCitrine-C1 in two steps. For this, mCitrin-C1 was modified with an additional *Fse*I restriction site by mutagenesis PCR with the primers mCitrine-FseI FP and mCitrine-FseI-RP. Talin was subcloned with *EcoR*I and *Sal*I.

eGFP-**tensin** was a gift of [Hall et al., 2009]. Tensin was amplified by PCR with the primers Tensin-FP and Tensin-RP. The PCR product was subcloned with *Sal*I and *Kpn*I.

VASP was amplified with primers VASP N1 FP1 and VASP N1 RP1 using HeLa cDNA as template. The product was cut with *EcoR*I and *BamH*I and inserted into the expression vectors.

mKO-**vinculin**-C1 was a gift from Miguel Vicente-Manzanares [Choi et al., 2008]. The restriction sites *BspE*I and *Sal*I for subcloning were introduced by PCR using primers Vinculin FP1 and Vinculin RP1.

Cerulian-**zyxin**-C1 was a gift from Irina Kaverina [Efimov et al., 2008]. It was subcloned with *EcoR*I and *BamH*I.

For FLIM experiments mCitrine (a gift from Joel Swanson) and mCherry (Clontech) were used as a FRET pair. CAS, Csk, FAK, ILK, parvin, paxillin and VASP were tagged with mCitrine as donors, while Csk, Paxillin, Tensin and Vinculin were labeled with mCherry as acceptors.

Constructs with two SH2-domains tagged N-terminally with meGFP or mCherry were used as a sensor for tyrosine phosphorylation, as described in [Kirchner, 2003]. For this, YFP-dSH2 (a gift from Benjamin Geiger) was sub-cloned into meGFP-C1 with the restriction enzymes *Nhe*I and *Xho*I and adjusted to the right reading frame by mutagenesis PCR, using primers meGFP-dSH2 FP1 and RP1.

For the expression of eGFP-FKBP and FRB for quantum dot labeling, the backbones pOPIN-EGFP and pOPIN-SUMO from the Dortmund Protein Facility were used.

2.3 Cell culture and media

2.3.1 Cell growth medium

E. coli cells were grown in autoclaved LB (lysogeny broth) medium with the composition 10 g/l tryptone, 5 g/l yeast extract and 5 g/l NaCl in H_2O bidest, adjusted to pH 7.

All eucaryotic cells were cultivated in Dulbecco's Modified Eagle Medium (DMEM, PAN-Biotech GmbH, Aidenbach, Germany) with 4.5 g/l glucose with 10% FBS (PAN), 2 mM glutamine and 1% non-essential glutamic acids (PAN). No antibiotics were added. For the microscopy experiments the medium was replaced with HEPES-buffered imaging medium (PAN).

2.3.2 Cell culture supplements

- PBS for both cell culture and *in vitro* experiments without calcium and magnesium was purchased from PAN-Biotech GmbH, Aidenbach, Germany.

- Cells were detached with trypsin solution from PAN-Biotech GmbH (Aidenbach, Germany).

- As transfection reagent, Lipofectamin 2000 (Invitrogen / Life Technologies, Carlsbad, USA) was used.

- Cells were cultured in 25 cm^2 Falcon flasks (BD, Franklin Lakes, USA) and seated for microscopy in MatTek glass bottom culture dishes (MatTek Corporation, Ashland, USA)

2.4 Chemicals

- Y-27632 was purchased as dihydrochloride from Sigma-Aldrich (St.Louis, USA). Cells were treated with a final concentration of 100 μM.

- To prepare sodium orthovanadate, vanadium-(V)-oxide (Sigma-Aldrich) was dissolved in 0.3 M NaOH resulting in a stock concentration of 29 mM and

boiled until the solution became colorless. Cells were treated with a final concentration of 100 μM vanadate for 30 min.

- Rapamycin was purchased from Bioaustralis, Smithfield, Australia.

- All quantum dots used in this work are from Invitrogen / Life Technologies (Carlsbad, USA).

- The linker Sulfosuccinimidyl-4-(N-maleimidomethyl)cyclohexane-1-carboxylate (sSMCC) was purchased from Pierce Biotechnology (Rockford, USA).

- The calibration fluorophore Atto655-maleimide was purchased from Sigma-Aldrich (St.Louis, USA).

2.5   Instruments

- FCCS, FRAP and photoactivation experiments were performed on a Zeiss LSM 510 META ConfoCor 3 with a 40x water NA 1.5 objective.

- For FLIM and FLCS experiments an Olympus FV1000 microscope with a 40x water NA 1.5 objective was used. Pulsed excitation and detection was performed with a Sepia II and PicoHarp 300 time correlated single photon counting system from PicoQuant (Berlin, Germany).

- Microinjections were done with a FemtoJet and InjectMan NI 2 combination and Femtotips 2 microinjection needles from Eppendorf (Hamburg, Germany).

Chapter 3

Methods

3.1 Cloning

3.1.1 Polymerase chain reaction

For most applications the polymerase PfuUltra from Stratagene (La Jolla, USA) was used with the accompanying buffer. The following composition was used for the PCR mix:

1 µl	Template DNA (approx. 300 µg/ml)
1 µl	Forward primer (approx. 100 µM)
1 µl	dNTPs (10 µM)
3 µl	PfuUltra buffer
1 µl PfuUltra polymerase	
22 µl	H_2O

To amplify a short DNA fragment, the following program was used:

Step 1	2 min	95°C
Step 2	30 s	95°C
Step 3	30 s	55°C
Step 4	1 min	72°C
Step 5	10 min	72°C

Steps 2-4 were repeated 30 times.

For mutagenesis PCR the following program was used:

Step 1   2 min   95°C
Step 2   30 s   95°C
Step 3   30 s   55°C
Step 4   6 min   72°C
Step 5   10 min   72°C
Steps 2-4 were repeated 18 times.

In case of very long fragments and primers with a very high or low melting temperature, the values in amplification step 4 were adjusted. If the removal of the template plasmid was necessary, methylated template DNA was digested with the restriction enzyme *Dpn*I from NEB, by incubating the PCR solution with 1 μl *Dpn*I for 1 h at 37°C.

The PCR product was purified by agarose gel electrophoresis.

3.1.2   Restriction digestions

All DNA digestions were performed with restriction enzymes from New England Biolabs (Ipswich, USA) in the supplied buffers. For preparative use, approximately 3 μg plasmids or PCR products were digested with 1 μl of each enzyme for at least 3 h. In case of methylation sensitive restriction enzymes, plasmids prepared from the dam-methylase negative *E. coli* strain SCS110 were used.

3.1.3   Agarose gel electrophoresis

To seperate cut DNA fragments from other products and enzymes, agarose gel electrophoresis was used. Gels were prepared in TAE buffer containing 40 mM TRIS, 0.1% acetic acid and 1 mM EDTA with 1% agarose and 0.005% red safe dye from iNtRON biotechnology (south korea). The DNA was mixed with 10% sample buffer with a final concentration of 5% glycerol, 0.01% Orange G and 0.01% EDTA and pipetted into the gel pockets. The DNA was separated using an electrophoresis system from BioRad (Hercules, USA). The bands of interest were cut out and extracted from the gel using a gel extraction kit from Qiagen (Hilden, Germany).

3.1.4 Ligation of DNA-fragments

To avoid unspecific religation, backbones were treated with calf intestine alkaline phosphatase from NEB. 8.5 µl backbone solution were incubated with 1 µl CIAP buffer and 0.5 µl CIAP for 1 h at 37°C. The phosphatase was inactivated by heating the solution to 95°C for 15 min.

Subsequently 2.5 µl dephosporylated backbone, 6 µl insert, 1 µl ligation buffer and 0.5 µl T4-ligase from Invitrogen were incubated over night at 18°C.

3.1.5 Transformation of *E. coli*

Chemically competent *E. coli* cells were thawed and supplemented with dithiothreitol. They were incubated with the DNA for 30 min on ice, heatshocked for 45 s to permeabilize them, cooled on ice for 2 min and incubated with antibiotics free medium for 1 h at 37°C. In case of purified plasmid, 0.5 µl were used and in case of freshly ligated plasmids, 10 µl were used per 50 µl bacterial suspension. After the transformation, the suspension was plated on LB-medium agar plates.

3.1.6 Overnight culture and plasmid preparation

3-5 ml LB-medium with 50 µg/ml kanamycin or 100 µg/ml ampicillin, depending on the resistance of the plasmid, was inoculated with a sterile pipette tip by picking a single colony from an agar plate or scratching away a small portion of a frozen stock. The cells were incubated over night at 37°C in a shaker with 200 rotations per minute. The bacteria were pelleted at 13000 rpm and the plasmid was extracted and purified with a Quiagen plasmid purification kit following the manufacturer's protocol. For long term storage 1 ml bacterial suspension from an overnight culture was mixed with 10% DMSO and frozen at -80°C.

3.1.7 DNA sequencing

Plasmid sequences were verified in house by using chain termination sequencing. The following PCR mixture was used:

0.5 μl	Template DNA (approx. 300 μg/ml)
0.25 μl	Sequencing primer (10 μM)
1 μl	5x sequencing buffer
1 μl BigDye terminator mix	
7.25 μl	H_2O

with the following program:

1	1 min	96°C
2	10 s	96°C
3	5 s	50°C
4	4 min	60°C

Steps 2-4 were repeated 25 times.

The PCR product was purified with Qiagen DyeEx kits following the protocol.

3.2 Labeling of quantum dots

FRB with an additional cysteine at its N-terminus separated by a SAGSAG linker was expressed and purified by the Dortmund Protein Facility based on the plasmid pJH48. 10 μl 8 μM quantum dots modified with amine groups (QD655 ITM amino PEG) were washed 3 times with PBS using an Amicon 100 column from Millipore (Darmstadt, Germany) and resuspended in 100 μl PBS containing 1 mM EDTA. 2 μl 60 mM sSMCC in DMSO was added to the quantum dot suspension and incubated for 60 min under gentle shaking. The activated quantum dots were purified using a NAP-5 column from GE Healthcare (Freiburg, Germany) and concentrated again to 100 μl with an Amicon 100 column. 1.2 mg FRB construct was incubated with 5 mM TCEP (tris(2-carboxyethyl)phosphine) to reduce the cysteines and incubated with the activated quantum dots over night at 4°C. The product was washed 8 times with PBS on a Amicon 100 column and stored at 4°C.

For biotinylation, QD655 ITM amino PEG were incubated with 60 mM N-hydroxy-succinimidyl-biotin for 60 min and then washed over a NAP-5 column as described above.

3.3 Cell culture

3.3.1 Passaging of cell lines

Both REF52 and NIH3T3 cells were cultured in 25 cm^2 flasks at 37°C with 5% CO_2 until they were 90% confluent. For passaging, cells were washed with 4.5 ml PBS, incubated for 5 min with 0.5 ml trypsin solution and resuspended in 4.5 ml medium. For regular passaging, cells were diluted 10 fold to be confluent again after 2-3 days. For microscopy experiments, 40000 cells were seated in a MatTek dish in 2 ml growth medium.

3.3.2 Cryopreservation

For long term storage cells were suspended as described above, mixed with 10% DMSO as a cryoprotectant and slowly cooled down to -70°C in NUNC cryo boxes. They were then stored at -150°C. Cells were thawed on ice and seated in a culture flask with growth medium. After one day the medium was changed to fresh growth medium to remove traces of DMSO.

3.3.3 Transfections

Cells seated on MatTek dishes were transfected at 50% confluency approximately one day after passaging. 1 ml of culture medium was removed before transfection. Approximately 0.4 µg of each plasmid was incubated with Lipofectamin 2000 following the protocol. For big or slowly expressing proteins like TDmKate2-talin a higher amount of plasmid was used. The solution containing plasmids and transfection reagent was added to the cells and incubated for one day.

3.3.4 Drug treatments

Cells were treated with drugs on stage by adding the stock solution directly to the imaging medium. In case of hydrophobic drugs they were mixed with 100 µl imaging medium before. Y-27632 and vanadate were used 100 µM and rapamycin 5 µM. Cells were incubated for 30-60 min for Y-27632 and vanadate and 5 min for rapamycin.

3.3.5   Microinjection

Quantum dots were shortly centrifuged before being loaded to the femtotip to avoid large aggregates. Quantum dots were injected into cells either with 50 hPa constant pressure or with 150 hPa injection pressure for 0.2 s and checked for injection success and viability with fluorescence microscopy.

3.3.6   Fixation and immunostaining

For fixation, cells were washed with warm PBS and then treated with freshly prepared 3% paraformaldehyde solution for 10 min.

For immunostaining cells were permeabilized for 5 min with 0.2% TritonX-100 in PBS. All antibodies were diluted in PBS containing 0.2% TritonX-100. Cells were incubated with the primary antibody solution for 1 h, washed three times for 10 min with PBS, incubated with the secondary antibody solution for 1 h and washed again. All incubation steps were carried out in the dark at room temperature.

3.3.7   Cell extracts

Cells were seated on a 10 cm culture dish and transfected with 10 μg of each plasmid. 100 μl cell lysis buffer was supplemented with 1% phenylmethanesulfonylfluoride solution and phosphatase inhibitor cocktails 2 and 3 each, as well as 6% protease inhibitor solution. The cells were washed wish PBS and incubated for 5 min with this lysis buffer, after which they were removed from the dish with a scraper. The suspension was centrifuged for 20 min at 14000 rpm and 4°C and the supernatant collected. If not immediately used the cell extract was frozen at -70°C.

3.4 Microscopy

3.4.1 FRAP

FRAP measurements were performed on a Zeiss LSM 510 META using a 40x
1.2 NA water objective at 37°C. REF52 cells expressing meGFP-tagged proteins
were excited with a 488 nm argon laser at 10% intensity. Emission light was split
with a 565 nm dichroic mirror and further filtered with a 505-550 nm bandpass
filter, using an 896 μm (12.5 airy units) pinhole. One image was taken every 3 s.
After 30 s a single focal adhesion site was bleached by 30 iterations of 100% laser
intensity over a period of 1-2 s and observed for at least 180 s. The bleaching
of a whole adhesion site with a wide pinhole ensured that all fluorescent material
within this site was bleached and recovery could only happen due to exchange of
material with the cytosol, not by exchange within the adhesion site. This had
the side effect that the bleached area was not constant but changed from cell
to cell. The mean fluorescence intensity $I(t)$ in the observed adhesion site was
measured in ImageJ and corrected for background by subtracting the intensity of
an equally sized cytosolic region. The fluorescence intensity $I(t)$ was normalized
to $I_{norm}(t)$ according to equation 3.1 with I_{pre} being the average intensity of the
nine frames before bleaching and $I_{bleached}$ the intensity in the frame right after
bleaching. $I_{norm}(t)$ ranged between 0 right after bleaching and 1 before bleaching,
both background-subtracted.

$$I_{norm}(t) = \frac{I(t) - I_{bleached}}{I_{pre} - I_{bleached}} \tag{3.1}$$

The recovery curves were fitted in Matlab between 0 and 180 s after bleaching
with the single exponential model described in equation 3.2, with M being the
mobile fraction and $\tau_{1/2}$ the recovery half-time.

$$I_{norm}(t) = M \cdot (1 - e^{-\tau_{1/2} \cdot t}) \tag{3.2}$$

Only fits with a coefficient of determination (R^2) above 0.7 were used for further
analysis.

3.4.2 FCCS

FCCS measurements were conducted on a Zeiss LSM 510 META ConfoCor 3 System using a 40x 1.2 NA water objective, at 37°C. meGFP and TDmKate2 were selected as fluorophores for high molecular brightness and good spectral separation. For regular imaging, proteins were excited simultaneously with a 488 nm argon laser and a 594 nm helium-neon laser, both at at 10% intensity, using a 405/488/594 dichroic mirror. Emission light was split with a 565 nm dichroic mirror and further filtered with a 505-550 nm bandpass or 615 nm longpass filter, respectively. For both channels an 896 μm (12.5 airy units for green, 10.4 for red.) pinhole was used before detection with the internal PMTs. For FCCS, an AOTF dampening factor of 10% and a laser intensity of 5% (488 nm) and 8% (594 nm) were used to excite the fluorophores. Emission light was split with a 565 nm dichroic mirror and further filtered via a 505-540 nm bandpass and a 655 nm longpass filter for the green and red channel, respectively, and collected by the internal APDs. The pinhole was set to 64 μm, corresponding to 1 airy unit for the green and 0.82 for the red channel. For each session the correction ring of the objective, as well as the pinhole position, was calibrated for highest count rate with an oregon green solution. Only spread cells with visible focal adhesions were selected for FCCS measurements. The measurement spot was set in a region far away (>5 μm) from focal adhesion that was not in the nucleus or other visible static structures like the stress fibers, or very close (<1.5 μm) to a focal adhesion when indicated. The z-focus was adjusted to the highest count rate, corresponding to a spot in the middle of the cell. For each measurement 10 traces of 10 s each were sequentially acquired. Measurements which showed obvious macroscopic noise in the fluorescence trace, e.g. focus drift or cellular movement, were repeated. The traces were auto- and cross-correlated with the Zeiss ConfoCor 3 software according to equations 1.2 and 1.7 for 175 logarithmically spaced τ between $2 \cdot 10^{-7}$ s and 3.4 s. Autocorrelation curves were fitted in Matlab as described by Bierbaum et al. [Bierbaum and Bastiaens, 2013] with the model shown in equation 3.3 from $2 \cdot 10^{-6}$ s onward, to exclude detector afterpulse and triplet state.

$$G(\tau) = \frac{1}{N \cdot (1 + \frac{\tau}{\tau_D}) \cdot \sqrt{1 + \frac{\tau}{\tau_D \cdot S^2}}} + G_\infty \qquad (3.3)$$

N is the number of particles in the confocal volume, τ_D the dwell time of the particle, S the structural parameter and G_∞ the offset of the curve that is caused

by movements on large timescales that are independent from the diffusion of fluorescent particles. Cross-correlation curves were not fitted, because negative or noisy curved don't give meaningful values. Instead the association score was derived according to equation 3.4 by dividing the offset-subtracted amplitude of the curve by the median absolute deviation (MAD) of the amplitude, which is shown in equation 3.5.

$$\text{score} = \frac{\text{median(amplitude)} - \text{median(offset)}}{\text{MAD(amplitude)}} \tag{3.4}$$

$$\text{MAD}(x) = \text{median}|x_i - \text{median}(x)| \tag{3.5}$$

The amplitude is sampled from the 41 data points between τ=25.6 μs and 81.92 μs and the offset from the 21 data points between τ=157.3 ms and 838.9 ms. While not containing absolute information about the association strength between two fluorophores, the score is a good and robust measure to estimate if they are associating. In absence of association the noise and therefore the MAD will be high compared to the curve amplitude while positive cross-correlation curves will also yield a high score. Negative scores were set to 0. The medians of amplitude and offset of the auto- and cross-correlation curves were also used to calculate the association constant according to equations 1.3, 1.8 and 1.9. To calculate the absolute protein concentrations, the confocal volumes were determined by measuring fluorophores with known diffusion coefficients, as described in [Rüttinger et al., 2008]. Oregon green with $D(25°C)$=4.11 · $10^{-6}cm^2s^{-1}$ [Müller et al., 2008] and Atto655-maleimide with $D(25°C)$=4.09 · $10^{-6}cm^2s^{-1}$ [Korlann et al., 2008] were solved in water and used to calibrate the green and red volume, respectively. Because measurements were performed at 37°C, the diffusion coefficient was adjusted according to equation 3.6

$$D(T_2) = D(T_2) \cdot \frac{T_1}{T_1} \cdot \frac{\eta(T_1}{\eta(T_1} \tag{3.6}$$

with T_1 being the reference and measurement temperatures of 298.15 K (25°C) and 310.15 K (37°C) and $\eta(T_1$ and $\eta(T_2$ the corresponding viscosities of the medium. Since the viscosity of water is also temperature dependent, it was calculated with equation 3.7.

$$\eta(T) = 2.414 \cdot 10^{-5} \cdot 10^{248.8/(T-140)} Pa \cdot s \tag{3.7}$$

The resulting diffusion coefficients of $D(37°C)$=5.51·$10^{-6}cm^2s^{-1}$ and $D(37°C)$=5.49·$10^{-6}cm^2s^{-1}$ for oregon green and Atto655-maleimide were used to determine the waist of the confocal volume ω following equation 1.5, with diffusion times of

τ_D=16.38±1.23 µs and τ_D=23.34±2.24 µs derived from fitting autocorrelation curves of oregon green and Atto655-maleimide solutions with the model from equation 3.3. Here, no offset was observed and the structural parameter S was set to 10, a value consistently observed when fitting the autocorrelation curves of fluorescent proteins. With the waist size ω and the structural parameter S available the size of a Gaussian shaped confocal volume V_{conf} was calculated according to 3.8.

$$V_{conf} = \left(\frac{\pi}{2}\right)^{2/3} \cdot \omega^3 \cdot S \qquad (3.8)$$

This resulted in confocal volumes of V_{green}=0.38 fl and V_{red}=0.67 fl. The overlap of the green and red confocal volumes was determined by expressing a fusion protein consisting of meGFP and TDmKate2 separated by the inert yeast protein Don1 [Maeder et al., 2007] and measuring the auto- and cross-correlation in REF52 cells. The apparent overlap was found to be 48±6%. However, the relatively slow maturation rate of mKate2 has to be considered, resulting in not all proteins being visible in both channels. To attribute for this, the correction ratio φ was calculated by multiplying the ratio of the number of particles of both channels with the volume ratio, according to equation 3.9.

$$\varphi = \frac{N_{red}}{N_{green}} \cdot \frac{V_{green}}{V_{red}} = 0.94 \cdot \frac{0.38}{0.67} = 0.53 \qquad (3.9)$$

Therefore the volume corrected affinity constant K_a can be calculated according to equation 3.10.

$$K_a = \frac{\frac{N_{complex}}{V_{overlap} \cdot \varphi}}{\left(\frac{N_{red}}{V_{red} \cdot \varphi} - \frac{N_{complex}}{V_{overlap} \cdot \varphi}\right) \cdot \left(\frac{N_{green}}{V_{green}} - \frac{N_{complex}}{V_{overlap} \cdot \varphi}\right)} \qquad (3.10)$$

The missing parameter $V_{overlap}$, the overlapping confocal volume, is obtained by solving equation 3.10 for the positive control measurements mentioned above, resulting in a $V_{overlap}$ of 0.34 fl.

FCCS raw data were filtered by the following criteria to sort out problematic measurements:

1) Cells with a low expression level of one or both proteins and high background fluorescence were sorted out, when the counts per molecule cpm=count rate/N was lower than 215 Hz, as these measurements resulted in noisy and unfitable autocorrelation curves.

2) If the offset G_∞ is ≥0.0025 or ≤-0.002, the curve is excluded to avoid inaccurate

fits.

3) If the ratio between the count rates in the green and red channel, after dark count subtraction, is ≥ 20, the measurement is excluded to avoid false cross-correlation signals due to bleedthrough. This was found to be the safe ratio below no cross-correlation could be observed in negative control cells expressing the fluorophores meGFP and TDmKate2 alone. Bleedthrough from red to green was not observed.

4) Negative K_a are excluded as they are biologically impossible and are likely to be an result of noisy correlation curves.

To identify significant association between two proteins, between 9 and 60 FCCS measurements were performed for each pair in different REF52 cells in at least 2 sessions with independent transfections. A negative control population was obtained by measuring 126 cells expressing untagged meGFP and TDmKate2 with different transfection ratios. The hypothesis that the median association score of the investigated protein pair was bigger than the negative control was tested with Fisher's exact test, which is a nonparametric test suitable for small sample sizes [Agresti, 1992, Fisher, 1922]. The resulting p-value denotes the confidence that the pair is physically associated, with lower p-values indicating a higher confidence. To quantify the statistical significance of changes between different conditions, i.e. close vs far from focal adhesions and before vs after adding Y-27632, cell-wise coupled association scores were compared for all investigated protein pairs. T-test and the Wilcoxon signed-rank test [Wilcoxon, 1945] were used to test the hypothesis that mean (t-test) or median (Wilcoxon test) difference in association scores between the compare conditions is different from 0. The same method was used to detect global changes, by batching together all investigated pairs but retaining the cell-wise couples information. In addition, the change in association score was investigated without cell-wise coupling globally and for individual pairs by using Fisher's exact test. To support this analysis, the change in the logarithm of the mean between different conditions was investigated with a t-test, assuming normal distribution. Again, the hypothesis was that the difference between the two conditions is different from 0.

Experiments with the quantum dot-FRB probe were carried out on the Zeiss LSM510 meta as described above for fluorescent proteins, with the exception that both eGFP and QD655 were excited at 488 nm, eliminating the need to calibrate

for confocal volume overlap.

3.4.3   FLIM

FLIM-experiments were performed on an Olympus Fluoview 1000 laser scanning microscope with a Sepia II and PicoHarp 300 time correlated single photon counting system from PicoQuant (Berlin, Germany). All experiments were carried out at 37°C with a 60x water objective. For regular fluorescence imaging samples were simultaneously excited with 488 nm (10% laser intensity) and 561 nm (31% laser intensity) light using a 405/488/561/633 dichroic mirror. Excitation light was splitted with another dichroic mirror at 560 nm and detected between 500-550 nm (780 detector power, green channel) and 580-680 nm (610 detector power, red channel). The pinhole was set to 300 µm. FLIM images were acquired using 470 nm excitation (36% intensity) with a pulse frequency of 40 mHz, a 405/470 nm dichroic mirror and a 525/15 nm band path filter. Proteins were labeled with mCitrine (donor) and mCherry (acceptor), with two-fold excess of acceptor. mCitrine is better suited as a donor than meGFP for its approximately monoexponential lifetime and mCherry does not have a immature green state like mKate2 that would cause noise in the donor channel. They also have a better spectral overlap than the fluorophores used for FCCS. On every day, a donor-only sample was measured for every donor construct used. As an internal control, after a FRET experiment cells were deprived of acceptor by photobleaching and an additional FLIM measurement was performed. Over the course of approximately 5 min lifetime images were acquired until 200-300 photons arrived from each pixel in focal adhesions. The images were binned 2x2 pixels and exported to IGOR Pro (Version 6.22A, Wave Metrics, Lake Oswego, USA). Data analysis was performed with pFLIM3, developed by Walther et al [Walther et al., 2011]. For this, the photon counting histogram of a whole donor-only image was fitted with a monoexponential model to derive the donor-only lifetime τ_1 which was around 3 ns for mCitrine. This value was fixed for the two-exponential fit of the photon counting histogram of the FRET image to derive τ_2. With these parameters available, the FRETing fraction α was calculated for each pixel.

3.4.4 FLCS

FLCS experiments were performed on an Olympus Fluoview 1000 microscope, as described above. All fluorophores were excited with 470 nm laser light with a pulse frequency of 20 mHz. The calculation of the filter functions and unmixing/cross-correlating of fluorescence traces was carried out with the included SymPhoTime software from PicoQuant (Berlin, Germany).

Chapter 4

Results

4.1 FCCS

4.1.1 Diffusion speed of focal adhesion proteins in the cytosol

To characterize the cytosolic mobility of components of adhesion sites in the cytosol, REF52 cells were transfected with proteins of interest labeled with meGFP. FCS autocorrelation curves were fitted with a single-component free diffusion model as described in section 3.4.2. The resulting dwell times are displayed in figure 4.1, together with a control measurement of the fluorophore alone. Interestingly, a clear size dependency was not observed, as the largest protein talin ranges in the middle of the field, while the rather small protein VASP is by far the slowest. This indicates that the diffusion speed of the proteins is dependent on the complexes they appear in or the structures they bind to. While spots with visible stress fibers were excluded from measurements, the binding to actin fibers might still be partly responsible for the slow diffusion of VASP, α-actinin and zyxin. The exact values for the dwell time τ_D and the derived apparent diffusion coefficient D are listed in the appendix.
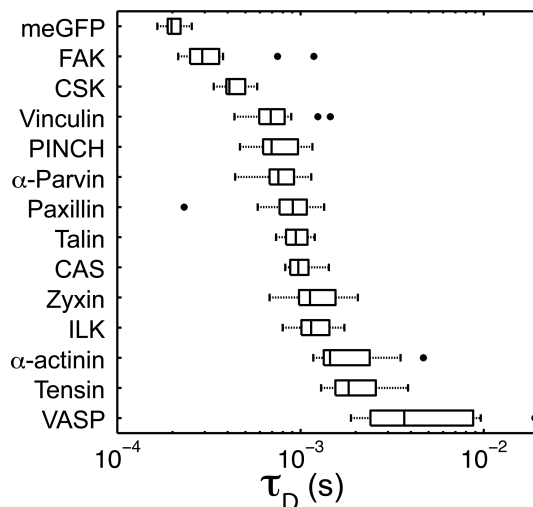
FIGURE 4.1: Dwell times of focal adhesion proteins in the cytosol: Box plots of dwell times τ_D for all investigated proteins labeled with meGFP, measured by FCS.

4.1.2 Pairwise physical associations

Two-color FCCS was used to quantify the physical associations between each two of the 13 selected proteins and derive a cytosolic association network. For this, REF52 cells were transfected pairwise with focal adhesion proteins tagged with meGFP and TDmKate2 and association was measured by FCCS as described in section 3.4.2. The association score was calculated for each measurement as a robust indicator of positive cross-correlation curves. Figure 4.2A shows the score distribution of all 1914 pairwise measurements compared with 126 negative control measurements of non-associating proteins. Compared to the negative control, the distribution for protein-protein association scores has an elongated tail towards higher scores, resulting from measurements with strong cross correlation. When looking at individual protein pairs, most have median scores around the negative control value, while some are shifted to the right. With the non parametric Fisher's exact test a p-value was calculated for each pair, that shows the confidence that the score distribution for this pair is higher than the negative control. Therefore a lower p-value means stronger association. The color coded p-values for each protein pair were plotted as an association matrix, as shown in figure 4.2B. Protein pairs with a low p-value were confirmed in another fibroblast cell line, NIH3T3, in 764 independent measurements. Only pairs with a p-value <0.0001 in REF52 and <0.05 in NIH3T3 were regarded as positive. All association constants, association scores and p-values for both cell lines are listed in the appendix.
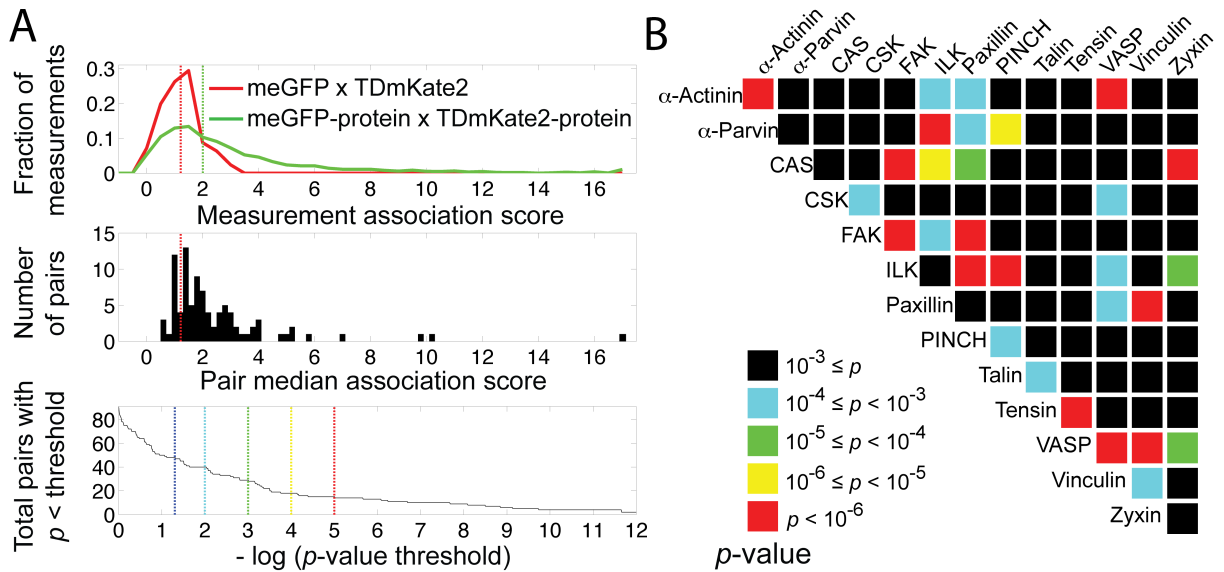
FIGURE 4.2: Pairwise physical protein-protein associations: A) Top: Normalized histograms of association scores obtained from all FCCS measurements (green) compared with the negative control (red). Center: Histogram of median association scores for each protein pair. The red dashed line is the median score of the negative control. Bottom: Distribution of p-values for all protein pairs. The p-value is the probability that the median association score of the given pair is higher than the negative control by coincidence. A lower p-value indicates stronger confidence in association. Dashed lines show the p-value thresholds used in later analysis. B) A matrix of all pairwise protein-protein associations, including the diagonal that indicates di- or multimerization. The p-value is color coded.

4.1.3 Dependency of association strength on distance from focal adhesions

The model of asymmetric material exchange between focal adhesions and cytosol would predict gradients of primed building blocks around adhesion sites, while the absence of such gradients would indicate symmetric exchange. To detect gradients in protein-protein association strength, FCCS measurements were performed in spots very near to (<1.5 µm) focal adhesions and far away in the cytosol in the same cell. Not all 91 pairs were investigated, only those that showed significant association and those that were expected to interact in adhesion sites based on literature data. Figure 4.3A+B show logarithmic scatter plots of the adhesions scores near and far from focal adhesions for all measurements batched together (A) and for individual pairs (B). It can be seen that most measurements cluster around the equality diagonal, indicating no spatial gradient, while outliers appear

mostly in the noise-dominated low score region. The same can be observed in the histogram that shows the difference in score near and far and also shows no shift. In figure 4.3C the median scores for each investigated pair are plotted and lie around the diagonal as well. Therefore no protein pair shows a spatial gradient in its association strength around focal adhesions.
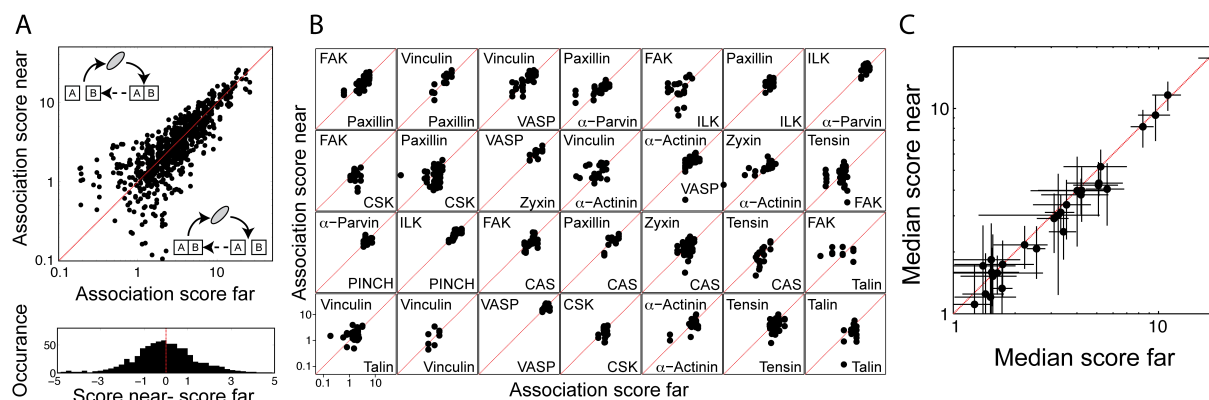
FIGURE 4.3: Distance dependency of association strength: A) The scatter plot shows logarithmic association scores measured near (<1.5 μm) and far away from focal adhesions in the same cell (n=755). The models indicate the asymmetric exchange mode that would be supported by points in that corner. Points on the diagonal indicate no gradient and symmetric exchange. The histogram shows the difference in score for all measurements. B) Scatter plots for individual protein pairs. C) Median association scores near and far from focal adhesions for every pair shown in B.

4.1.4 The cytosolic tyrosine phosphorylation level of FAK, paxillin and CAS

Other than protein-protein interactions, posttranslational modification such as phosphorylation can change when a protein is recruited to focal adhesions and can be used as in indicator for the exchange mode. To detect the cytosolic tyrosine phosphorylation level of the three key proteins FAK, paxillin and CAS, a sensor composed of the phophotyrosine binding SH2 domains and meGFP was co-transfected with the TDmKate2-labeled protein of interest and association was measured by FCCS. The localization of the sensor is shown in figure 4.4A in comparison with paxillin. Interestingly, the localization to focal adhesions is stronger than that of any target protein used in this work, indicating an adhesion site specific tyrosine phosphorylation. Association scores for the interaction of the
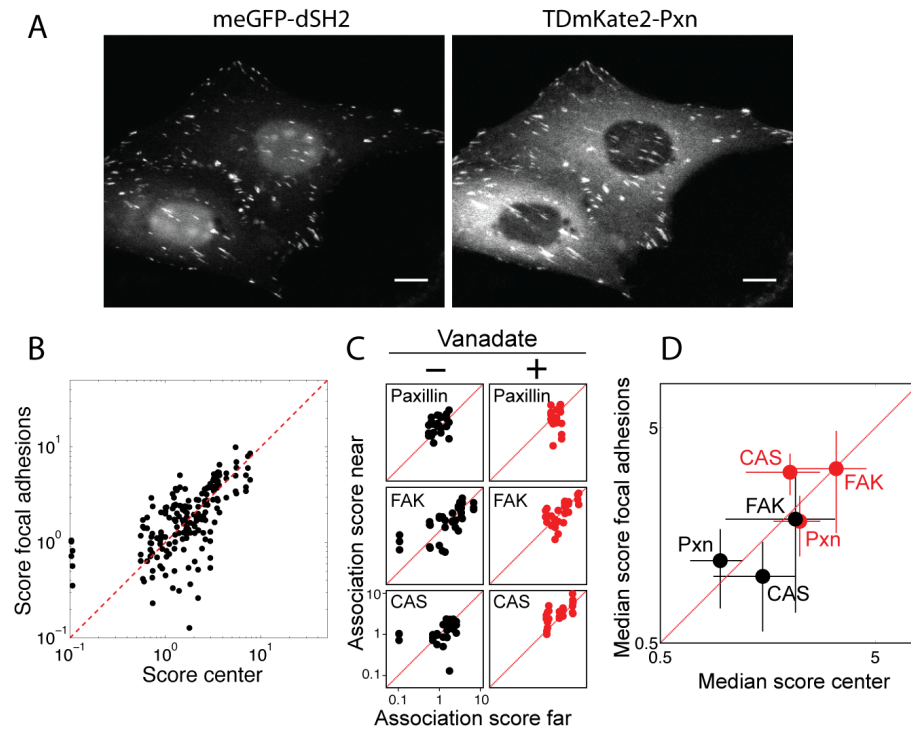
FIGURE 4.4: Cytosolic tyrosine phosphorylation levels of FAK, Pxn and CAS: A) Fluorescence microscopy images of REF52 cells transfected with TDmKate2-paxillin and the tyrosine phosphorylation sensor meGFP-dSH2. Scale bars = 10 µm. B) Scatter plot of association scores of CAS, FAK, Paxillin and CAS with the phosphorylation sensor near (<1.5 µm) and far away from focal adhesions. The association was measured before and after treatment with 100 µM vanadate. C) Scatter plot association scores of all measurements for the indicated protein before and after treatment with 100 µM vanadate. D) Scatter plot of median association scores of the indicated proteins with the phosphorylation sensor near and far away from focal adhesions. Black dots indicate measurements before vanadate treatment, red dots measurements after treatment.

proteins with the sensor are shown in figure 4.4B-D, for pairwise measurements near and far from focal adhesions, analog to section 4.1.3. The score for all three proteins is relatively low, below the level of strong protein-protein associations. A difference in score near and far and therefore a gradient around adhesion sites was not observed. Upon phosphatase inhibition by vanadate, the association with the sensor increases for all investigated proteins, again without showing a distance dependency to focal adhesions.

4.1.5   Response of association strength to perturbation of actomyosin contractility

So far, all FCCS measurements were performed in cells with intact focal adhesions in steady state. This state was perturbed by inhibiting the actomyosin contractility with Y-27632 and thereby disrupting the focal adhesions. After 30 min most adhesion sites were lost, with the exception of small, force-independent, focal complexes. Figure 4.5A shows the effect of Y-27632 on REF52 cells expressing paxillin and vinculin. For all 91 protein pairs, FCCS measurements were conducted before and 30-90 min after addition of Y-27632 in the same cell and, if possible, in the same spot. The first observation is an increase in count rate, both globally and for individual proteins, as shown in figure 4.5B and C. The count rate is proportional to the concentration of the labeled protein in the cytosol and shows the release of material upon disruption of adhesion sites and stress fibers. The color of the fluorescent label does not influence the increase in count rate for any of the proteins. By calculating the relative increase in count rate for each protein, as shown in figure 4.5D, the fraction of material normally bound to static structures is obtained. For example, the concentration of α-actinin increases by over 50% upon disruption of adhesion sites, which shows that approximately one third of the protein is bound to focal adhesions or stress fibers in unperturbed cells.

The association scores, retrieved from FCCS measurements in the same cell before and after addition of Y-27632, were plotted globally for all protein pairs together (n=1278). While most measurements cluster around the equality diagonal, the histogram in figure 4.6A reveals that the population is slightly shifted towards higher scores. During the experiments, morphological changes were observed in some cells as they retracted their lamellipodia and rounded up during the action of Y-27632. This might lead to a higher thickness of the cell in respect to the z-axis of the confocal volume and therefore a higher apparent protein concentration. While this by itself might lower the amplitude of the cross-correlation curve, it would also affect the noise of the curve which is also incorporated in the score. Importantly the measurements showed that the association score is not correlated with the count rate. Figure 4.6B and C show scatter plots of the scores before and after drug treatment for each individual pair and the median score of the respective pair. No single pair is observed to stray far from the equality diagonal, therefore no individual protein pair shows a clear reaction to the treatment.
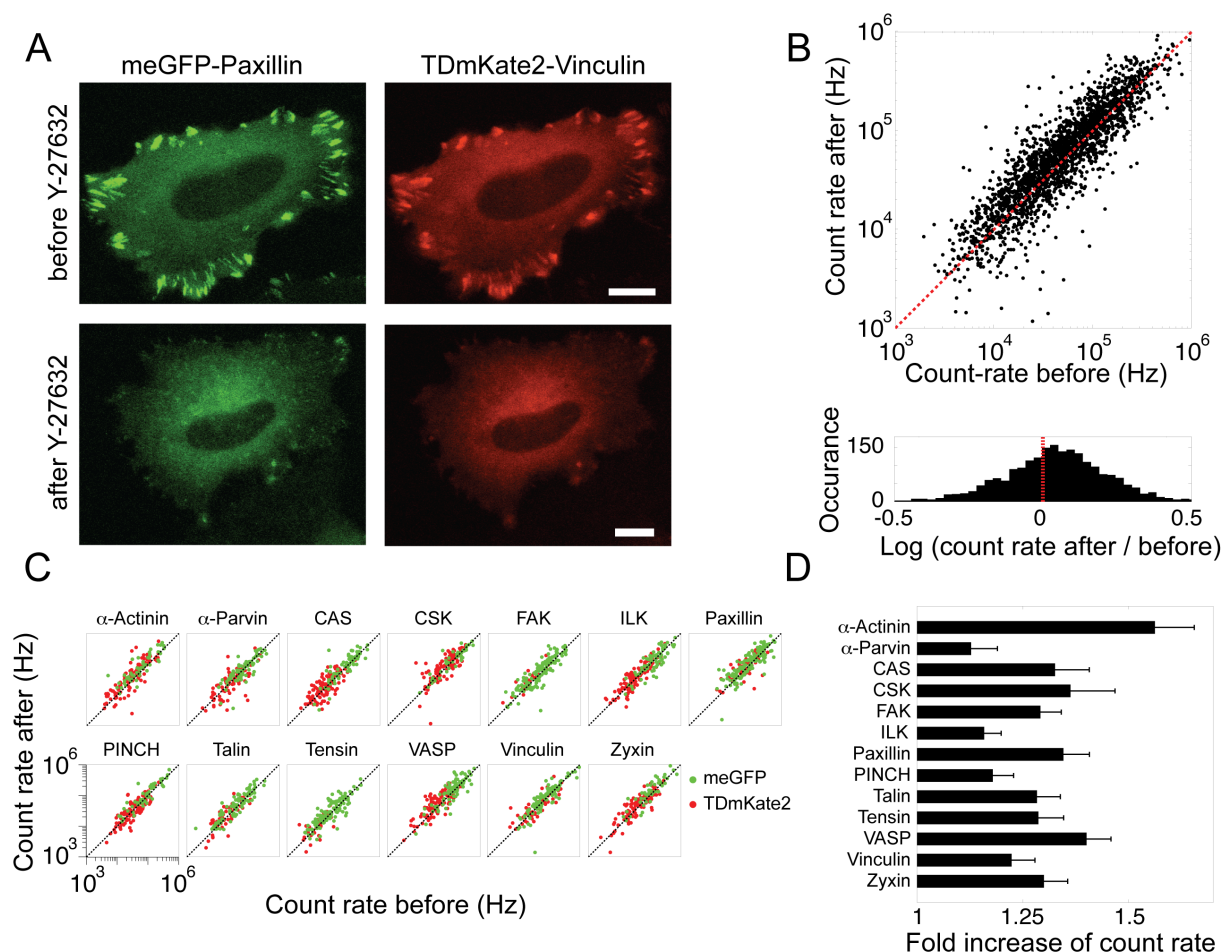
FIGURE 4.5: Inhibition of actomyosin contractility increases protein concentration in the cytosol: A) Fluorescence images of a REF52 cell expressing meGFP-paxillin and TDmKate2-vinculin before and after 30 min incubation with 100 μM Y-27632. Scale bars = 10 μm. B) The count rate, which correlates with the protein concentration, was measured in the same spot before and after addition of Y-27632. The histogram shows a systematic shift towards higher count rate upon addition of the drug. C) Logarithmic scatter plots for the count rates of individual proteins labeled with either meGFP or TDmKate2. D) Relative change in count rate for individual proteins after disruption of focal adhesions. Error bars indicate the median absolute deviation.
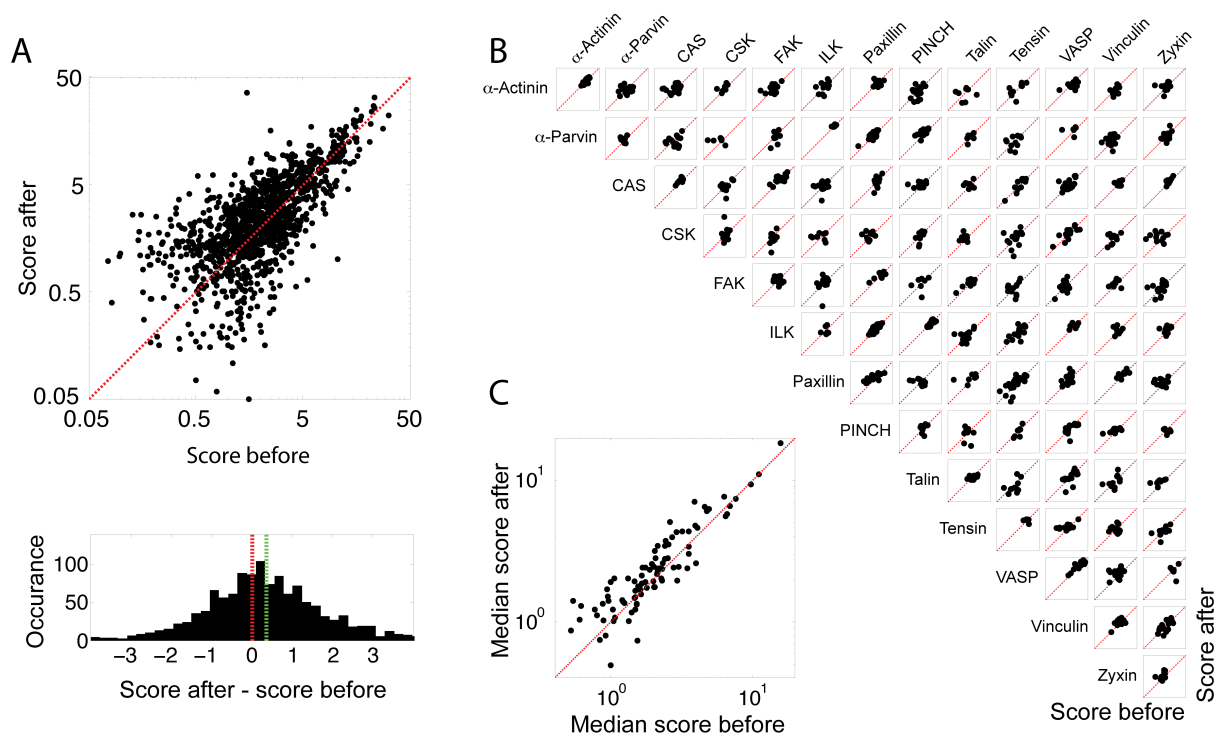
FIGURE 4.6: The effect of focal adhesion disruption on cytosolic associations:
A) Scatter plot of association scores before and after addition of Y-27632 for
individual cells. The histogram shows the difference in score upon treatment.
The median of the population (green line) is slightly different from 0 (red line).
B) Scatter plots of association scores for each protein pair. C) Scatter plot of
the median scores for each pair before and after disruption of focal adhesions.
Most pairs lie on the equality diagonal, indicating no change in association.

4.2 FRAP

To quantify the exchange of proteins between focal adhesions and cytosol and
investigate the dynamics of this process, FRAP was used. For each of the 13
investigated proteins several individual adhesion sites were bleached and their flu-
orescence recovery was recorded as described in 3.4.1. Figure 4.7A shows represen-
tative FRAP measurements for each protein. It can be seen that after bleaching,
fluorescence in the targeted adhesion site is lost almost completely, while surround-
ing sites remain unperturbed. About 9 s after bleaching a partial recovery can be
observed, depending on the dwell time of the protein, and within 180 s most of
the fluorescence has recovered.

Figure 4.7B-C shows average recovery curves for the different proteins as well
as the parameter dwell time $\tau_{1/2}$ and mobile fraction M derived from fitting be-
tween x and y individual recovery curves. All proteins show a fast recovery with a
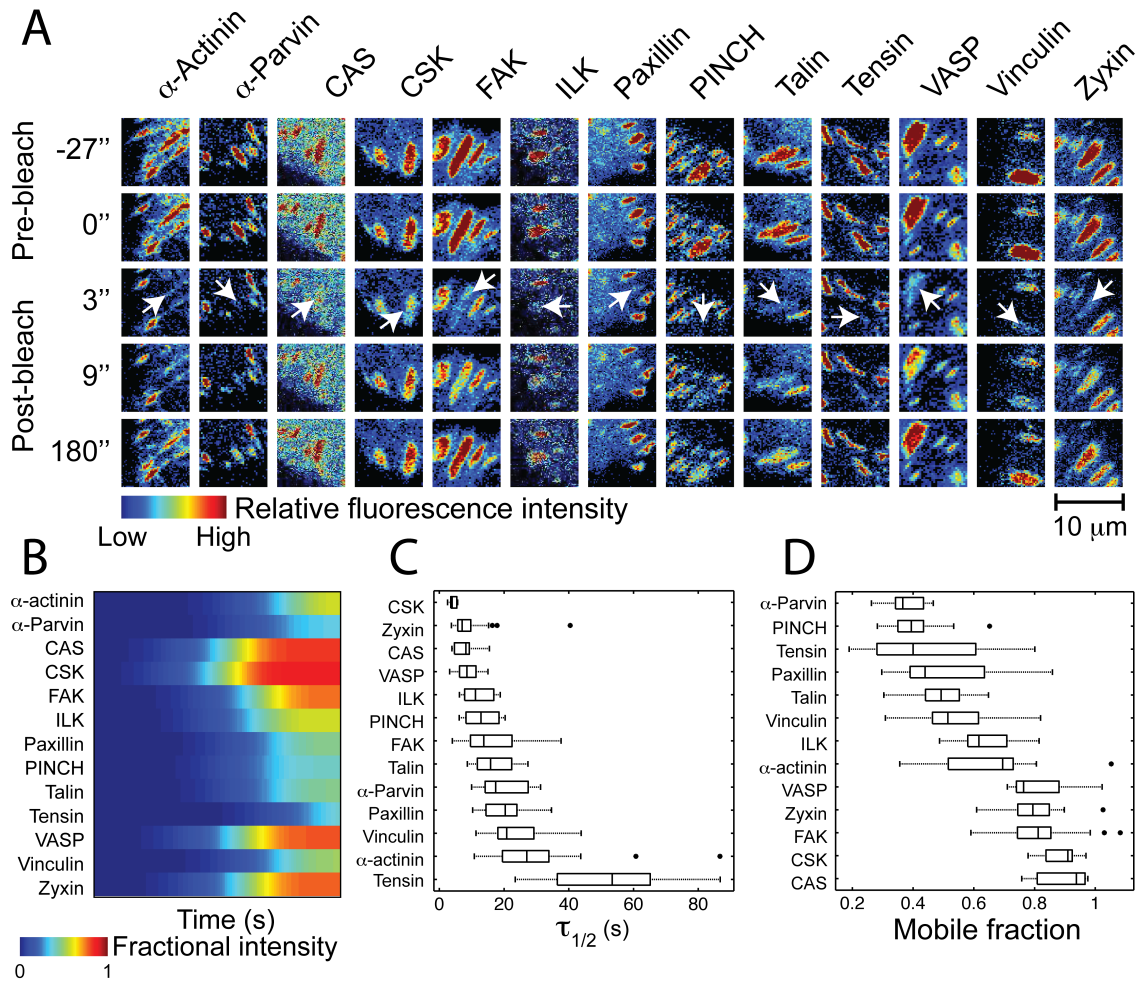
FIGURE 4.7: FRAP experiments: A) Intensity pictures of representative focal adhesions for all 13 proteins at different timepoints during the FRAP experiment. Arrows indicate the specific adhesions that were bleached. Image size = 10·10 μm. B) Average recovery curves for the single proteins. C) Box plot of the recovery half-time $\tau_{1/2}$ derived from a monoexponential fit. D) Box plot of mobile fractions M derived from the fit.

half-time in the seconds range, indicating a rapid exchange of adhesion site-bound material with the cytosol. Still, there is a big variance between the fast exchanging proteins csk and zyxin ($\tau_{1/2} < 10$ s) and tensin ($\tau_{1/2} > 50$ s). The mobile fraction that measures how much of the protein is readily exchanged with the cytosol ranges between 50 and 90%.
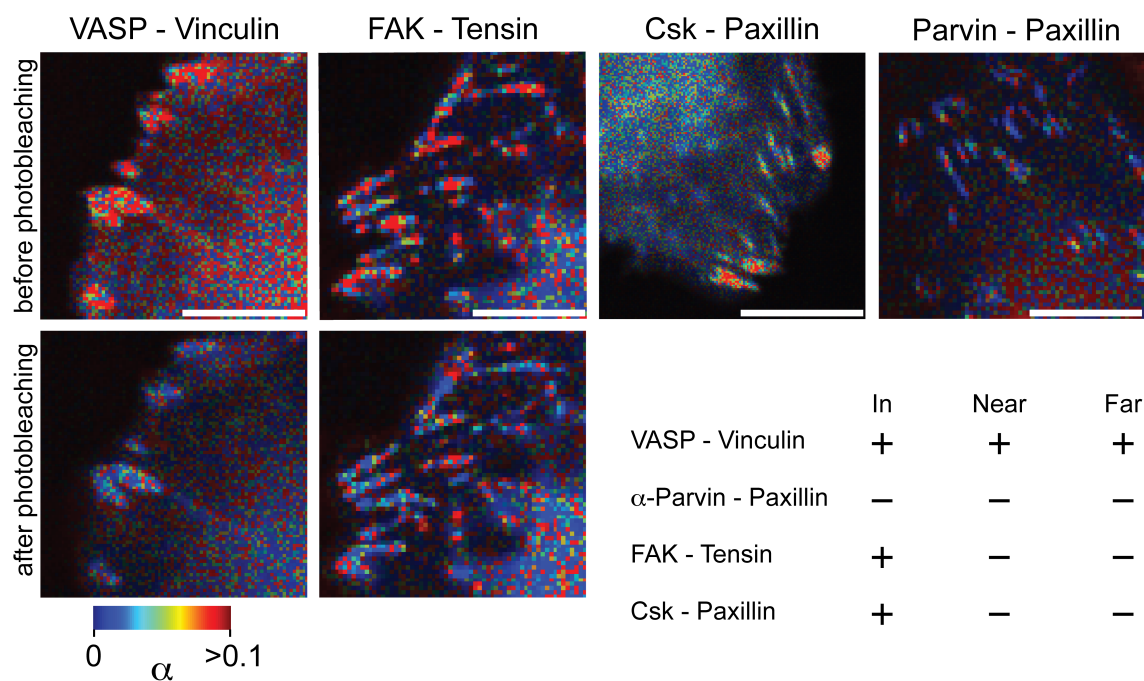
FIGURE 4.8: FLIM results: α-maps of four selected protein pairs. The first name indicates the donor fluorophore tagged protein, the second the acceptor. The lower row shows pictures of the same regions after acceptor photobleaching, where available. Scale bars = 10 μm. The table lists if interaction is visible in focal adhesions and compares it with the FCCS results from section 4.1.2.

4.3 FLIM

FLIM is a complementary method for the measurement of protein-protein interactions and in contrast to FCCS measures direct interactions, not associations. To further characterize the cytosolic interactome of adhesion proteins and the spatial distribution of the interaction strength, selected protein interactions were investigated with FLIM, as described in section 3.4.3. Figure 4.8 shows the α-maps for these protein pairs and as a control for two of them the map after acceptor photobleaching that the change in lifetime was indeed caused by the presence of the acceptor. VASP and vinculin, that were found to be associated in the cytosol by FCCS, are interacting in both, the cytosol and at adhesion sites, with an interacting fraction of around 10%. FAK-tensin and Csk-paxillin did not display association in the cytosol and show FRET exclusively in focal adhesions, indicating that their interaction is limited to these structures. Parvin and Paxillin were found to be non-interacting by both FCCS and FLIM and are not expected to interact, according to the literature.

Figure 4.9 shows the interaction of the four proteins FAK, paxillin, CAS and ILK,
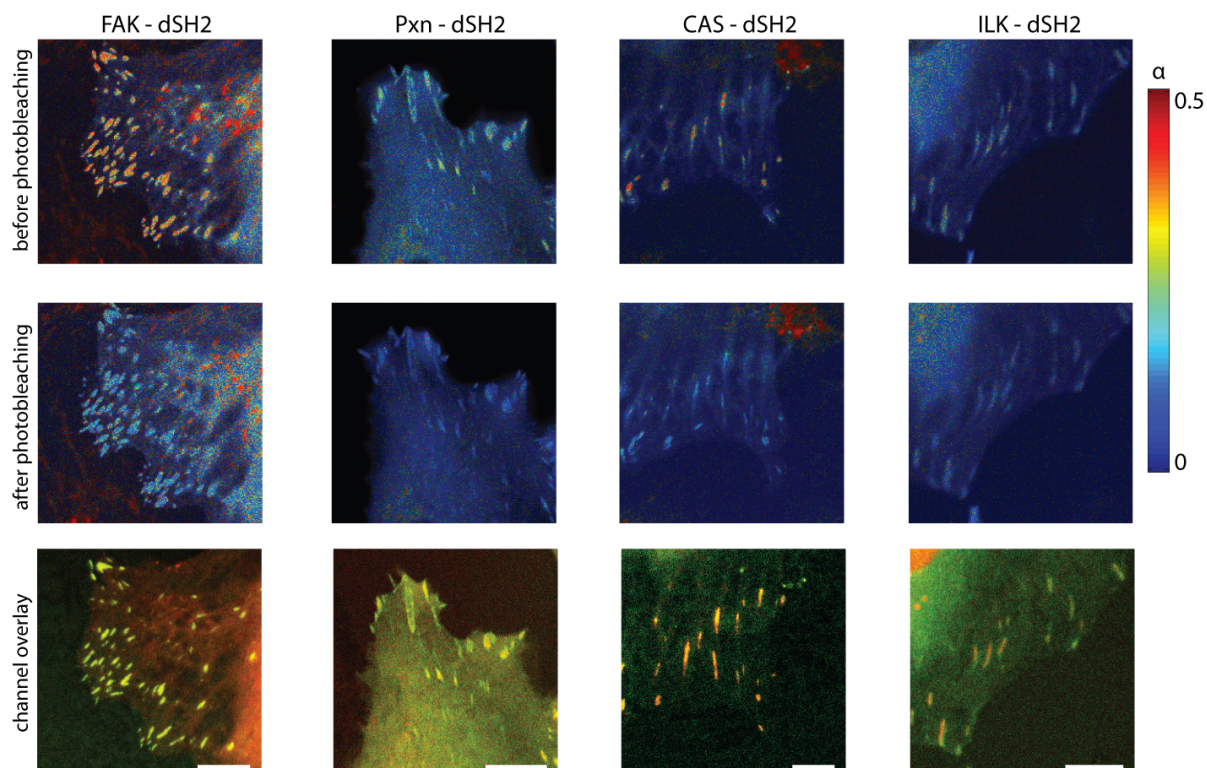
FIGURE 4.9: Map of protein phosphorylation: α-maps of cells expressing the focal adhesion proteins FAK, Paxillin, CAS and ILK as donor and the dSH2-sensor as acceptor before and after acceptor photobleaching. The lower row shows overlays of donor (green) and acceptor (red) channels. Scale bars = 10 μm

labeled with the donor fluorophore, with the double SH2-domain sensor tagged with the acceptor. FAK, paxillin and CAS have well characterized tyrosine phosphorylation sites [Leopoldt et al., 2000, Yu et al., 2004], while ILK has no known tyrosine phosphorylation site and was therefore selected as a control. It can be seen that all three proteins show clear interaction with the SH2-sensor in focal adhesions with an interacting fraction of about 50% donor protein, while there is much less interaction in the cytosol. ILK shows little to no FRET signal. This can be attributed to the proximity of ILK to other phosphorylated proteins in the dense environment of focal adhesions.

4.4   Imaging controls

4.4.1   Immunostaining for CAS, FAK and paxillin phosphorylation

To prove that FAK, paxillin and CAS are indeed phosphorylated in focal adhesions of REF52 cells, immunostaining experiments were conducted with antibodies against characteristic phosphotyrosines, as shown in figure 4.10.
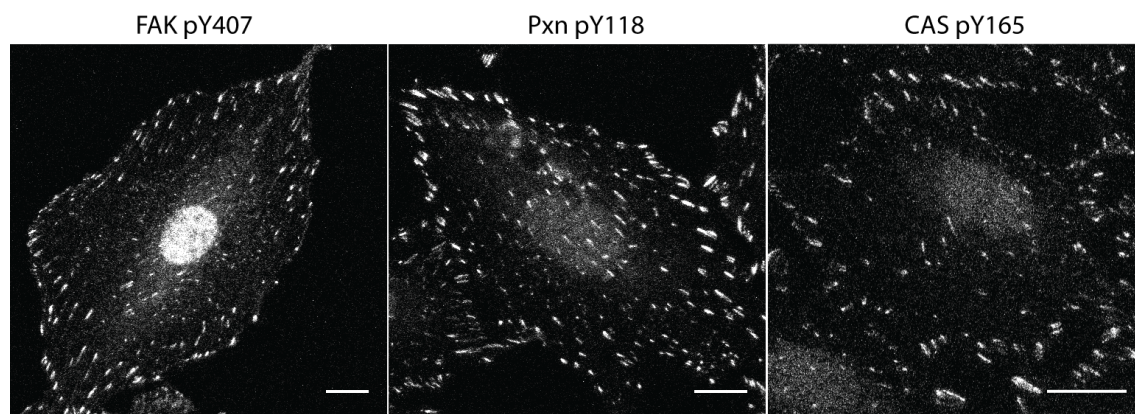
FIGURE 4.10: Immunostaining of REF52 cells with antibodies against FAK pY407, paxillin pY118 and CAS pY165. Scale bars = 15 μm.

4.4.2   Focal adhesion recovery after washout of Y-27632

The effect of the incubation time of Y-27632 on the recovery of focal adhesions was investigated in REF52 cells with a stable expression of YFP-paxillin. By using this cell line, all cell are roughly comparable intensity-wise, which is not the case for transiently transfected cells that differ a lot in their expression level. Cells were treated with 100 μM Y-27632 for 30 min, the minimum time to guarantee complete loss of focal adhesions, and 170 min, after which they were washed twice with imaging medium containing 10% FBS. As a comparison, the FCCS experiments described in section 4.1.5 were conducted after 30-90 min incubation. The cells were fixed at different timepoints during their recovery from Y-27632. Using fixed cells ensured a more accurate control over the time after washout, in comparison to on-stage washing and live cell imaging. Figure 4.11A shows representative cells at selected timepoints. It can be seen that 10 min after washout the cells

incubated for 170 min showed a higher intensity in focal adhesions, while directly before washout the focal adhesion level was equally low. This indicates that the incubation time has an effect on the recovery speed of focal adhesions. The model shown in figure 4.11B states that the disruption of focal adhesions lead to an enrichment of primed complexes in the cytosol that perturb the steady state. This inhomogeneous environment inhibits the recovery of focal adhesions and slows it down. After long incubation times, the cytosolic pool has returned to a steady state. This ensures the rapid assembly of adhesion sites, after actomyosin contractility is restored by washout.

The effect could be reproduced in independent experiments using both fixed and live cells. To test that the difference in recovery speed cannot be attributed to loss in activity of the drug after long incubation times, the supernatant of REF52 cells, treated for 170 min with Y-27632, was collected and applied to a fresh sample. The cells showed a regular response to the drug.
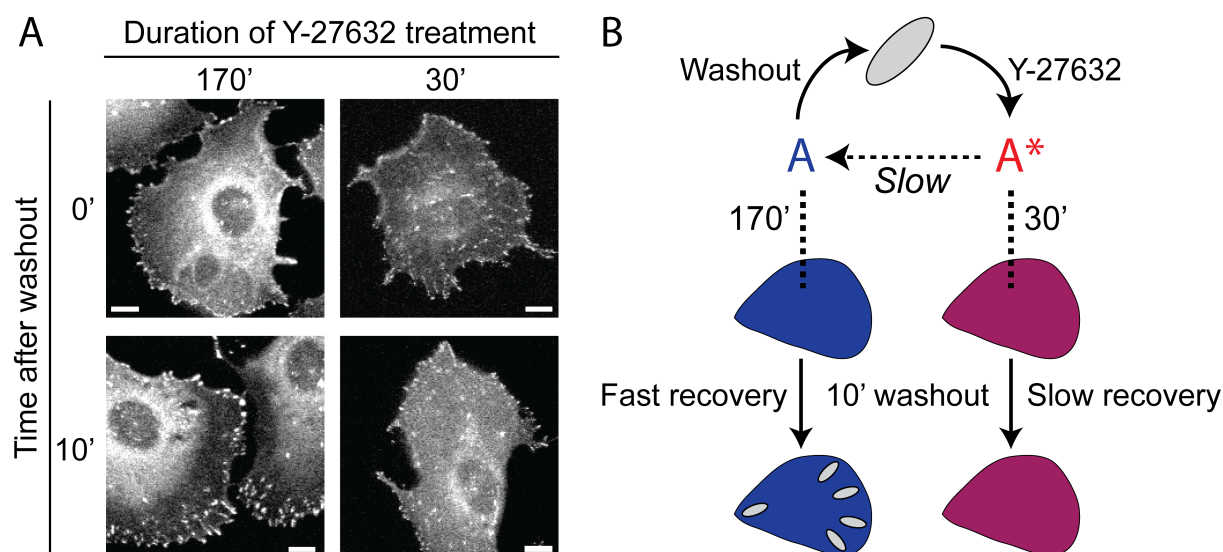
FIGURE 4.11: The incubation time with Y-27632 influences focal adhesion recovery after washout: A) REF52 cells with a stable expression of YFP-paxillin were treated with 100 μM Y-27632 for 30 or 170 minutes and washed twice with imaging medium. After the indicated time they were fixed with paraformaldehyde. Scale bars = 10 μm. B) A model for the effect of the duration of the treatment on focal adhesion recovery: After short incubation the cytosol still contains primed material released from the disassembling adhesion sites that impairs with the recovery of focal adhesions. After longer incubation, the primed building blocks had enough time to relax to steady state, leading to normal focal adhesion recovery.

4.5 Development of new FCCS techniques

4.5.1 A switchable sensor for protein association

Fluorescent proteins are limited in their use in FCCS because of their comparatively low quantum yield and photostability. For the detection of low affinity associations, quantum dots with their superior molecular brightness and possibly multiparametric readout can provide a useful tool. Furthermore, the ability to switch on the binding of the fluorophore to the protein of interest allows internal negative controls in the same conditions than the actual measurement. Therefore, red quantum dots were labeled with FRB as described in section 3.2 and figure 4.12A. To characterize their function, they were mixed with eGFP labeled FKBP *in vitro*, shown in figure 4.12B. Without rapamycin, absolutely no association is observed between QD655-FRB and eGFP-FKBP, while after addition of 5 µM rapamycin clear cross-correlation can be observed. The sensor is also working when injected into REF52 cells expressing the eGFP-FKBP construct, as can be seen in figure 4.12C. Figure 4.12D shows a bait-prey experiment with QD655-FRB injected into REF52-cells expressing eGFP-VASP (prey) and mTagBFP-VASP-FKBP (bait). The pair VASP-VASP was selected because it displayed the strongest association in previous FCCS experiments (section 4.1.2). The blue fluorescent protein in the bait construct is not required for the experiment and serves as an expression control. The curves show auto- and cross-correlation between sensor and prey after addition of rapamycin. Clear association can be observed between them, with around 20% of the proteins being in complex with each other.

During the experiment it was observed that the labeled quantum dots tended to form aggregates that frequently blocked the injection needle, making the reliable high-throughput injection of cells challenging. Additionally, the QDs, while initially being dispersed in the cytosol right after injection, formed clusters after several minutes, making long term experiments inside the same cell difficult. An alternative to microinjection could be electroporation, which would allow the introduction of the sensor into many cells at the same time. However, initial experiments were not successful. Some quantum dots ended up in cells, but were not freely diffusing in the cytosol and may have been the result of unspecific uptake by endocytosis. The QD655-FRB sensor was difficult to store because quantum dots are not suited for long term freezing and the FRB domain lost activity after
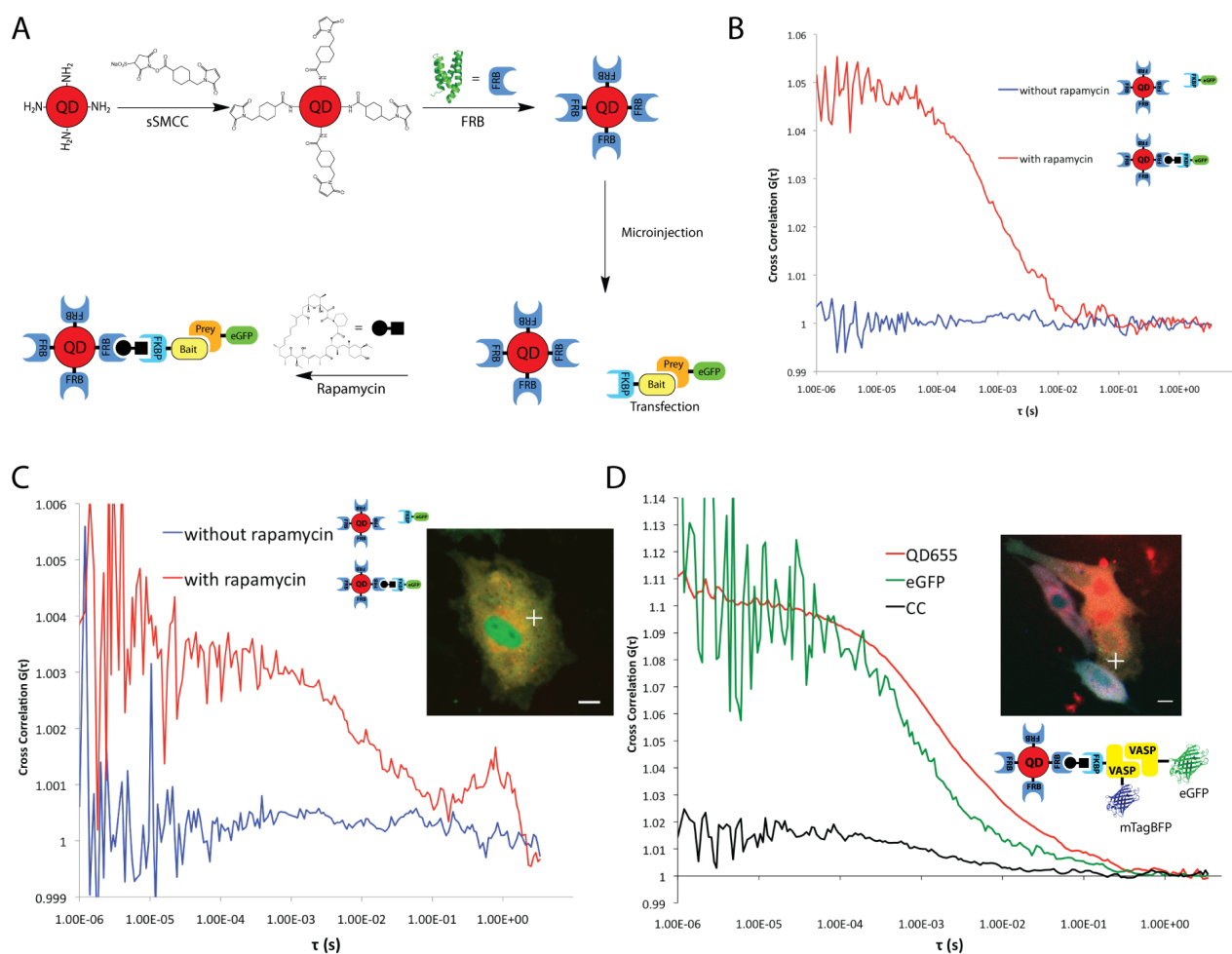
FIGURE 4.12: A switchable quantum dot-based sensor for FCCS: A) Principle of the sensor: An amino-functionalyzed QD655 is activated with the bifacial linker sSMCC and labeled with the heterodimerization domain FRB. This sensor can then be microinjected into cells that express a bait protein linked to the other dimerization domain FKBP and a prey protein labeled with eGFP. Addition of rapamycin brings the proteins together. If bait and prey are associating, cross-correlation between QD655 and eGFP can be measured. B) *In vitro* experiment to test the sensor: The FRB labeled QD655 is mixed with eGFP-FKBP. In blue is the cross-correlation curve between the fluorophores before and in red after the addition of rapamycin. C) REF52 cells expressing eGFP-FKBP were injected with the sensor. The insert shows the injected cell and the point of measurement. Blue and red curves show the cross-correlation before and after addition of 5 μM rapamycin. D) REF52 cells expressing the bait construct mTagBFP-VASP-FKBP and the prey construct eGFP-VASP were injected with the sensor and treated with 5 μM rapamycin. Green and red curves show the autocorrelation of eGFP and QD655 respectively, while the black curve shows the positive cross-correlation between them. The insert shows the injected cell and the point of measurement. Scale bars = 10 μm.

a few weeks when stored at 4°C, so fresh conjugate had to be prepared before expreriments.

4.5.2   Detection of high order associations

So far, all FCCS experiments were performed with two spectrally different fluorophores detected in separate channels. While potential high order associations can be infered from pairwise measurements of the involved proteins, the exact complex composition can only be derived if all components are observable at the same time. For the simultaneous measurement of associations between three fluorophores, FLCS was used as described in section 1.2.5. Figure 4.13A shows the successful unmixing of eGFP and QD525 autocorrelation curves from a mixture containing both fluorophores. For biological applications it is necessary to label proteins of interest with the quantum dot. Therefore QD525 labeled with donkey-anti-mouse antibodies was mixed with REF52 cell extract containing meGFP-ILK. The association between both components was generated by adding a specific mouse-anti-ILK antibody. Figure 4.13B shows cross-correlation curves between meGFP-ILK and QD525 after unmixing by FLCS. Even though the fluorescence of both fluorophores was measured in the same channel, no false cross-correlation was detected, while after addition of the primary antibody clear association was visible. This shows that it is possible to observe the association of two spectrally similar fluorophores. ILK was chosen as the target protein because its complex with α-parvin and PINCH is of particular interest for the detection of high order associations. However, the targeting of α-parvin and PINCH with the combination of primary antibodies and QD-labeled secondary antibodies was not successful, possibly because the affinity of one or both antibodies was too low in the complex environment of the cell extract. Another problem was the emergence of anticorrelation between the two fluorophores separated by lifetime when the count rate of one or both fluorophores was too high. This happened already when the concentration of QD525 exceeded 0.2 particles per confocal volume and limited the application to diluted samples. To test the ability of FLCS to observe three fluorophores at the same time, a mixture of unlabeled eGFP with QD525 and QD655 labeled with streptavidin or biotin was measured *in vitro*. Figure 4.13C+D show the pairwise cross-correlation curves that were obtained simultaneously from this mixture. In case of non-interacting fluorophores, no cross-correlation between any

of them is observed, while the cross-correlation curve of QD525 and QD655 becomes positive when they bind to each other via streptavidin and biotin. The other cross-correlation curves are not influenced and stay negative, proving that no bleedthrough between channels unmixed by spectra or lifetime is happening.
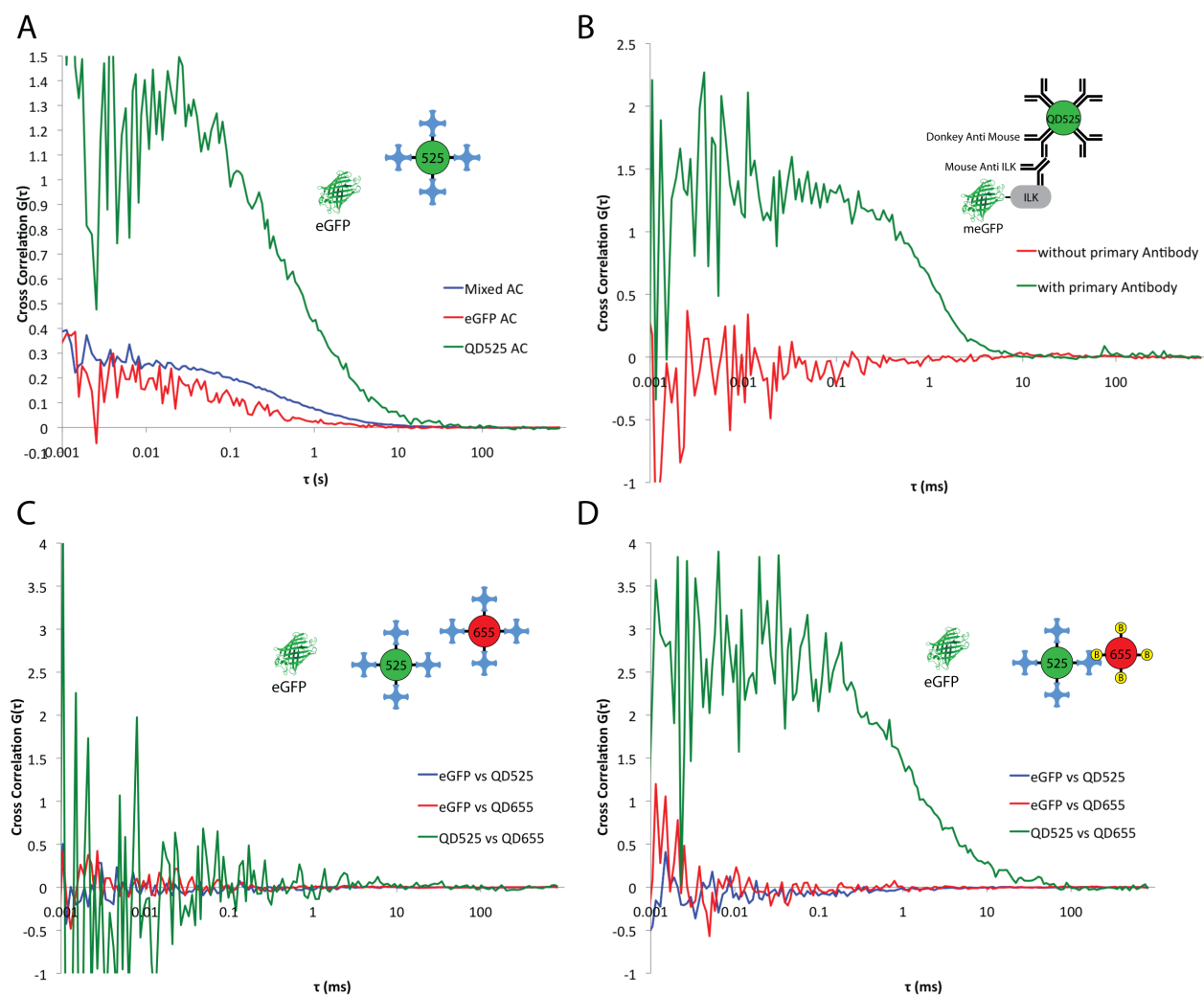
FIGURE 4.13: Results of FLCS experiments: A) An *in vitro* sample with eGFP and QD525, which have a similar emission spectrum, are observed in the same channel. The blue curve shows the autocorrelation of the mixture, while the red and green curves show the autocorrelation of the single species after applying FLCS filters. B) REF52 cell extract containing meGFP-ILK is mixed with an donkey-anti-mouse antibody labeled QD525. After application of FLCS filters, the two resulting channels are cross-correlated. The red curve shows no cross-correlation in the non-interacting state, while after addition of a secondary antibody that links the species cross-correlation can be observed (green curve). C) eGFP, QD525-Streptavidin and QD655-Streptavidin are observed *in vitro* in two spectrally separate channels. No cross-correlation is observed between any of the three species in non-interacting state. D) The same setup as in C, except that QD655-Streptavidin is exchanged against QD655-Biotin, which binds to QD525-Streptavidin. Cross-correlation is observed between the green and red QDs, while the other associations are still negative.

Chapter 5

Discussion

5.1 The cytosolic interactome of cell-matrix adhesion components

5.1.1 Pairwise associations in the cytosol

The study of pairwise associations between 13 key proteins of cell-matrix adhesions, as described in section 4.1.2, reveals a surprisingly high amount of interconnection in the cytosol, with a total of 18 different protein-protein associations found below a p-value of 10^{-3}, meaning high confidence. Figure 5.1 shows the association constants of these pairs and a network of binary associations with a color-coded p-value and association constants represented by edge thickness. Many of these associations are known to be direct or mediated interactions, however, their occurrence in the cytosol was not always investigated previously. The following section describes the cytosolic associations found, sorted by association constant, and the previous knowledge about them, if available.

VASP-VASP
VASP forms a tetramer, mediated by a 45 amino acid long right handed α-helical coiled-coil domain located towards the C-terminus. The interaction is very stable, with a melting point of 120 °C [Kühnel et al., 2004].
α-Parvin-ILK
There is direct and binary [Cabodi et al., 2010] interaction between C-terminus of ILK pseudokinase domain and the second calpoin homology domain of α-parvin
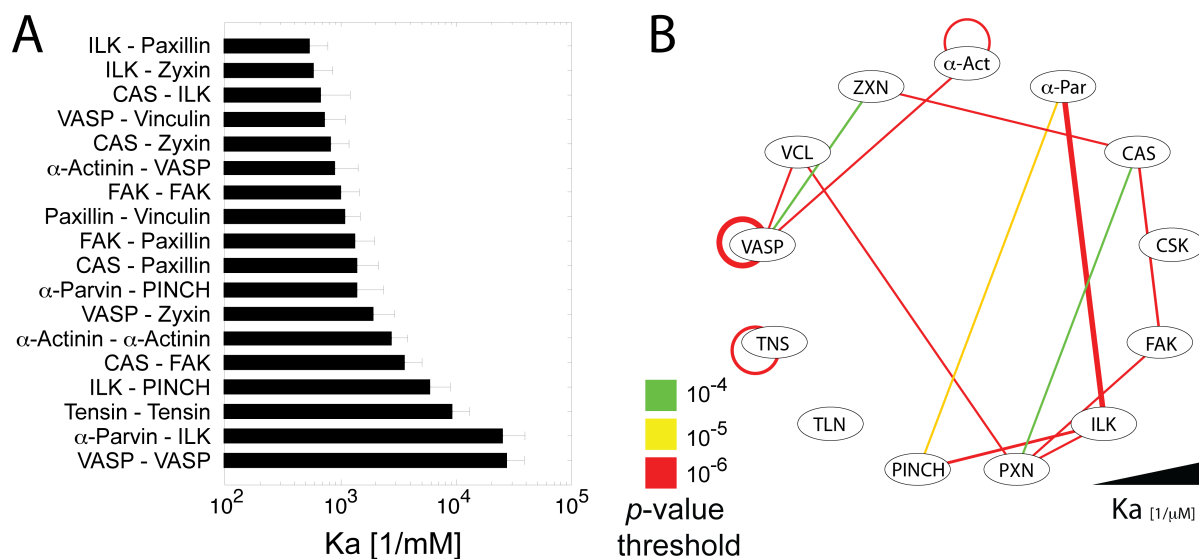
FIGURE 5.1: A) List of median apparent association constants for cytosolic protein pairs found to be associating by FCCS. Error bars indicate the median absolute deviation. B) Association network of all 13 investigated proteins. Pairs with a p-value below 10^{-4} are shown as edges between nodes, with the significance of the association coded as color and the affinity constant coded as thickness of the edge.

[Stiegler et al., 2013]. The formation of the complex is necessary for the recruitment to adhesion sites [Zhang, 2002].

Tensin-Tensin

Tensin potentially forms a homodimer. Interaction via the C-terminus was suggested [Lo et al., 1994a,b], however no strong evidence was found yet. Mediated interaction is unlikely, as no other investigated proteins associate with tensin in the cytosol.

ILK-PINCH

There is a direct, binary [Cabodi et al., 2010] interaction between the five ankyrin repeat domains of ILK and the LIM1 domain of PINCH [Stiegler et al., 2013]. Formation of the complex is necessary for the recruitment to adhesion sites [Zhang, 2002].

CAS-FAK

A proline rich repeat at the C-terminus of FAK, which does not belong to the focal-adhesion-targeting domain, interacts with the SH3 domain of CAS [Harte et al., 1996].

α-Actinin-α-Actinin

Two copies of α-actinin form an antiparallel dimer that is mediated by the rod

domains [Sjöblom et al., 2008].

VASP-Zyxin

Zyxin binds VASP through its N-terminal proline rich domain and a LIM domain. The interaction is necessary for VASP recruitment to focal adhesion and changes actin binding properties of VASP [Grange et al., 2013].

α-Parvin-PINCH

There is no direct interaction known, the association is probably mediated by ILK. However, it was suggested that low affinity interaction, between parvin and PINCH or the ILK subdomains they are bound to, is possible [Stiegler et al., 2013].

CAS-Paxillin

No evidence for direct interaction was found, however, association can be mediated by the Crk SH2 domains [Angers-Loustau et al., 1999, Zaidel-Bar et al., 2005]. Additionally, the association could be mediated by FAK, as both proteins bind to FAK on non-overlapping sites.

FAK-Paxillin

There is direct interaction between the C-terminal focal-adhesion-targeting (FAT) domain of FAK [Cooley et al., 2000, Hildebrand et al., 1995, Scheswohl et al., 2008] and paxillin LD2 (Amino acids 143-168) and LD3 domains [Brown et al., 1996]. The interaction is not necessary for focal adhesion targeting of both proteins.

Paxillin-Vinculin

There is direct interaction between the paxillin LD2 domain [Brown et al., 1996] and Vinculin amino acids 978-1000 [Wood et al., 1994].

FAK-FAK

No stable dimerization of FAK was reported in the literature, however, FAK is known to autophosphorylate [Schaller et al., 1994], so it could potentially bind and phosphorylate other copies of FAK.

α-Actinin-VASP

There was no indication of direct interaction in the literature. LPP is supposed to link VASP and α-actinin [Hansen and Beckerle, 2008].

CAS-Zyxin

Direct interaction was reported between the Zyxin LIM domain and the CAS SH2 domain binding region [Yi et al., 2002].

VASP-Vinculin

VASP binds to vinculin with its N-terminal EVH1 domain [Harbeck et al., 2000]. The interaction is independent of VASP phosphorylation.

CAS-ILK and **ILK-Zyxin**

No indication for direct interaction was found in the literature for both protein pairs. They could be newly identified interactions or mediated interactions, e.g. by paxillin in case of CAS-ILK.

Paxillin-ILK

There is a direct interaction between the paxillin LD domain and the ILK pseudokinase domain (amino acids 386 and 387) [Moik et al., 2013, Nikolopoulos and Turner, 2001]. Whether paxillin binding is required for ILK localization to adhesion sites is disputed.

Other known associations between focal adhesion proteins appear not to occur in the cytosol, notably the well characterized interactions between talin and vinculin [Izard et al., 2004] and FAK and talin [Chen et al., 1995, Zheng et al., 1998]. This indicates that their interaction is limited to the focal adhesion, possibly as part of their regulation, while being absent in other parts of the cell. A dimerization of talin was also not observed with high significance. This dimerization is mediated by the C-terminal helix 2496-2529 [Gingras et al., 2008] of talin and required for focal adhesion targeting and actin binding [Smith and McCann, 2007]. This confirms the model that talin is in a closed, autoinhibited conformation within the cytosol and opens up when recruited to early adhesion, possibly by contact with phosphatidylinositol 4,5-bisphosphate (PIP2), where it reveals its binding sites for vinculin and FAK [Wang, 2012]. The quantitative approach in this work shows that almost 100% of cytosolic talin is inactive.

Tensin is known to bind directly to CAS with its SH2 domain in a phosphorylation dependent manner [Qian et al., 2009]. The absence of this interaction in the cytosol indicates lack of tyrosine phosphorylation of CAS.

Another absent interaction is the one between α-actinin and zyxin [Crawford et al., 1992, Li and Trueb, 2001, Reinhard et al., 1999], that is important for the localization of zyxin fo focal adhesions.

The interaction of Csk with paxillin [Rathore et al., 2007, Sabe et al., 1994] does not occur in the cytosol with FCCS, but the FLIM analysis in section 4.3 reveals that the proteins are interacting in focal adhesions with around 10% of the paxillin present bound to csk. Csk binds to phosphorylated paxillin, as well as FAK, with its SH2 domain [Bergman et al., 1995]. This shows how the two complementary methods FCCS and FLIM detect highly localized interactions.

The network of pairwise cytosolic associations in figure 5.1B gives insight into possible complexes and interaction dependencies between the investigated proteins. By breaking down the whole network into subnetworks, potential higher order complexes and mutual exclusive interactions can be derived, as shown in figure 5.2. This makes use of the fact that FCCS does not only measure direct interactions, but also associations mediated by another protein. The two motifs identified are i) ternary complexes, where all three components associate with each other and ii) mutual exclusive associations, where two proteins both associate with a third one, but not with each other. The two ternary complexes found in the analysis in this work are the well characterized ILK-PINCH-α-parvin-complex, that is mediated by ILK [Stiegler et al., 2013] and the CAS-FAK-paxillin-complex. This potentially trimeric complex was not yet reported in the literature. While the interactions of FAK with CAS and paxillin are well characterized, it was not clear if these interactions are mutually exclusive. The binding sites for both proteins on FAK are both C-terminal, but do not overlap. Therefore it is possible that both proteins bind to the same copy of FAK at the same time. The fact that this is happening already in the cytosol has implications for focal adhesion signaling, since binding do FAK is required for the Src dependent phosphorylation of CAS [Provenzano and Keely, 2009] and paxillin [Mitra and Schlaepfer, 2006] and activation of their signaling acitivity [Mitra et al., 2005, Schlaepfer et al., 1999]. However, with these data it is still possible that the associations of CAS, FAK and paxillin do not happen at the same time, but are mutually exlusive. To investigate this, techniques that image 3 or more proteins at once are required. It should be noted that all complexes including the proteins α-actinin, FAK, tensin and VASP are, by definition, also potential higher order complexes, as they form di- or multimers.

The discovered potential mutual exclusive interactions are displayed on the right side of figure 5.2. They include the association of paxillin with FAK and vinculin, that both bind to the LD2 domain of paxillin [Brown et al., 1996] and the binding of CAS and VASP to the LIM domain of zyxin. Others, like the association of VASP with α-actinin, vinculin and zyxin, were not yet reported in the literature. However, it is possible that the FCCS approach in this work might not be sensitive enough to capture very weak associations that are mediated by low affinity binding to a third protein, especially if this protein is not overexpressed.
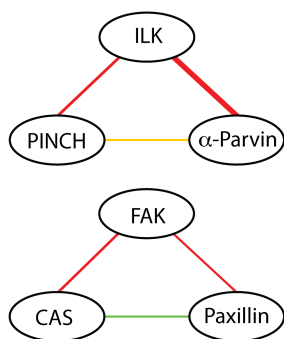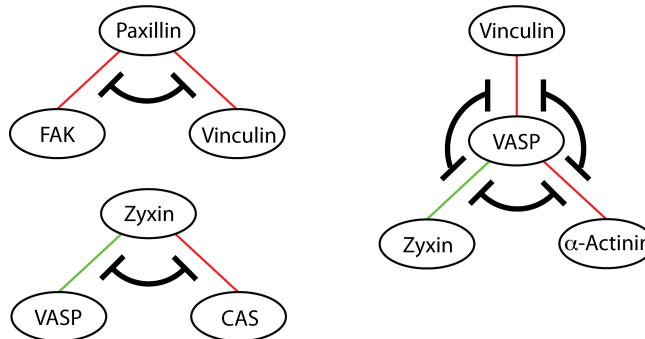
FIGURE 5.2: Deduction of high order interactions: The network of pairwise associations shown in figure 5.1 reveals possible ternary protein complexes and mutually exclusive interactions.

5.1.2 The diversity of cytosolic building blocks

The measurement of pairwise cytosolic associations by FCCS already revealed a high interconnectivity between components of adhesion sites. The question that arises is, whether the building blocks of focal adhesions are homogeneous in the cytosol or rather composed of many different types. In the former case, proteins that associate in the cytosol would always enter and leave adhesion sites together, while in the second case one protein may be in different kinds of complexes. To test these hypotheses, as illustrated in figure 5.3A, the aforementioned FCCS measurements were combined with FRAP measurements of whole adhesion sites, as explained in section 4.2. In figure 5.3B, recovery half time $\tau_{1/2}$ and mobile fraction M of all 13 proteins are plotted against each other. If two proteins enter focal adhesions mostly as a complex, they are expected to share similar $\tau_{1/2}$ and M and therefore a short Euclidian distance in the plot. This co-dynamics distance of two proteins is compared with the association score of the respective pair in figure 5.3C. Protein pairs in the upper left corner of this plot show both a similar recovery behavior and association in the cytosol. This is the case for the α-parvin-ILK-PINCH complex where, interestingly, the indirectly binding proteins α-parvin and PINCH display a shorter co-dynamics distance than their respective pairings with ILK. This indicates that both protein always enter focal adhesions in complex with ILK, while ILK is also present in other building blocks. Other candidates for building blocks that follow a confined assembly path are VASP-zyxin, paxillin-vinculin and CAS-FAK. α-actinin-VASP, though being one of the highest affinity complexes in the cytosol, show no exceptionally short co-dynamics

distance, suggesting that α-actinin is not always present when VASP enters adhesion sites, in contrast to zyxin. This in in agreement with literature sources that report that zyxin recruits VASP to focal adhesions [Grange et al., 2013]. In figure 5.3D the association score is plotted against the difference in cytosolic diffusion speed τ_D of two proteins, determined by FCCS in section 4.1.1. Again, the α-parvin-ILK-PINCH complex displays similar behavior, also, the aforementioned pairs paxillin-vinculin and CAS-FAK show a similar diffusion speed. All pairs including VASP have a high difference in τ_D, resulting from the exceptionally slow diffusion of VASP. This might be caused by VASP binding to static or slow moving structures like actin filaments, however, other actin-binders like zyxin don't show such a slow diffusion.

Overall there is no correlation between the parameters association strength, diffusion speed, recovery half time and mobile fraction. This leads to the conclusion that, with the exception of a few protein pairs, the composition of cytosolic building blocks are highly diverse and most proteins can enter adhesion sites as part of different complexes.

5.2 Symmetric and asymmetric exchange of building blocks between adhesion sites and cytosol

The analysis of the composition of cytosolic building blocks and their recovery to focal adhesions after photobleaching proofs that there is a constant and rapid exchange of material between the cytosol and adhesion sites in steady state. As discussed in the introduction, a fundamental question for understanding the regulation of focal adhesion assembly and maintenance is, whether they exchange material symmetrically or asymmetrically. Asymmetric material exchange would lead to a gradient of primed building blocks around adhesion sites, this would allow communication and feedback between focal adhesion. By using the high spatial resolution of FCCS, the association between proteins was quantified near and far from focal adhesions, as described in section 4.1.3. No significant change in association score was detected, neither for all measurements batched together (Figure 5.4A), nor for individual pairs. FLIM experiments with selected pairs show
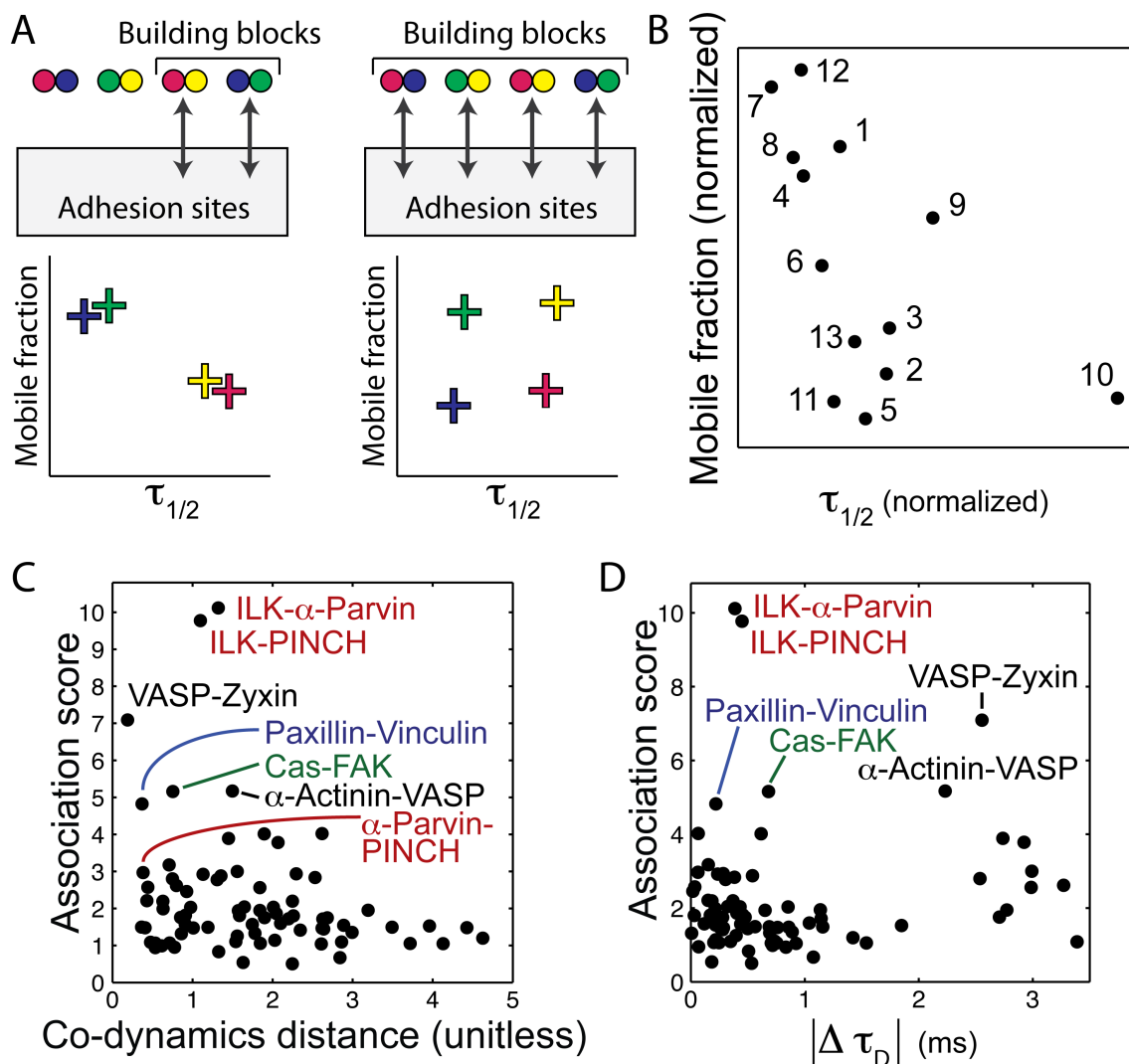
FIGURE 5.3: Composition of cytosolic building blocks: A) Two possible models for the building block composition. Proteins could exchange between adhesion sites and cytosol only in specific complexes, leading to a high correlation between the FRAP parameters of these proteins. They could also be able to enter and leave as part of diverse complexes, resulting in a low correlation between the FRAP parameters. B) The normalized mobile fraction is plotted against the normalized recovery half time that were derived from FRAP measurements. Numbers correspond to the proteins 1, α-actinin; 2, α-parvin; 3, CAS; 4, Csk; 5, FAK; 6, ILK, 7, paxillin; 8, PINCH; 9, talin; 10, tensin; 11, VASP; 12, vinculin and 13, zyxin C) The Euclidian distance between two proteins in D is called the co-dynamics distance. The association score of these proteins measured by FCCS is plotted against this co-dynamics distance. D) The association score of each protein pair is plotted against the difference in dwell time τ_D, that was measured by FCCS.

that there is, in fact, a difference in interaction between cytosolic and focal adhesion bound proteins for some pairs, but no gradient was detected. This strongly indicates that there is no distance dependency in the composition of protein complexes and all proteins leave adhesion sites with the same interaction partners as they entered.

Other than protein-protein interactions, the phosphorylation state is a major property of focal adhesion building blocks, as many important functions are regulated by transient protein phosphorylation. Therefore, the tyrosine phosphorylation of the phosphoproteins CAS, FAK and paxillin was measured with FCCS and FLIM, using the double SH2-domain sensor in sections 4.1.4 and 4.3. The general localization of the sensor indicates an enrichment of phosphotyrosine in focal adhesions and the FLIM results show strong phosphorylation of CAS, FAK and paxillin in focal adhesions. However, outside of adhesion sites the interaction between the proteins and the dSH2 sensor is much lower, which is supported by the relatively low association detected by FCCS. The inhibition of tyrosine phosphatases by vanadate increases the association with the sensor, showing that the novel application of FCCS to detect phosphorylation was successful. Both FLIM and FCCS show no phosphorylation gradient around adhesion sites. This shows that the tyrosine phosphorylation level of CAS, FAK and paxillin is lower in the cytosol than in focal adhesions, but homogeneously distributed within the cytosol.

The lack of a gradient around adhesion sites for both complex composition and protein phosphorylation supports the model of symmetric material exchange that is shown schematically in figure 5.4B. Certain protein interactions and modifications are exclusive to adhesion sites and get switched off before or during the protein leaves the site. This ensures that the cytosolic pool of building blocks for focal adhesions is uniform and standardized and prevents cross-talk.

The symmetric exchange model is true for focal adhesions in steady-state. During the experiments shown in section 4.1.5 the cells were perturbed by the inhibition of actomyosin contractility and therefore the disassembly of force-dependent focal adhesions. Analysis of the response of protein association to this perturbation for all investigated protein pairs reveals a low but significant increase in association (Figure 5.4A). This means that overall the complex concentration increases in cells with disassembling adhesion sites, indicating a release of big complexes that dissociate only slowly. This asymmetric disassembly happens on top of the steady-state symmetric material exchange which together leads to an inhomogeneous pool of building blocks. The corresponding model is presented in figure 5.4B. The Y-27632
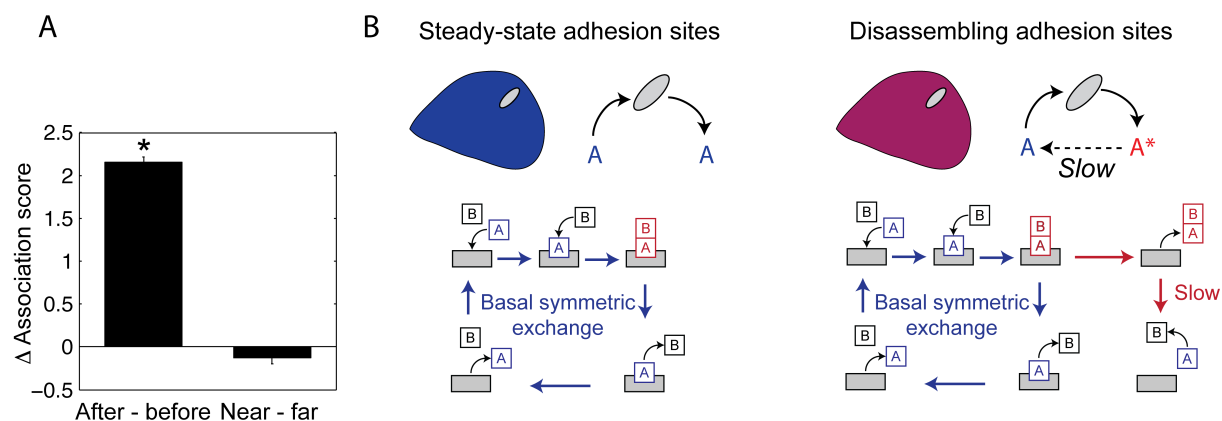
FIGURE 5.4: Exchange mode of focal adhesions and cytosol: A) Bar plot showing the mean effect of focal adhesion disruption by Y-27632 and the distance to focal adhesions on the difference in association score for all paired measurements batched together, as shown in figures 4.6 and 4.3. Error bars are standard error of the mean. The disruption of focal adhesions cause a significant increase in cytosolic association, according to Wilcoxon signed rank test, while the distance to adhesion sites does not have a significant influence. According to Wilcoxon signed rank test, the p-values for the hypothesis that the score changes are 0.0003155 (after-before, highly significant) and 0.3634801 (near-far, not significant). B) Models of exchange of material between adhesion sites and cytosol for the steady state and for disassembling focal adhesions. In steady state the exchange is symmetric and protein complexes leave adhesion sites in the same state as they entered. Disassembling adhesion sites additionally release material in bigger complexes that slowly fall apart in the cytosol.

washout experiments in section 4.4.2 suggest that the presence of asymmetrically released building blocks impairs the assembly of focal adhesions and that the large complexes dissociate on a fairly large time scale.

5.3 Novel FCCS techniques allow the measurement of high order associations

The discovery of possible ternary cytosolic complexes in the cytosol underlines the necessity for new approaches to detect higher order complexes while retaining the high resolution of light microscopy. Additionally, regular FCCS with two fluorescent proteins reaches its limit when dealing with low affinity complexes in a noisy environment. The analysis of pairwise associations in section 4.1.2, while clearly identifying strong interactors, shows some protein pairs with scores in the

medium range where low affinity association could not be definitely proven or excluded. A technique with higher sensitivity would allow the investigation of these candidates. While not well suited for the screening of many different protein combinations, due to the difficulty of specific labeling and microinjection, quantum dot based probes with their superior fluorescence properties could be used for selected protein-protein combinations, previously identified by purely transfection based methods. The experiments discussed in section 4.5.1 show that the switchable sensor works well *in vitro*. It is also feasible to inject it into cells and measure protein associations there. The proof-of-principle experiment using VASP as bait and prey was successful, however, the obtained cross-correlation signal was less clear than that of regular fluorescent protein FCCS. On top of that, the associating fraction was likely underestimated because endogenous proteins and unlabeled quantum dots interfere with the detection of the complex. This shows that, while working in principle, the sensor is not yet suited for biological applications and requires further optimization. Especially the stability of the sensor needs to be improved, both in cells and for long term storage.

FLCS was successfully used to observe three fluorophores at the same time and separate them by spectrum or lifetime, as shown in section 4.5.2. This opens the door for high order correlation spectroscopy without the need for complex instrumental setup with three detection channels. However, in this work the application was limited to *in vitro* experiments with artificial probes. The selective targeting of quantum dots to proteins of interest with antibodies was only achieved for ILK, but not yet for other proteins. The use of this targeting strategy has the drawbacks that additional binding steps of the primary and secondary antibodies reduce the effective affinity and, even more importantly, may lead to artificial crosslinking between proteins. The use of cell extract as an alternative for the challenging microinjection proved to be well suited for proof-of-principle experiments, but for the investigation of possibly regulated protein associations, live cell experiments are a necessity.

5.4 Conclusions and outlook

The investigation of the molecular complexity of focal adhesions from the perspective of the cytosolic pool is an approach that was long rather neglected in the

field. This work reveals a high level of interconnectivity in the cytosolic protein-protein associations, in the absence of big multi-protein complexes. Many of these interactions are also known to occur in focal adhesions, while other important interactions were strikingly absent in the cytosol. CAS-FAK-paxillin was indentified as a potential ternary complex and the associations between CAS and ILK and ILK and zyxin were newly discovered. Several interactions are mutually exclusive, confining the potential size of cytosolic building blocks. The combination of FRAP and FCCS reveals a rapid exchange of material between focal adhesions and the cytosol. Most proteins are able to enter adhesion sites in more than one complex and cytosolic complexes are highly diverse.

The 13 proteins investigated in this work cover many important key players in focal adhesions and contain examples for all cytosolic protein classes. It might still give additional insight into the cytosolic adhesion to expand the matrix by other major scaffold proteins, like crk and filamin. Proteins of particular interest are effectors downstream of focal adhesions. For example, the rho-GEF pix is supposed to regulate the reorganization of the cytoskeleton by being recruited to focal adhesions [Filipenko et al., 2005]. Investigating if its association with ILK and other focal adhesion scaffold proteins exists already in the cytosol might help understand how the spatial regulation of rho family proteins is achieved.

This work determined how material is exchanged between focal adhesions and the cytosol. Protein complexes are exchanged in a symmetric way where proteins leave adhesion sites in the same state as they entered. This ensures a standardized cytosolic pool and prevents cross talk between adhesion sites and unspecific aggregation. Also, the tyrosine phosphorylation, while much higher in adhesions sites than in the surrounding cytosol, behaves symmetrically, as proteins get dephosphorylated before or during leaving the adhesion sites.

So far, only the tyrosine phosphorylation of CAS, FAK and paxillin was investigated. This can be expanded for other proteins with known posttranslational modifications. Future experiments need to investigate the consequences of this asymmetric disassembly and what implications it has on cells that rapidly disassemble their focal adhesions in a controlled manner, e.g. at the trailing edge of migrating cells. Additionally, other kinds of perturbations can be used to further investigate the relationship between mechanisms to control focal adhesion behavior and the cytosolic pool. Nocodazole can be used to induce the reversible disassembly of focal adhesions by altering the dynamics of microtubules [Chang

et al., 2008, Ezratty et al., 2005], while PDGF can stimulate the cell motility and alter the phosphorylation pattern of focal adhesions [Higuchi et al., 2013, Hunger-Glaser et al., 2004].

The development of a novel method to measure high order associations between proteins was partly successful. In proof-of-principle experiments various sensors were used for switchable recruitment of proteins *in vivo* and for the simultaneous measurement of three associations, separated by spectrum and lifetime. However, the method is not yet able to measure associations between proteins in a cellular environment with the same precision as conventional FCCS with fluorescent proteins. In future experiments the protein targeting, the introduction into cells and the stability of the sensor needs to be optimized. Additionally, a monovalent organic fluorophore or even a fluorescent protein with a high lifetime would overcome the drawbacks of quantum dots and make the direct labeling of proteins possible.

Appendix A

Tables

The following tables show the number of valid measurements, the obtained average association constant, the association score and the p-value for each protein pair in REF52 and NIH3T3 cell lines. The total numbers of measurements are 1914 and 764, respectively. n is the number of measurements for the indicated pair that were found valid by the criteria described in chapter 3.4.2. The median association constant in 1/mM show the apparent association strength, not taking into account the unlabeled endogenous protein. It is only meaningful for measurements with high scores. The median association score is a measure for the significance of the cross-correlation amplitude. The p-value is the result of Fishers exact test, with the hypothesis that the score of the indicated protein pair is bigger than that of a negative control. Low p-value indicate significant association.

Table A.4 lists the dwell times τ_D in s for all proteins as described in chapter 4.1.1 and the diffusion coefficients D in cm^2/s.

Table A.5 lists all PCR primers that were used to create the plasmids used in this work, as described in chapter 2.2.

TABLE A.1: Pairwise association in REF52 cells

Protein pair	n (REF52)	Ka (REF52)	score (REF52)	p-value (REF52)
FAK - Paxillin	60	1.3352731	4.0129753	8.5942602261971603E-14
FAK - Vinculin	23	0.35912998	1.2544735	0.338258240669562
Paxillin - Vinculin	30	1.0832447	4.8237497	1.4121665964417801E-9
FAK - VASP	28	0.32181655	1.0872029	0.85191803673802102
Paxillin - VASP	30	0.36500375	1.9468359	9.7372070388263097E-4
VASP - Vinculin	40	0.72448591	2.9997601	2.09252886984689E-8
α-parvin - FAK	20	0.464982	1.7207366	0.114120216743684
α-parvin - Paxillin	39	0.41728534	2.209968	4.8260803774390998E-4
α-parvin - Vinculin	28	0.25469087	0.95104895	0.97062720715361095
α-parvin - VASP	21	0.64509017	3.7821471	9.2011550769844699E-3
FAK - ILK	29	0.40152132	2.0307671	4.3798987488777899E-4
ILK - Paxillin	40	0.54150449	2.9217802	1.9918870174786299E-7
ILK - Vinculin	19	0.23698249	1.8162966	0.170657547333632
ILK - VASP	17	0.6643682	2.7991446	6.9549678614588199E-4
α-parvin - ILK	28	24.962342	10.11698	1.83244723690646E-10
CSK - FAK	18	0.26295876	1.5749207	3.7761138858996401E-2
CSK - Paxillin	46	0.22732689	1.4440869	0.19460208537345
CSK - Vinculin	17	0.23885607	1.4146571	0.51238920144322997
CSK - VASP	27	0.29596661	2.6187061	2.87562991869522E-4
α-parvin - CSK	14	0.42306423	1.0954024	0.61037988122611597
CSK - ILK	20	0.28839712	1.1048168	0.59480729600971305
FAK - Zyxin	27	0.3107148	0.94202352	0.95913721264196306
Paxillin - Zyxin	20	0.23254521	1.1410442	0.885879783256316
Vinculin - Zyxin	19	0.41288799	1.5671561	0.170657547333632
VASP - Zyxin	13	1.8944548	7.0917473	7.2916513011586395E-5
α-parvin - Zyxin	15	0.25555495	2.1971111	2.5835441705845002E-3
ILK - Zyxin	17	0.57822213	2.456384	6.6945811910010594E-5
CSK - Zyxin	16	0.16705365	0.9890843	0.78659138044413601
α-actinin - FAK	19	0.28781622	1.4917946	0.170657547333632
α-actinin - Paxillin	19	0.3874253	2.8780424	1.7676161430524301E-4
α-actinin - Vinculin	35	0.2755488	1.474514	0.23512541790914199
α-actinin - VASP	26	0.88213664	5.1710529	8.2794364036803101E-7
α-actinin - α-parvin	18	0.3204891	1.3276298	0.40088638845415703
α-actinin - ILK	20	0.34854199	2.7759238	6.1688275984238402E-4
α-actinin - CSK	9	0.33546028	1.5950881	0.253762725803700601
α-actinin - Zyxin	33	0.57674728	2.0411365	2.7179469297772901E-2
FAK - Tensin	28	0.39411565	1.0545558	0.85191803673802102
Paxillin - Tensin	36	0.53130792	1.0408768	0.90728396315193605
Tensin - Vinculin	18	0.93112563	1.7173419	3.7761138858996401E-2
Tensin - VASP	15	0.91740943	1.5264389	0.14373315430384001
α-parvin - Tensin	17	0.20848703	0.67079955	0.98320691540386196
ILK - Tensin	24	0.56405097	1.4929922	0.41209686992910999
CSK - Tensin	18	0.53305385	1.1979617	0.774730542003633
Tensin-Zyxin	17	0.5098469	1.0500695	0.85641826521182396
α-actinin - Tensin	18	0.76112204	2.835187	0.225269457996367

TABLE A.2: Pairwise association in REF52 cells continued

Protein pair	n (REF52)	Ka (REF52)	score (REF52)	p-value (REF52)
FAK - PINCH	9	0.36415369	1.864921	0.25376272580370601
Paxillin - PINCH	10	0.33820865	1.9890281	0.16248106452006
PINCH - Vinculin	10	0.34166413	1.3183112	0.372182178279786
PINCH - VASP	18	0.77736363	2.5613019	2.20140016191931E-3
α-parvin - PINCH	25	1.3934461	2.9695503	2.1431168201741901E-6
ILK - PINCH	46	5.9303266	9.7743455	3.2998646876373799E-18
CSK - PINCH	10	0.20585821	1.4650112	4.8182435481791602E-2
PINCH - Zyxin	9	0.29903388	2.0326536	1.57671107447634E-3
α-actinin - PINCH	20	0.19752377	1.0560286	0.76449080875436903
PINCH - Tensin	10	0.30341979	1.9518602	0.16248106452006
CAS - FAK	28	3.5376147	5.1575872	8.0847572092313799E-9
CAS - Paxillin	24	1.3917978	4.0218973	4.0518397422885502E-5
CAS - Vinculin	10	1.2329107	2.9354021	8.5675697355736304E-3
CAS - VASP	24	0.72988025	1.755873	6.52708635004533E-3
α-parvin - CAS	18	0.48806311	1.5439631	0.40088638845415703
CAS - ILK	26	0.66489394	1.8078357	9.5780520689773007E-6
CAS - CSK	16	0.52157228	1.4974233	3.02485204867423E-2
CAS - Zyxin	31	0.81233395	3.1749758	7.3378084927556296E-10
a-actinin - CAS	30	0.57648049	1.7525454	7.7134733728255703E-2
CAS - Tensin	28	1.263358	1.4805454	0.148081963261979
CAS - PINCH	16	0.261514	1.747898	7.3422427205941396E-3
FAK - Talin	14	0.57997963	1.9412743	4.48702359058836E-3
Paxillin - Talin	9	1.6174184	2.5733123	8.6001834795924506E-2
Talin - Vinculin	21	0.27305846	1.4789023	3.0988316409255701E-2
Talin - VASP	16	0.95255999	3.8905568	7.3422427205941396E-3
α-parvin - Talin	10	0.41151008	2.1936898	8.5675697355736304E-3
ILK - Talin	19	0.29605688	1.0671947	0.93506020630069098
CSK - Talin	20	0.11453299	0.50587417	0.99992309780527
Talin - Zyxin	10	0.10060631	0.5413897	0.99143243026442596
α-actinin - Talin	10	0.1344319	0.83243936	0.99143243026442596
Talin - Tensin	15	0.49138765	1.3535057	0.51174254055597002
PINCH - Talin	10	0.22770135	1.0631867	0.62781782172021405
CAS - Talin	9	0.77305535	1.7998766	0.25376272580370601
FAK - FAK	19	0.99442317	3.6095836	5.7077263698329699E-7
Paxillin - Paxillin	21	0.38331208	2.2118381	3.0988316409255701E-2
Vinculin - Vinculin	14	0.45801702	3.9671494	5.4010302852153605E-4
VASP - VASP	33	27.363935	17.133137	2.2277698225394501E-12
α-parvin - α-parvin	10	0.32466015	1.0351729	0.99143243026442596
ILK - ILK	14	0.93383	2.8327376	2.2682996351303199E-2
CSK - CSK	18	0.38419693	2.3614596	3.1574723921170899E-4
Zyxin - Zyxin	10	0.2331874	1.4706248	0.372182178279786
α-actinin - α-actinin	33	2.7308877	5.8288517	3.2049111532351201E-9
Tensin - Tensin	33	9.2486966	5.0196906	2.2277698225394501E-12
PINCH - PINCH	10	0.70958254	2.561588	6.8401436319194097E-4
CAS - CAS	9	1.1103583	3.1673154	1.57671107447634E-3
Talin - Talin	18	0.83602031	3.383629	3.1574723921170899E-4

TABLE A.3: Pairwise association in NIH3T3 cells

Protein pair	n (NIH3T3)	Ka (NIH3T3)	score (NIH3T3)	p-value (NIH3T3)
FAK - Paxillin	29	1.9267987	3.9109301	1.2054112895770301E-6
Paxillin - Vinculin	21	0.70343835	3.1276369	2.1123176582123998E-3
Paxillin - VASP	0	0.46548769	1.387012	NA
VASP - Vinculin	21	1.5295119	6.4872379	9.2011550769844699E-3
α-parvin - Paxillin	0	0.36578679	1.0836397	NA
α-parvin - VASP	34	0.77120463	2.0392783	8.7634081175268501E-5
FAK - ILK	0	0.23355113	0.79548509	NA
ILK - Paxillin	11	0.68095572	2.4969788	4.71210834908039E-3
ILK - VASP	21	0.40244194	1.6353082	8.3121881025761804E-2
α-parvin - ILK	31	12.606637	9.2039368	1.45744878858949E-11
CSK - VASP	0	0.27404095	1.0214646	NA
Vinculin - Zyxin	16	0.53286559	2.0459613	9.1637344900019096E-2
VASP - Zyxin	9	1.592497	4.2833736	1.7422657372963501E-2
ILK - Zyxin	20	0.50956733	1.574287	4.5078469008311403E-2
α-actinin - Paxillin	12	0.442307	1.4209217	0.381978434689
α-actinin - VASP	28	1.0276642	3.0293001	2.9464241259203102E-3
α-actinin - Zyxin	11	0.55275701	1.8466686	0.108251787969057
Tensin - Vinculin	17	0.84457503	2.5835014	6.3304041324660498E-2
Tensin - VASP	14	1.0632625	2.3248786	4.48702359058836E-3
α-actinin - Tensin	13	0.76596169	1.4231831	0.51103798812261203
PINCH - VASP	10	0.57763742	1.2325372	0.62781782172021405
α-parvin - PINCH	33	1.9353634	4.0168418	3.2049111532351201E-9
ILK - PINCH	21	9.9263711	6.6242229	1.06271897185037E-7
CAS - FAK	28	1.8652175	3.8096873	1.6704459662422701E-7
CAS - Paxillin	19	2.0162253	4.8972356	1.7676161430524301E-4
CAS - Vinculin	27	0.71812995	1.7296317	1.4124657793525501E-3
CAS - VASP	15	0.41707866	2.2816123	1.40366830536586E-2
CAS - ILK	20	0.48305542	2.3406298	4.5078469008311403E-2
CAS - Zyxin	11	0.42091926	3.1319673	4.71210834908039E-3
a-actinin - CAS	0	0.83989141	2.0029433	NA
CAS - Tensin	29	1.0791077	1.5306231	5.3210667955255697E-2
Paxillin - Talin	14	0.54552787	1.64495	2.2682996351303199E-2
Talin - VASP	20	0.23530832	1.187018	0.59480729600971305
α-parvin - Talin	0	0.38682576	1.2714169	NA
CAS - Talin	13	0.30869878	1.7760157	0.127295432297444
FAK - FAK	41	0.46424489	1.5704748	8.1366003360776595E-2
Vinculin - Vinculin	12	0.27844229	1.4436372	0.18281704322668599
VASP - VASP	31	16.586911	17.468865	1.45744878858949E-11
ILK - ILK	15	1.5105404	3.439877	1.4948993321068401E-5
α-actinin - α-actinin	14	1.33709267	3.4901723	2.9687437440431601E-5
Tensin - Tensin	25	4.1540627	4.4349148	1.2386102895665899E-7
PINCH - PINCH	17	0.49017189	2.393321	1.95162085263791E-2
CAS - CAS	26	0.92746057	3.7271114	8.2794364036803101E-7
Talin - Talin	15	0.83020007	1.8623722	5.2404698311956703E-2

TABLE A.4: Diffusion speed in REF52 cells

Protein	tauD	D
meGFP	1.9763241E-4	4.5667509696410612E-7
FAK	2.9079849E-4	3.103654355289121E-7
paxillin	9.0765088E-4	9.9436690900360255E-8
vinculin	6.878687E-4	1.3120788894741102E-7
VASP	3.6801047E-3	2.4524791373462821E-8
a-parvin	7.5640562E-4	1.1931931441757397E-7
ILK	1.1433865E-3	7.8935513057045862E-8
csk	4.0852366E-4	2.2092673898006295E-7
zyxin	1.1255134E-3	8.0189005301935968E-8
a-actinin	1.4482948E-3	6.2317285127309703E-8
tensin	1.8310853E-3	4.9289784588407753E-8
pinch	6.9438832E-4	1.2997597655444433E-7
cas	9.7241475E-4	9.2814100156337591E-8
talin	9.4183819E-4	9.5827288549426929E-8

TABLE A.5: PCR primers used for cloning

eGFP-meGFP-FP	tgagcacccagtccaagctgagcaaagacccca
eGFP-meGFP-RP	tggggtctttgctcagcttggactgggtgctca
mKate2 FP1	ccaccggtcgccaccatggtgagcgagctgattaagg
mKate2 RP1	ggctcgagatctgagtccggatctgtgccccagtttgctagg
mKate2 C1 FP1	gcgcaccggtgcaggtgctggaatggtgagcgagctgattaagg
mKate2 C1 RP1	gcgctccggatctgtgccccagtttgctagg
mKate2 N1 FP1	gcgcaccggtcgccaccatggtgagcgagctgattaagg
mKate2 N1 RP1	gcgctccggaccggctctgtgccccagtttgctagg
Don1-FP	tatagatctagcgcgggcggaaagaaaaatagaaagggaaaagaaaat
Don1-RP	tatgaattcgcccgcgctcgtaaaacttaattcttgtctagatggatgaa
meGFP-FP	atagtcgaccaatggtgagcaagggcgaggagc
meGFP-RP	ataggatccttacttgtacagctcgtccatgccga
Parvin C1 FP1	ggctcgagctatggccacctccccgcagaagtcg
Parvin C1 RP1	ccgaattctcactccacgttacggtacttgg
CAS C1 FP1	cgcgcgctcgagcgatgaaccacctgaacgtgctggc
CAS C1 RP1	gcgcgcgaattctcaggcggctgccagctg
Csk N1 FP1	ccgtcgacatgtcagcaatacaggccgcctgg
Csk N1 RP1	ccggatccgccaggtgcagctcgtgggttttg
FAK C1 FP1	ggagatctgggatggcagctgcttaccttgacc
FAK C1 RP1	ccgtcgactcagtgtggtctcgtctgccc
ILK C1 FP1	ggctcgagctatggacgacattttcactcagtgc
ILK C1 RP1	ccgaattcctacttgtcctgcatcttctcaagg
PINCH-FP2	tatagatctgcaggttccgctggtatggccaacgccctggccagcgcc
PINCH-RP2	tatgtcgacttatttccttcctaaggtctcagctagtttcttaagtcttttcttcagctcc
Talin C1 FP2	gcgcgaattcgatggttgcactttcactgaagatcagc
Talin C1 RP2	gcgcgtcgacttagtgctcatctcgaagctctgaagg
mCitrine-FseI FP	ccggactcagatctcgagctcaagcttcgaattctgcagggccggccctgcagtcgacggtaccgcgggcccg
mCitrine-FseI RP	cgggcccgcggtaccgtcgactgcagggccggccctgcagaattcgaagcttgagctcgagatctgagtccgg
Tensin-FP	atagtcgacatgagtgtgagccggaccatggag
Tensin-RP	ataggtaccttatctctttttggccggcattcagcatgac
VASP N1 FP1	ccgaattcatgagcagcgagacggtcatctg
VASP N1 RP1	ccggatccgcgggagaaccccgcttcctcagc
Vinculin FP1	ggtccggaagtgctggtagtgctggtatgccagtgtttcatacgcgcac
Vinculin RP1	ccgtcgacctactggtaccagggagtctttctaaccca
meGFP-dSH2 FP1	tacaagtccggactcagatccgagctcaagcttaagagca
meGFP-dSH2 RP1	tgctcttaagcttgagctcggatctgagtccggacttgta

Bibliography

Alan Agresti. A survey of exact inference for contingency tables. *Statistical Science*, 7(1):131–153, 1992.

S Ai, M Kuzuya, T Koike, T Asai, S Kanda, K Maeda, T Shibata, and a Iguchi. Rho-Rho kinase is involved in smooth muscle cell migration through myosin light chain phosphorylation-dependent and independent pathways. *Atherosclerosis*, 155(2):321–7, April 2001. ISSN 0021-9150.

A Angers-Loustau, J F Côté, A Charest, D Dowbenko, S Spencer, L a Lasky, and M L Tremblay. Protein tyrosine phosphatase-PEST regulates focal adhesion disassembly, migration, and cytokinesis in fibroblasts. *The Journal of cell biology*, 144(5):1019–31, March 1999. ISSN 0021-9525.

Eva Arnspang Christensen, Pasad Kulatunga, and B Christoffer Lagerholm. A single molecule investigation of the photostability of quantum dots. *PloS one*, 7 (8):e44355, January 2012. ISSN 1932-6203. doi: 10.1371/journal.pone.0044355.

Angela Barrett, Caroline Pellet-Many, Ian C Zachary, Ian M Evans, and Paul Frankel. p130Cas: a key signalling node in health and disease. *Cellular signalling*, 25(4):766–77, April 2013. ISSN 1873-3913. doi: 10.1016/j.cellsig.2012. 12.019.

J Henri Bayle, Joshua S Grimley, Kryn Stankunas, Jason E Gestwicki, Thomas J Wandless, and Gerald R Crabtree. Rapamycin analogs with differential binding specificity permit orthogonal control of protein activity. *Chemistry & biology*, 13 (1):99–107, January 2006. ISSN 1074-5521. doi: 10.1016/j.chembiol.2005.10.017.

James E Bear and Frank B Gertler. Ena/VASP: towards resolving a pointed controversy at the barbed end. *Journal of cell science*, 122(Pt 12):1947–53, June 2009. ISSN 0021-9533. doi: 10.1242/jcs.038125.

M Bergman, V Joukov, I Virtanen, and K Alitalo. Overexpressed Csk tyrosine kinase is localized in focal adhesions, causes reorganization of alpha v beta 5 integrin, and interferes with HeLa cell spreading. *Molecular and cellular biology*, 15(2):711–22, February 1995. ISSN 0270-7306.

Martin Bierbaum and Philippe I H Bastiaens. Cell cycle-dependent binding modes of the ran exchange factor RCC1 to chromatin. *Biophysical journal*, 104(8): 1642–51, May 2013. ISSN 1542-0086. doi: 10.1016/j.bpj.2013.03.024.

Megan L Blades, Ekaterina Grekova, Holly M Wobma, Kun Chen, Warren C W Chan, and David T Cramb. Three-color fluorescence cross-correlation spectroscopy for analyzing complex nanoparticle mixtures. *Analytical chemistry*, 84 (21):9623–31, November 2012. ISSN 1520-6882. doi: 10.1021/ac302572k.

Martin Böhmer, Michael Wahl, Hans-Jürgen Rahn, Rainer Erdmann, and Jörg Enderlein. Time-resolved fluorescence correlation spectroscopy. 2002.

M C Brown, J a Perrotta, and C E Turner. Identification of LIM3 as the principal determinant of paxillin focal adhesion localization and characterization of a novel motif on paxillin directing vinculin and focal adhesion kinase binding. *The Journal of cell biology*, 135(4):1109–23, November 1996. ISSN 0021-9525.

K Burridge and M Chrzanowska-Wodnicka. Focal adhesions, contractility, and signaling. *Annual review of cell and developmental biology*, 12:463–518, January 1996. ISSN 1081-0706. doi: 10.1146/annurev.cellbio.12.1.463.

Sara Cabodi, Maria del Pilar Camacho-Leal, Paola Di Stefano, and Paola Defilippi. Integrin signalling adaptors: not only figurants in the cancer story. *Nature reviews. Cancer*, 10(12):858–70, December 2010. ISSN 1474-1768. doi: 10.1038/ nrc2967.

David a Calderwood, Yosuke Fujioka, Jose M de Pereda, Begoña García-Alvarez, Tetsuya Nakamoto, Ben Margolis, C Jane McGlade, Robert C Liddington, and Mark H Ginsberg. Integrin beta cytoplasmic domain interactions with phosphotyrosine-binding domains: a structural prototype for diversity in integrin signaling. *Proceedings of the National Academy of Sciences of the United States of America*, 100(5):2272–7, March 2003. ISSN 0027-8424. doi: 10.1073/pnas.262791999.

Alex Carisey and Christoph Ballestrem. Vinculin, an adapter protein in control of cell adhesion signalling. *European journal of cell biology*, 90(2-3):157–63, 2011. ISSN 1618-1298. doi: 10.1016/j.ejcb.2010.06.007.

Mariola R. Chacón and Pietro Fazzari. FAK: Dynamic integration of guidance signals at the growth cone. *Cell Adhesion & Migration*, 5(1):52–55, January 2011. ISSN 1933-6918. doi: 10.4161/cam.5.1.13681.

Yuan-Chen Chang, Perihan Nalbant, Jörg Birkenfeld, Zee-Fen Chang, and Gary M Bokoch. GEF-H1 couples nocodazole-induced microtubule disassembly to cell contractility via RhoA. *Molecular biology of the cell*, 19(5):2147–53, May 2008. ISSN 1939-4586. doi: 10.1091/mbc.E07-12-1269.

H C Chen, P A Appeddu, J T Parsons, J D Hildebrand, M D Schaller, and J L Guan. Interaction of focal adhesion kinase with cytoskeletal protein talin. *The Journal of biological chemistry*, 270(28):16995–9, July 1995. ISSN 0021-9258.

Jiji Chen and Joseph Irudayaraj. Fluorescence lifetime cross correlation spectroscopy resolves EGFR and antagonist interaction in live cells. *Analytical chemistry*, 82(15):6415–21, August 2010. ISSN 1520-6882. doi: 10.1021/ac101236t.

Colin K Choi, Miguel Vicente-Manzanares, Jessica Zareno, Leanna a Whitmore, Alex Mogilner, and Alan Rick Horwitz. Actin and alpha-actinin orchestrate the assembly and maturation of nascent adhesions in a myosin II motor-independent manner. *Nature cell biology*, 10(9):1039–50, September 2008. ISSN 1465-7392. doi: 10.1038/ncb1763.

M a Cooley, J M Broome, C Ohngemach, L H Romer, and M D Schaller. Paxillin binding is not the sole determinant of focal adhesion localization or dominant-negative activity of focal adhesion kinase/focal adhesion kinase-related nonkinase. *Molecular biology of the cell*, 11(9):3247–63, September 2000. ISSN 1059-1524.

Sean R Coyer, Ankur Singh, David W Dumbauld, David A Calderwood, Susan W Craig, Emmanuel Delamarche, and Andrés J García. Nanopatterning reveals an ECM area threshold for focal adhesion assembly and force transmission that is regulated by integrin activation and cytoskeleton tension. *Journal of cell science*, 125(Pt 21):5110–23, November 2012. ISSN 1477-9137. doi: 10.1242/jcs.108035.

a W Crawford, J W Michelsen, and M C Beckerle. An interaction between zyxin and alpha-actinin. *The Journal of cell biology*, 116(6):1381–93, March 1992. ISSN 0021-9525.

D R Critchley. Genetic, biochemical and structural approaches to talin function. *Biochemical Society transactions*, 33(Pt 6):1308–12, December 2005. ISSN 0300-5127. doi: 10.1042/BST20051308.

Andrew B Cubitt, Roger Heim, Stephen R Adams, E Aileen, Larry A Gross, Roger Y Tsien, A E Boyd, Larry A Gross, and Roger Y Tsien. Understanding, improving and using green fluorescent proteins. *Trends in biochemical sciences*, 20(11):448–55, November 1995. ISSN 0968-0004.

EHJ Danen. Integrin Signaling as a Cancer Drug Target. *ISRN Cell Biology*, 2013: 1–14, 2013. ISSN 2090-7389. doi: 10.1155/2013/135164.

Nicholas O Deakin and Christopher E Turner. Paxillin comes of age. *Journal of cell science*, 121(Pt 15):2435–44, August 2008. ISSN 0021-9533. doi: 10.1242/jcs.018044.

MA Michelle A Digman, Paul W PW Wiseman, Colin Choi, Alan R Horwitz, and Enrico Gratton. Stoichiometry of molecular complexes at adhesions in living cells. *Proceedings of the National Academy of Sciences of the United States of America*, 106(7):2170–5, February 2009a. ISSN 1091-6490. doi: 10.1073/pnas. 0806036106.

Michelle a Digman, Paul W Wiseman, Alan R Horwitz, and Enrico Gratton. Detecting protein complexes in living cells from laser scanning confocal image sequences by the cross correlation raster image spectroscopy method. *Biophysical journal*, 96(2):707–16, January 2009b. ISSN 1542-0086. doi: 10.1016/j.bpj.2008.09.051.

Chenxi Duan, Virgile Adam, Martin Byrdin, Jacqueline Ridard, Sylvie Kieffer-Jaquinod, Cecile Morlot, Delphine Arcizet, Isabelle Demachy, and Dominique Bourgeois. Structural evidence for a two-regime photobleaching mechanism in a reversibly switchable fluorescent protein. *Journal of the American Chemical Society*, September 2013. ISSN 1520-5126. doi: 10.1021/ja406860e.

Andrey Efimov, Natalia Schiefermeier, Ilya Grigoriev, Ryoma Ohi, Michael C Brown, Christopher E Turner, J Victor Small, and Irina Kaverina. Paxillin-dependent stimulation of microtubule catastrophes at focal adhesion sites. *Journal of cell science*, 121(Pt 2):196–204, January 2008. ISSN 0021-9533. doi: 10.1242/jcs.012666.

Elliot L Elson. Fluorescence correlation spectroscopy: past, present, future. *Biophysical journal*, 101(12):2855–70, December 2011. ISSN 1542-0086. doi: 10.1016/j.bpj.2011.11.012.

Ellen J Ezratty, Michael a Partridge, and Gregg G Gundersen. Microtubule-induced focal adhesion disassembly is mediated by dynamin and focal adhesion kinase. *Nature cell biology*, 7(6):581–90, June 2005. ISSN 1465-7392. doi: 10.1038/ncb1262.

Nolan R Filipenko, Sarah Attwell, Calvin Roskelley, and Shoukat Dedhar. Integrin-linked kinase activity regulates Rac- and Cdc42-mediated actin cytoskeleton reorganization via alpha-PIX. *Oncogene*, 24(38):5837–49, September 2005. ISSN 0950-9232. doi: 10.1038/sj.onc.1208737.

Ronald Aylmer Fisher. On the Interpretation of x2 from Contingency Tables, and the Calculation of P. *Journal of the Royal Statistical Society*, 85(1):87–94, 1922.

Th. Förster. Zwischenmolekulare Energiewanderung und Fluoreszenz. *Annalen der Physik*, 437(1-2):55–75, 1948. ISSN 00033804. doi: 10.1002/andp.19484370105.

B Geiger and a Bershadsky. Assembly and mechanosensory function of focal contacts. *Current opinion in cell biology*, 13(5):584–92, October 2001. ISSN 0955-0674.

Sushmita Ghatak, Jessica Morgner, and Sara A Wickström. ILK: a pseudokinase with a unique function in the integrin-actin linkage. *Biochemical Society transactions*, 41(4):995–1001, August 2013. ISSN 1470-8752. doi: 10.1042/BST20130062.

Alexandre R Gingras, Neil Bate, Benjamin T Goult, Larnele Hazelwood, Ilona Canestrelli, J Günter Grossmann, HongJun Liu, Nicholas S M Putz, Gordon C K Roberts, Niels Volkmann, Dorit Hanein, Igor L Barsukov, and David R Critchley. The structure of the C-terminal actin-binding domain of talin. *The EMBO journal*, 27(2):458–69, January 2008. ISSN 1460-2075. doi: 10.1038/sj. emboj.7601965.

Jacob Grange, James D Moody, Marc P a Ascione, and Marc D H Hansen. Zyxin-VASP interactions alter actin regulatory activity in zyxin-VASP complexes. *Cellular & molecular biology letters*, 18(1):1–10, March 2013. ISSN 1689-1392. doi: 10.2478/s11658-012-0035-2.

Emily H Hall, Abbi E Daugherty, Colin K Choi, Alan F Horwitz, and David L Brautigan. Tensin1 requires protein phosphatase-1alpha in addition to RhoGAP DLC-1 to control cell polarization, migration, and invasion. *The Journal of biological chemistry*, 284(50):34713–22, December 2009. ISSN 1083-351X. doi: 10.1074/jbc.M109.059592.

Douglas Hanahan and Robert a Weinberg. Hallmarks of cancer: the next generation. *Cell*, 144(5):646–74, March 2011. ISSN 1097-4172. doi: 10.1016/j.cell.2011.02.013.

Marc D H Hansen and Mary C Beckerle. alpha-Actinin links LPP, but not zyxin, to cadherin-based junctions. *Biochemical and biophysical research communications*, 371(1):144–8, June 2008. ISSN 1090-2104. doi: 10.1016/j.bbrc.2008.04.018.

B Harbeck, S Hüttelmaier, K Schluter, B M Jockusch, and S Illenberger. Phosphorylation of the vasodilator-stimulated phosphoprotein regulates its interaction with actin. *The Journal of biological chemistry*, 275(40):30817–25, October 2000. ISSN 0021-9258. doi: 10.1074/jbc.M005066200.

M T Harte, J D Hildebrand, M R Burnham, A H Bouton, and J T Parsons. p130Cas, a substrate associated with v-Src and v-Crk, localizes to focal adhesions and binds to focal adhesion kinase. *The Journal of biological chemistry*, 271(23):13649–55, June 1996. ISSN 0021-9258.

Elke Haustein and Petra Schwille. Fluorescence correlation spectroscopy: novel variations of an established technique. *Annual review of biophysics and biomolecular structure*, 36:151–69, January 2007. ISSN 1056-8700. doi: 10.1146/annurev.biophys.36.040306.132612.

Nissim Hay and Nahum Sonenberg. Upstream and downstream of mTOR. *Genes & development*, 18(16):1926–45, August 2004. ISSN 0890-9369. doi: 10.1101/gad.1212704.

Katrin G Heinze, Michael Jahnz, and Petra Schwille. Triple-color coincidence analysis: one step further in following higher order molecular complex formation.

Biophysical journal, 86(1 Pt 1):506–16, January 2004. ISSN 0006-3495. doi: 10.1016/S0006-3495(04)74129-6.

J Nathan Henderson, Hui-Wang Ai, Robert E Campbell, and S James Remington. Structural basis for reversible photobleaching of a green fluorescent protein homologue. *Proceedings of the National Academy of Sciences of the United States of America*, 104(16):6672–7, April 2007. ISSN 0027-8424. doi: 10.1073/pnas.0700059104.

Jelle Hendrix and Don C Lamb. *Pulsed interleaved excitation: principles and applications.*, volume 518. Elsevier Inc., 1 edition, January 2013. ISBN 9780123884220. doi: 10.1016/B978-0-12-388422-0.00009-1.

Maiko Higuchi, Rina Kihara, Tomohiko Okazaki, Ichiro Aoki, Shiro Suetsugu, and Yukiko Gotoh. Akt1 promotes focal adhesion disassembly and cell motility through phosphorylation of FAK in growth factor-stimulated cells. *Journal of cell science*, 126(Pt 3):745–55, February 2013. ISSN 1477-9137. doi: 10.1242/jcs.112722.

J D Hildebrand, M D Schaller, and J T Parsons. Paxillin, a tyrosine phosphorylated focal adhesion-associated protein binds to the carboxyl terminal domain of focal adhesion kinase. *Molecular biology of the cell*, 6(6):637–47, June 1995. ISSN 1059-1524.

T Hirota, T Morisaki, Y Nishiyama, T Marumoto, K Tada, T Hara, N Masuko, M Inagaki, K Hatakeyama, and H Saya. Zyxin, a regulator of actin filament assembly, targets the mitotic apparatus by interacting with h-warts/LATS1 tumor suppressor. *The Journal of cell biology*, 149(5):1073–86, May 2000. ISSN 0021-9525.

R a Hoebe, H T M Van der Voort, J Stap, C J F Van Noorden, and E M M Manders. Quantitative determination of the reduction of phototoxicity and photobleaching by controlled light exposure microscopy. *Journal of microscopy*, 231(Pt 1):9–20, July 2008. ISSN 1365-2818. doi: 10.1111/j.1365-2818.2008.02009.x.

Mark Howarth, Wenhao Liu, Sujiet Puthenveetil, Yi Zheng, Lisa F Marshall, Michael M Schmidt, K Dane Wittrup, Moungi G Bawendi, and Alice Y Ting. Monovalent, reduced-size quantum dots for imaging receptors on living cells.

Nature methods, 5(5):397–9, May 2008. ISSN 1548-7105. doi: 10.1038/nmeth. 1206.

Isabel Hunger-Glaser, Robert S Fan, Eduardo Perez-Salazar, and Enrique Rozengurt. PDGF and FGF induce focal adhesion kinase (FAK) phosphorylation at Ser-910: dissociation from Tyr-397 phosphorylation and requirement for ERK activation. *Journal of cellular physiology*, 200(2):213–22, August 2004. ISSN 0021-9541. doi: 10.1002/jcp.20018.

R O Hynes. Integrins: a family of cell surface receptors. *Cell*, 48(4):549–54, February 1987. ISSN 0092-8674.

Giovanni a Infusino and Jeffrey R Jacobson. Endothelial FAK as a therapeutic target in disease. *Microvascular research*, 83(1):89–96, January 2012. ISSN 1095-9319. doi: 10.1016/j.mvr.2011.09.011.

Hellen C Ishikawa-Ankerhold, Richard Ankerhold, and Gregor P C Drummen. Advanced fluorescence microscopy techniques–FRAP, FLIP, FLAP, FRET and FLIM. *Molecules (Basel, Switzerland)*, 17(4):4047–132, January 2012. ISSN 1420-3049. doi: 10.3390/molecules17044047.

T Ishizaki, M Uehata, I Tamechika, J Keel, K Nonomura, M Maekawa, and S Narumiya. Pharmacological properties of Y-27632, a specific inhibitor of rho-associated kinases. *Molecular pharmacology*, 57(5):976–83, May 2000. ISSN 0026-895X.

Tina Izard, Gwyndaf Evans, Robert A Borgon, Christina L Rush, Gerard Bricogne, and Philippe R J Bois. Vinculin activation by talin through helical bundle conversion. 427(January):171–175, 2004. doi: 10.1038/nature02273. Published.

J L Jainchill, S a Aaronson, and G J Todaro. Murine sarcoma and leukemia viruses: assay using clonal lines of contact-inhibited mouse cells. *Journal of virology*, 4(5):549–53, November 1969. ISSN 0022-538X.

Pakorn Kanchanawong, Gleb Shtengel, Ana M Pasapera, Ericka B Ramko, Michael W Davidson, Harald F Hess, Clare M Waterman, W Davidson, Harald F Hess, and Clare M Waterman. Nanoscale architecture of integrin-based cell adhesions. *Nature*, 468(7323):580–4, November 2010. ISSN 1476-4687. doi: 10.1038/nature09621.

Peter Kapusta, Radek Macháň, Aleš Benda, and Martin Hof. Fluorescence Lifetime Correlation Spectroscopy (FLCS): Concepts, Applications and Outlook. *International journal of molecular sciences*, 13(10):12890–910, January 2012. ISSN 1422-0067. doi: 10.3390/ijms131012890.

J. Kirchner. Live-cell monitoring of tyrosine phosphorylation in focal adhesions following microtubule disruption. *Journal of Cell Science*, 116(6):975–986, January 2003. ISSN 00219533. doi: 10.1242/jcs.00284.

Takako Kogure, Hiroyuki Kawano, Yukiko Abe, and Atsushi Miyawaki. Fluorescence imaging using a fluorescent protein with a large Stokes shift. *Methods (San Diego, Calif.)*, 45(3):223–6, July 2008. ISSN 1095-9130. doi: 10.1016/j.ymeth.2008.06.009.

You Korlann, Thomas Dertinger, Xavier Michalet, Shimon Weiss, and Jörg Enderlein. Measuring diffusion with polarization-modulation dual-focus fluorescence correlation spectroscopy. *Optics express*, 16(19):14609–16, October 2008. ISSN 1094-4087.

Jane Kovalevich, Brittany Tracy, and Dianne Langford. PINCH: More than just an adaptor protein in cellular response. *Journal of cellular physiology*, 226(4): 940–7, April 2011. ISSN 1097-4652. doi: 10.1002/jcp.22437.

Kristopher E Kubow and Alan Rick Horwitz. Reducing background fluorescence reveals adhesions in 3D matrices. *Nature cell biology*, 13(1):3–5; author reply 5–7, January 2011. ISSN 1476-4679. doi: 10.1038/ncb0111-3.

Karin Kühnel, Thomas Jarchau, Eva Wolf, Ilme Schlichting, Ulrich Walter, Alfred Wittinghofer, and Sergei V Strelkov. The VASP tetramerization domain is a right-handed coiled coil based on a 15-residue repeat. *Proceedings of the National Academy of Sciences of the United States of America*, 101(49):17027–32, December 2004. ISSN 0027-8424. doi: 10.1073/pnas.0403069101.

Joseph R. Lakowicz and Klaus W. Berndt. Lifetime-selective fluorescence imaging using an rf phase-sensitive camera. *Review of Scientific Instruments*, 62(7):1727, 1991. ISSN 00346748. doi: 10.1063/1.1142413.

Irena Lavelin, Haguy Wolfenson, Israel Patla, Yoav I Henis, Ohad Medalia, Tova Volberg, Ariel Livne, Zvi Kam, and Benjamin Geiger. Differential effect of actomyosin relaxation on the dynamic properties of focal adhesion proteins.

PloS one, 8(9):e73549, January 2013. ISSN 1932-6203. doi: 10.1371/journal.
pone.0073549.

Soon-Hyouk Lee, Gyu-Chang Lim, Soo-Yong Kim, Eun-Kyung Kim, Hak-Sung
Kim, and Sok-Won Kim. Statistical Analysis of Fluorescence Correlation Spec-
troscopy of Ultra Low Concentration Molecules with a Confocal Microscope.
Journal of the Optical Society of Korea, 12(3):170–173, September 2008. ISSN
1226-4776. doi: 10.3807/JOSK.2008.12.3.170.

Kyle R Legate, Seiichiro Takahashi, Navid Bonakdar, Ben Fabry, David Boettiger,
Roy Zent, and Reinhard Fässler. Integrin adhesion and force coupling are inde-
pendently regulated by localized PtdIns(4,5)2 synthesis. *The EMBO journal*, 30
(22):4539–53, November 2011. ISSN 1460-2075. doi: 10.1038/emboj.2011.332.

Tanmay P Lele, Charles K Thodeti, Jay Pendse, and Donald E Ingber. Investigat-
ing complexity of protein-protein interactions in focal adhesions. *Biochemical
and biophysical research communications*, 369(3):929–34, May 2008. ISSN 1090-
2104. doi: 10.1016/j.bbrc.2008.02.137.

D Leopoldt, H F Yee, S Saab, and E Rozengurt. Tyrosine phosphorylation
of p125(Fak), p130(Cas), and paxillin does not require extracellular signal-
regulated kinase activation in Swiss 3T3 cells stimulated by bombesin or
platelet-derived growth factor. *Journal of cellular physiology*, 183(2):208–20,
May 2000. ISSN 0021-9541. doi: 10.1002/(SICI)1097-4652(200005)183:2⟨208::
AID-JCP7⟩3.0.CO;2-5.

Steven V Ley, Miles N Tackett, Matthew L Maddess, James C Anderson,
Paul E Brennan, Michael W Cappi, Jag P Heer, Céline Helgen, Masakuni
Kori, Cyrille Kouklovsky, Stephen P Marsden, Joanne Norman, David P Os-
born, María a Palomero, John B J Pavey, Catherine Pinel, Lesley a Robinson,
Jürgen Schnaubelt, James S Scott, Christopher D Spilling, Hidenori Watanabe,
Kieron E Wesson, and Michael C Willis. Total synthesis of rapamycin. *Chem-
istry (Weinheim an der Bergstrasse, Germany)*, 15(12):2874–914, January 2009.
ISSN 1521-3765. doi: 10.1002/chem.200801656.

B Li and B Trueb. Analysis of the alpha-actinin/zyxin interaction. *The Journal of
biological chemistry*, 276(36):33328–35, September 2001. ISSN 0021-9258. doi:
10.1074/jbc.M100789200.

Jun Liang, Jungwon Choi, and Jon Clardy. Refined structure of the FKBP12–rapamycin–FRB ternary complex at 2.2 A resolution. *Acta Crystallographica Section D Biological Crystallography*, 55(4):736–744, April 1999. ISSN 09074449. doi: 10.1107/S0907444998014747.

Daniel Lietha, Xinming Cai, Derek F J Ceccarelli, Yiqun Li, Michael D Schaller, and Michael J Eck. Structural basis for the autoinhibition of focal adhesion kinase. *Cell*, 129(6):1177–87, June 2007. ISSN 0092-8674. doi: 10.1016/j.cell.2007.05.041.

L Liu, L Chen, J Chung, and S Huang. Rapamycin inhibits F-actin reorganization and phosphorylation of focal adhesion proteins. *Oncogene*, 27(37):4998–5010, August 2008. ISSN 1476-5594. doi: 10.1038/onc.2008.137.

S H Lo, Q An, S Bao, W K Wong, Y Liu, P A Janmey, J H Hartwig, and L B Chen. Molecular cloning of chick cardiac muscle tensin. Full-length cDNA sequence, expression, and characterization. *The Journal of biological chemistry*, 269(35): 22310–9, September 1994a. ISSN 0021-9258.

S H Lo, P A Janmey, J H Hartwig, and L B Chen. Interactions of tensin with actin and identification of its three distinct actin-binding domains. *The Journal of cell biology*, 125(5):1067–75, June 1994b. ISSN 0021-9525.

Su Hao Lo. Tensin. *The International Journal of Biochemistry & Cell Biology*, 36 (1):31–34, January 2004. ISSN 13572725. doi: 10.1016/S1357-2725(03)00171-7.

John Logan, Jean Claude Nicolas, William C Topp, Marc Girard, Thomas Shenk, and Arnold J Levine. Thomas shenk,* and arnold j. levine**'. 422:419–422, 1981.

Celine I Maeder, Mark a Hink, Ali Kinkhabwala, Reinhard Mayr, Philippe I H Bastiaens, and Michael Knop. Spatial regulation of Fus3 MAP kinase activity through a reaction-diffusion mechanism in yeast pheromone signalling. *Nature cell biology*, 9(11):1319–26, November 2007. ISSN 1465-7392. doi: 10.1038/ncb1652.

M. Maekawa, T Ishizaki, S Boku, N Watanabe, A Fujita, A Iwamatsu, T Obinata, K Ohashi, K Mizuno, and S Narumiya. Signaling from Rho to the Actin Cytoskeleton Through Protein Kinases ROCK and LIM-kinase. *Science*, 285(5429): 895–898, August 1999. ISSN 00368075. doi: 10.1126/science.285.5429.895.

Satyajit K Mitra and David D Schlaepfer. Integrin-regulated FAK-Src signaling in normal and cancer cells. *Current opinion in cell biology*, 18(5):516–23, October 2006. ISSN 0955-0674. doi: 10.1016/j.ceb.2006.08.011.

Satyajit K Mitra, Daniel a Hanson, and David D Schlaepfer. Focal adhesion kinase: in command and control of cell motility. *Nature reviews. Molecular cell biology*, 6(1):56–68, January 2005. ISSN 1471-0072. doi: 10.1038/nrm1549.

Daniel Moik, Anika Boettcher, Tatiana Makhina, Carsten Grashoff, Nada Bulus, Roy Zent, and Reinhard Faessler. Mutations in the Paxillin-binding site of Integrin-linked-kinase (ILK) destabilize the pseudokinase domain and cause embryonic lethality in mice. *The Journal of biological chemistry*, May 2013. ISSN 1083-351X. doi: 10.1074/jbc.M113.470476.

Barbara K Müller, Evgeny Zaychikov, Christoph Bräuchle, and Don C Lamb. Pulsed interleaved excitation. *Biophysical journal*, 89(5):3508–22, November 2005. ISSN 0006-3495. doi: 10.1529/biophysj.105.064766.

C. B. Müller, a. Loman, V. Pacheco, F. Koberling, D. Willbold, W. Richtering, and J. Enderlein. Precise measurement of diffusion by multi-color dual-focus fluorescence correlation spectroscopy. *EPL (Europhysics Letters)*, 83(4):46001, August 2008. ISSN 0295-5075. doi: 10.1209/0295-5075/83/46001.

S Nada, M Okada, A MacAuley, J A Cooper, and H Nakagawa. Cloning of a complementary DNA for a protein-tyrosine kinase that specifically phosphorylates a negative regulatory site of p60c-src. *Nature*, 351(6321):69–72, May 1991. ISSN 0028-0836. doi: 10.1038/351069a0.

Philipp Niethammer, Iva Kronja, Stefanie Kandels-Lewis, Sonja Rybina, Philippe Bastiaens, and Eric Karsenti. Discrete states of a protein interaction network govern interphase and mitotic microtubule dynamics. *PLoS biology*, 5(2):e29, February 2007. ISSN 1545-7885. doi: 10.1371/journal.pbio.0050029.

S N Nikolopoulos and C E Turner. Integrin-linked kinase (ILK) binding to paxillin LD1 motif regulates ILK localization to focal adhesions. *The Journal of biological chemistry*, 276(26):23499–505, June 2001. ISSN 0021-9258. doi: 10.1074/jbc.M102163200.

Masato Okada. Regulation of the SRC family kinases by Csk. *International journal of biological sciences*, 8(10):1385–97, January 2012. ISSN 1449-2288. doi: 10.7150/ijbs.5141.

M Ormö, a B Cubitt, K Kallio, L a Gross, R Y Tsien, and S J Remington. Crystal structure of the Aequorea victoria green fluorescent protein. *Science (New York, N.Y.)*, 273(5280):1392–5, September 1996. ISSN 0036-8075.

Eleonora Petryayeva, W Russ Algar, and Igor L Medintz. Quantum dots in bioanalysis: a review of applications across various platforms for fluorescence spectroscopy and imaging. *Applied spectroscopy*, 67(3):215–52, March 2013. ISSN 1943-3530. doi: 10.1366/12-06948.

Kiryl D Piatkevich, James Hulit, Oksana M Subach, Bin Wu, Arian Abdulla, Jeffrey E Segall, and Vladislav V Verkhusha. Monomeric red fluorescent proteins with a large Stokes shift. *Proceedings of the National Academy of Sciences of the United States of America*, 107(12):5369–74, March 2010. ISSN 1091-6490. doi: 10.1073/pnas.0914365107.

David W Piston and Gert-Jan Kremers. Fluorescent protein FRET: the good, the bad and the ugly. *Trends in biochemical sciences*, 32(9):407–14, September 2007. ISSN 0968-0004. doi: 10.1016/j.tibs.2007.08.003.

Paolo P Provenzano and Patricia J Keely. The role of focal adhesion kinase in tumor initiation and progression. *Cell adhesion & migration*, 3(4):347–50, 2009. ISSN 1933-6926.

Xiaolan Qian, Guorong Li, William C Vass, Alex Papageorge, Renard C Walker, Laura Asnaghi, Peter J Steinbach, Giovanna Tosato, Kent Hunter, and Douglas R Lowy. The Tensin-3 protein, including its SH2 domain, is phosphorylated by Src and contributes to tumorigenesis and metastasis. *Cancer cell*, 16 (3):246–58, September 2009. ISSN 1878-3686. doi: 10.1016/j.ccr.2009.07.031.

Jun Qin and Chuanyue Wu. ILK: a pseudokinase in the center stage of cell-matrix adhesion and signaling. *Current opinion in cell biology*, 24(5):607–13, October 2012. ISSN 1879-0410. doi: 10.1016/j.ceb.2012.06.003.

Vipul B Rathore, Masato Okada, Peter J Newman, and Debra K Newman. Paxillin family members function as Csk-binding proteins that regulate Lyn activity in human and murine platelets. *The Biochemical journal*, 403(2):275–81, April 2007. ISSN 1470-8728. doi: 10.1042/BJ20061618.

BI I Ratnikov, A W Partridge, and M H Ginsberg. Integrin activation by talin. *Journal of thrombosis and haemostasis : JTH*, 3(8):1783–90, August 2005. ISSN 1538-7933. doi: 10.1111/j.1538-7836.2005.01362.x.

M. Reinhard, J Zumbrunn, D Jaquemar, M Kuhn, U Walter, and B Trueb. An alpha -Actinin Binding Site of Zyxin Is Essential for Subcellular Zyxin Localization and alpha -Actinin Recruitment. *Journal of Biological Chemistry*, 274 (19):13410–13418, May 1999. ISSN 00219258. doi: 10.1074/jbc.274.19.13410.

Jonas Ries and Petra Schwille. Fluorescence correlation spectroscopy. *BioEssays : news and reviews in molecular, cellular and developmental biology*, 34(5):361–8, May 2012. ISSN 1521-1878. doi: 10.1002/bies.201100111.

Larisa Y Romanova and J Frederic Mushinski. Central role of paxillin phosphorylation in regulation of LFA-1 integrins activity and lymphocyte migration. *Cell adhesion & migration*, 5(6):457–62, 2011. ISSN 1933-6926. doi: 10.4161/cam.5.6.18219.

Verena Rombach-Riegraf, Peter Oswald, Roland Bienert, Jan Petersen, M P Domingo, Julian Pardo, P Gräber, and E M Galvez. Blinking effect and the use of quantum dots in single molecule spectroscopy. *Biochemical and biophysical research communications*, 430(1):260–4, January 2013. ISSN 1090-2104. doi: 10.1016/j.bbrc.2012.10.140.

S Rüttinger, V Buschmann, B Krämer, R Erdmann, R Macdonald, and F Koberling. Comparison and accuracy of methods to determine the confocal volume for quantitative fluorescence correlation spectroscopy. *Journal of microscopy*, 232 (2):343–52, November 2008. ISSN 1365-2818. doi: 10.1111/j.1365-2818.2008. 02105.x.

H Sabe, a Hata, M Okada, H Nakagawa, and H Hanafusa. Analysis of the binding of the Src homology 2 domain of Csk to tyrosine-phosphorylated proteins in the suppression and mitotic activation of c-Src. *Proceedings of the National Academy of Sciences of the United States of America*, 91(9):3984–8, April 1994. ISSN 0027-8424.

Harekrushna Sahoo and Petra Schwille. FRET and FCS–friends or foes? *Chemphyschem : a European journal of chemical physics and physical chemistry*, 12(3):532–41, February 2011. ISSN 1439-7641. doi: 10.1002/cphc.201000776.

M D Schaller, J D Hildebrand, J D Shannon, J W Fox, R R Vines, and J T Parsons. Autophosphorylation of the focal adhesion kinase, pp125FAK, directs SH2-dependent binding of pp60src. *Molecular and cellular biology*, 14(3):1680–8, March 1994. ISSN 0270-7306.

Danielle M Scheswohl, Jessica R Harrell, Zenon Rajfur, Guanghua Gao, Sharon L Campbell, and Michael D Schaller. Multiple paxillin binding sites regulate FAK function. *Journal of molecular signaling*, 3:1, January 2008. ISSN 1750-2187. doi: 10.1186/1750-2187-3-1.

D D Schlaepfer, C R Hauck, and D J Sieg. Signaling through focal adhesion kinase. *Progress in biophysics and molecular biology*, 71(3-4):435–78, January 1999. ISSN 0079-6107.

S N Sehgal, H Baker, and C Vézina. Rapamycin (AY-22,989), a new antifungal antibiotic. II. Fermentation, isolation and characterization. *The Journal of antibiotics*, 28(10):727–32, October 1975. ISSN 0021-8820.

Xingbo Shi, Yang Tu, Xiaojun Liu, Edward S Yeung, and Hongwei Gai. Photobleaching of quantum dots by non-resonant light. *Physical chemistry chemical physics : PCCP*, 15(9):3130–2, March 2013. ISSN 1463-9084. doi: 10.1039/c3cp43668c.

B Sjöblom, a Salmazo, and K Djinović-Carugo. Alpha-actinin structure and regulation. *Cellular and molecular life sciences : CMLS*, 65(17):2688–701, September 2008. ISSN 1420-682X. doi: 10.1007/s00018-008-8080-8.

Steven J Smith and Richard O McCann. A C-terminal dimerization motif is required for focal adhesion targeting of Talin1 and the interaction of the Talin1 I/LWEQ module with F-actin. *Biochemistry*, 46(38):10886–98, September 2007. ISSN 0006-2960. doi: 10.1021/bi700637a.

Fabio Stanchi, Carsten Grashoff, Carine Flore Nguemeni Yonga, Dominique Grall, Reinhard Fässler, and Ellen Van Obberghen-Schilling. Molecular dissection of the ILK-PINCH-parvin triad reveals a fundamental role for the ILK kinase domain in the late stages of focal-adhesion maturation. *Journal of cell science*, 122(Pt 11):1800–11, June 2009. ISSN 0021-9533. doi: 10.1242/jcs.044602.

Amy L Stiegler, Thomas D Grant, Joseph R Luft, David A Calderwood, Edward H Snell, and Titus J Boggon. Purification and SAXS analysis of the integrin linked kinase, PINCH, parvin (IPP) heterotrimeric complex. *PloS one*, 8(1):e55591, January 2013. ISSN 1932-6203. doi: 10.1371/journal.pone.0055591.

Yuansheng Sun, Horst Wallrabe, Soo-Ah Seo, and Ammasi Periasamy. FRET microscopy in 2010: the legacy of Theodor Förster on the 100th anniversary of

his birth. *Chemphyschem : a European journal of chemical physics and physical chemistry*, 12(3):462–74, February 2011. ISSN 1439-7641. doi: 10.1002/cphc. 201000664.

K Tobe, H Sabe, T Yamamoto, T Yamauchi, S Asai, Y Kaburagi, H Tamemoto, K Ueki, H Kimura, Y Akanuma, Y Yazaki, H Hanafusa, and T Kadowaki. Csk enhances insulin-stimulated dephosphorylation of focal adhesion proteins. *Molecular and cellular biology*, 16(9):4765–72, September 1996. ISSN 0270-7306.

Léa Trichet, Cécile Sykes, and Julie Plastino. Relaxing the actin cytoskeleton for adhesion and movement with Ena/VASP. *The Journal of cell biology*, 181(1): 19–25, April 2008. ISSN 1540-8140. doi: 10.1083/jcb.200710168.

Roger Y Tsien. The green fluorescent protein. *Annual review of biochemistry*, 67: 509–44, January 1998. ISSN 0066-4154. doi: 10.1146/annurev.biochem.67.1.509.

M Uehata, T Ishizaki, H Satoh, T Ono, T Kawahara, T Morishita, H Tamakawa, K Yamagami, J Inui, M Maekawa, and S Narumiya. Calcium sensitization of smooth muscle mediated by a Rho-associated protein kinase in hypertension. *Nature*, 389(6654):990–4, October 1997. ISSN 0028-0836. doi: 10.1038/40187.

Kirstin A Walther, Björn Papke, Maja B Sinn, Kirsten Michel, and Ali Kinkhab-wala. Precise measurement of protein interacting fractions with fluorescence lifetime imaging microscopy. *Molecular bioSystems*, 7(2):322–36, February 2011. ISSN 1742-2051. doi: 10.1039/c0mb00132e.

Jia-huai Wang. Pull and push: talin activation for integrin signaling. *Cell research*, 22(11):1512–4, November 2012. ISSN 1748-7838. doi: 10.1038/cr.2012.103.

Yuan Wang and Thomas D Gilmore. Zyxin and paxillin proteins: focal adhesion plaque LIM domain proteins go nuclear. *Biochimica et Biophysica Acta (BBA) - Molecular Cell Research*, 1593(2-3):115–120, February 2003. ISSN 01674889. doi: 10.1016/S0167-4889(02)00349-X.

Bernhard Wehrle-Haller. Assembly and disassembly of cell matrix adhesions. *Current opinion in cell biology*, 24(5):569–81, October 2012a. ISSN 1879-0410. doi: 10.1016/j.ceb.2012.06.010.

Bernhard Wehrle-Haller. Structure and function of focal adhesions. *Current opinion in cell biology*, 24(1):116–24, February 2012b. ISSN 1879-0410. doi: 10.1016/j.ceb.2011.11.001.

Matthias Weiss, Markus Elsner, Fredrik Kartberg, and Tommy Nilsson. Anomalous subdiffusion is a measure for cytoplasmic crowding in living cells. *Biophysical journal*, 87(5):3518–24, November 2004. ISSN 0006-3495. doi: 10.1529/biophysj.104.044263.

J White and E Stelzer. Photobleaching GFP reveals protein dynamics inside live cells. *Trends in cell biology*, 9(2):61–5, February 1999. ISSN 0962-8924.

Sara a Wickström, Anika Lange, Eloi Montanez, and Reinhard Fässler. The ILK/PINCH/parvin complex: the kinase is dead, long live the pseudokinase! *The EMBO journal*, 29(2):281–91, January 2010. ISSN 1460-2075. doi: 10.1038/emboj.2009.376.

Frank Wilcoxon. Individual comparisons by ranking methods. *Biometrics bulletin*, 1(6):80–83, 1945.

Holly M Wobma, Megan L Blades, Ekaterina Grekova, Dylan L McGuire, Kun Chen, Warren C W Chan, and David T Cramb. The development of direct multicolour fluorescence cross-correlation spectroscopy: towards a new tool for tracking complex biomolecular events in real-time. *Physical chemistry chemical physics : PCCP*, 14(10):3290–4, March 2012. ISSN 1463-9084. doi: 10.1039/c2cp23278b.

Haguy Wolfenson, Irena Lavelin, and Benjamin Geiger. Dynamic regulation of the structure and functions of integrin adhesions. *Developmental cell*, 24(5):447–58, March 2013. ISSN 1878-1551. doi: 10.1016/j.devcel.2013.02.012.

C K Wood, C E Turner, P Jackson, and D R Critchley. Characterisation of the paxillin-binding site and the C-terminal focal adhesion targeting sequence in vinculin. *Journal of cell science*, 107 (Pt 2):709–17, February 1994. ISSN 0021-9533.

F S Wouters and P I Bastiaens. Fluorescence lifetime imaging of receptor tyrosine kinase activity in cells. *Current biology : CB*, 9(19):1127–30, October 1999. ISSN 0960-9822.

Jinseong Yi, Susanne Kloeker, Christopher C Jensen, Susanne Bockholt, Hiroaki Honda, Hisamura Hirai, and Mary C Beckerle. Members of the Zyxin family of LIM proteins interact with members of the p130Cas family of signal transducers. *The Journal of biological chemistry*, 277(11):9580–9, March 2002. ISSN 0021-9258. doi: 10.1074/jbc.M106922200.

Cheng-han Yu, Jaslyn Bee Khuan Law, Mona Suryana, Hong Yee Low, and Michael P Sheetz. Early integrin binding to Arg-Gly-Asp peptide activates actin polymerization and contractile movement that stimulates outward translocation. *Proceedings of the National Academy of Sciences of the United States of America*, 108(51):20585–90, December 2011. ISSN 1091-6490. doi: 10.1073/pnas.1109485108.

Hong-Gang Yu, Henning Schrader, Jan-Michel Otte, Wolfgang E Schmidt, and Frank Schmitz. Rapid tyrosine phosphorylation of focal adhesion kinase, paxillin, and p130Cas by gastrin in human colon cancer cells. *Biochemical Pharmacology*, 67(1):135–146, January 2004. ISSN 00062952. doi: 10.1016/j.bcp.2003.08.015.

David A Zacharias, Jonathan D Violin, Alexandra C Newton, and Roger Y Tsien. Partitioning of lipid-modified monomeric GFPs into membrane microdomains of live cells. *Science (New York, N.Y.)*, 296(5569):913–6, May 2002. ISSN 1095-9203. doi: 10.1126/science.1068539.

Ronen Zaidel-Bar, Zvi Kam, and Benjamin Geiger. Polarized downregulation of the paxillin-p130CAS-Rac1 pathway induced by shear flow. *Journal of cell science*, 118(Pt 17):3997–4007, September 2005. ISSN 0021-9533. doi: 10.1242/jcs.02523.

Ronen Zaidel-Bar, Shalev Itzkovitz, Avi Ma'ayan, Ravi Iyengar, and Benjamin Geiger. Functional atlas of the integrin adhesome. *Nature cell biology*, 9(8):858–67, August 2007. ISSN 1465-7392. doi: 10.1038/ncb0807-858.

E Zamir and B Geiger. Molecular complexity and dynamics of cell-matrix adhesions. *Journal of cell science*, 114(Pt 20):3583–90, October 2001. ISSN 0021-9533.

E Zamir, M Katz, Y Posen, N Erez, K M Yamada, B Z Katz, S Lin, D C Lin, a Bershadsky, Z Kam, and B Geiger. Dynamics and segregation of cell-matrix adhesions in cultured fibroblasts. *Nature cell biology*, 2(4):191–6, April 2000. ISSN 1465-7392. doi: 10.1038/35008607.

Eli Zamir, Benjamin Geiger, and Zvi Kam. Quantitative multicolor compositional imaging resolves molecular domains in cell-matrix adhesions. *PloS one*, 3(4):e1901, January 2008. ISSN 1932-6203. doi: 10.1371/journal.pone.0001901.

Eli Zamir, Piet H M Lommerse, Ali Kinkhabwala, Hernán E Grecco, and Philippe I H Bastiaens. Fluorescence fluctuations of quantum-dot sensors capture intracellular protein interaction dynamics. *Nature methods*, 7(4):295–8, April 2010. ISSN 1548-7105. doi: 10.1038/nmeth.1441.

André Zeug, Andrew Woehler, Erwin Neher, and Evgeni G Ponimaskin. Quantitative intensity-based FRET approaches–a comparative snapshot. *Biophysical journal*, 103(9):1821–7, November 2012. ISSN 1542-0086. doi: 10.1016/j.bpj. 2012.09.031.

Xuejiao Zhang, Cheng Li, Huiling Gao, Hiroaki Nabeka, Tetsuya Shimokawa, Hiroyuki Wakisaka, Seiji Matsuda, and Naoto Kobayashi. Rho kinase inhibitors stimulate the migration of human cultured osteoblastic cells by regulating actomyosin activity. *Cellular & molecular biology letters*, 16(2):279–95, June 2011. ISSN 1689-1392. doi: 10.2478/s11658-011-0006-z.

Y. Zhang. Assembly of the PINCH-ILK-CH-ILKBP complex precedes and is essential for localization of each component to cell-matrix adhesion sites. *Journal of Cell Science*, 115(24):4777–4786, December 2002. ISSN 00219533. doi: 10.1242/jcs.00166.

C. Zheng, Z Xing, Z C Bian, C Guo, A Akbay, L Warner, and J L Guan. Differential Regulation of Pyk2 and Focal Adhesion Kinase (FAK). THE C-TERMINAL DOMAIN OF FAK CONFERS RESPONSE TO CELL ADHESION. *Journal of Biological Chemistry*, 273(4):2384–2389, January 1998. ISSN 00219258. doi: 10.1074/jbc.273.4.2384.

Wolfgang H Ziegler, Robert C Liddington, and David R Critchley. The structure and regulation of vinculin. *Trends in cell biology*, 16(9):453–60, September 2006. ISSN 0962-8924. doi: 10.1016/j.tcb.2006.07.004.

Wolfgang H Ziegler, Alex R Gingras, David R Critchley, and Jonas Emsley. Integrin connections to the cytoskeleton through talin and vinculin. *Biochemical Society transactions*, 36(Pt 2):235–9, April 2008. ISSN 0300-5127. doi: 10.1042/BST0360235.